MINISTRY OF HEALTH OF THE REPUBLIC OF UZBEKISTAN

BUKHARA STATE MEDICAL INSTITUTE

Radjabov Akhtam Boltaevich

Rasulova Mokhigul Matyokub kizi

Age-related histology of the rat prostate and their structural changes in chronic alcoholism

(monograph)

Bukhara – 2024

The monograph presents comprehensive information on the patterns of development and formation of microanatomical structures of the rat prostate gland during postnatal ontogenesis and under chronic exposure to ethyl alcohol. Research has shown that throughout all stages of postnatal ontogenesis, the structural components of the prostate develop in a consistent and interconnected manner, following general biological laws while also exhibiting individual features.The data obtained will improve the efficiency of assessing the degree of alcohol influence on the prostate of experimental animals at the microscopic level and reduce the duration of the study. A clear understanding of the histology of the prostate gland in animals is necessary for studying the etiology, development and treatment of human prostate diseases, for which rat models are modeled. The monograph is intended for scientific researchers of fundamental medicine, urologists, narcologists, and master's students. 16 The monograph provides comprehensive information on the regularities of development and formation of microanatomical structures of the rat prostate gland during postnatal ontogenesis and chronic exposure to ethyl alcohol. It was found that the development of the prostate components occurs sequentially and is interconnected at all stages of postnatal ontogenesis, obeys general biological laws and has individual characteristics. The data obtained increase the efficiency of microscopic assessment of the effects of alcohol on the prostate gland of experimental animals and reduces the duration of the study. A clear understanding of prostate histology through modeling in rats is necessary for studying the etiology, development and treatment of human prostate diseases. The monograph is intended for researchers in basic medicine, urologists, narcologists and master's students

Radjabov Akhtam Boltaevich

Rasulova Mokhigul Matyokub kizi

Age-related histology of the rat prostate and their structural changes in chronic alcoholism [text] / Radjabov Akhtam Boltaevich, Rasulova Mokhigul Matyokub kizi – Bukhara:

Authors:

Radjabov A.B. - Head of the Department of Anatomy, Clinical Anatomy (OSTA), DSc

Rasulova M.M. -assistant of the Department of Anatomy, Clinical Anatomy (OSTA)

Reviewers:

Oripov F.S. - Head of the Department of Histology, Cytology and Embryology of the Samarkand State Medical University, Associate Professor, DSc

Dustova N.K. - Associate Professor of the Department of Obstetrics and Gynecology No. 2 of the Bukhara State Medical Institute, DSc

CONTENTS

INTRODUCTION…….....5

CHAPTER I. MORPHOLOGY OF THE PROSTATE GLAND IN HUMANS AND ANIMALS IN NORMAL CONDITIONS AND UNDER THE INFLUENCE OF ENVIRONMENTAL FACTORS…….....…….. 8

1.1-§. Histological characteristics of the prostate gland in mammals…….…. 8

1.2-§. Microscopic structure of the prostate gland under the influence of environmental factors…….. 19

CHAPTER II. DESIGN AND METHODOLOGY OF CARRYING OUT A HISTOLOGICAL STUDY OF THE PROSTATE…..…….…. 23

2.1-§. Characteristics of experimental studies……..… 23

2.2-§. Research methods used…….…. 26

CHAPTER III. DEVELOPMENT AND MORPHOLOGICAL STRUCTURE OF THE PROSTATE IN RATS OF THE CONTROL GROUP IN POSTNATAL ONTOGENESIS……. 30

3.1-§. Microscopic structure of the prostate gland of rats in early postnatal ontogenesis…….…. 30

3.2-§. Histological characteristics of the prostate gland of rats in late postnatal ontogenesis…….. 45

3.3-§. Age immunohistochemical characteristics of the prostate gland of rats... 59

CHAPTER IV. MORPHOLOGICAL STRUCTURE OF THE PROSTATE GLAND IN RATS OF THE EXPERIMENTAL GROUP……. 74

4.1-§. Microscopic structure of the prostate gland of rats suffering from chronic alcoholism……... 74

4.2-§. Immunohistochemical characteristics of the prostate gland of rats of the experimental group…….. 95

DISCUSSION OF THE OBTAINED DATA AND CONCLUSION……. 102

LITERATURE……. 116

APPENDIX……...……...133

INTRODUCTION

The increased attention of practicing physicians and researchers in fundamental medicine to the study of the prostate gland is dictated by the high level of its pathology, "...sometimes disappointing indicators of diagnosis and treatment, the feasibility of studying the etiopathogenesis of diseases of the gland in order to provide high-quality medical care..."[1] . To date, the anatomical argumentation of surgical treatment of prostate diseases has not lost its relevance, although some success has been achieved in its surgical treatment. The process of formation of epithelial-stromal elements of the prostate gland in the dynamics of development and their relationship with the hemomicrocirculatory bed remains unstudied. Organometric parameters of the gland have not been studied taking into account the indicators of physical development and age-related variability. From a morphological perspective, age-related changes are important for refining age norms and considering them when evaluating pathological processes. Ultimately, prostate pathology acquires not only medical but also social significance.

Global research has shownthat the morphostructure of the prostate gland can be influenced by various environmental factors, including chemical agents. Among these, alcohol is one of the most toxic. According to the World Health Organization, harmful alcohol use is responsible for approximately 3 million deaths each year globally, representing 5.3% of all fatalities. The risk associated with alcohol stems

[1] " Aboyan I.A., Tolmachev A.N., Lemeshko S.I. Morphological characteristics of hyperplastic prostate tissue in chronic prostatitis. Experimental and Clinical Urology 2020(4):82-88. https://doi.org/10.29188/2222-8543-2020-13-4-82-88.

from its toxic effects on multiple organs and bodily systems. Alcohol misuse is identified as the third leading risk factor for diseases and disabilities worldwide and is associated with around 60 different medical conditions. Both experimental and clinical studies have been conducted to investigate the effects of alcohol on various organs and physiological systems. The most vulnerable organs are the brain, kidneys, liver, and lungs. There are no reports of comprehensive studies of organometric changes in the prostate gland in the age aspect, as well as with chronic alcohol exposure. To date, the effect of alcohol on the formation and morphological state of the prostate gland remains unclear. The precise stages of postnatal ontogenesis during which alcohol exerts the most detrimental effects on the development and morphological formation of the prostate remain undefined, rendering this issue highly relevant for both theoretical and clinical medicine.

In Uzbekistan, extensive efforts are currently being made to modernize the healthcare system, strengthen social protection, align medical services with international standards, improve early diagnosis, treatment, and disease prevention, and increase life expectancy. According to the Presidential Decree of the Republic of Uzbekistan No. UP-60 dated January 28, 2022, “On the Development Strategy of the NewUzbekistan for 2022–2026,” measures within the framework of ensuring public health include organizing primary healthcare in the regions based on the “one step” principle and implementing initiatives to provide primary care in mahallas, thereby creating more convenient conditions for the population to access high-quality medical services... "[2]

This research, to some extent, supports the implementation of the objectives outlined in the Presidential Decree of the Republic of Uzbekistan No. UP-60 “On the Development Strategy of the New Uzbekistan for 2022–2026” dated January 28, 2022, as well as in the Presidential Resolutions No. PP-5124 “On Additional

[2] “Decree of the President of the Republic of Uzbekistan No. PF-60 dated January 28, 2022 “On the Development Strategy of the New Uzbekistan for 2022-2026”

Measures for the Comprehensive Development of the Healthcare Sector" dated May 25, 2021, and No. PP-5199 "On Measures for Further Improvement of the System of Specialized Medical Care in Healthcare" dated July 28, 2021, along with other relevant regulatory and legal acts in this field.

CHAPTER I. MORPHOLOGY OF THE PROSTATE GLAND IN HUMANS AND ANIMALS IN NORMAL CONDITIONS AND UNDER THE INFLUENCE OF ENVIRONMENTAL FACTORS

1.2-§. Histological characteristics of the prostate gland in mammals

The prostate gland in mammals is a highly specialized tubular-alveolar exocrine gland [32, 82, 89, 90, 91, 106].

In rats, each lobe of the prostate is surrounded by a thin connective tissue capsule. Structurally, a lobe consists of individual glands (acini or alveoli) and a branching ductal network, with each duct opening separately into the urethra. The acini are separated by thin, loose connective tissue that contains stromal cells, smoothmusclefibers, blood vessels, and nerves. The epithelium lining both the acini and ducts is composed of luminal secretory cells, non-secretory basal cells, and a small population of neuroendocrine cells [73, 92, 123, 138]. Luminal cells range in shape from cuboidal to tall columnar, with their height reflecting the level of secretory activity and the extent of glandular distension. Each acinus is surrounded by smooth muscle fibers, which contract to expel prostatic secretions. Depending on the level of secretory activity, the lobes contain a protein rich secretion that exhibits mild eosinophilia[63]. Within the cane rodent, two histologically particular sorts of lobules were distinguished, comparing to two zones of the organ. The central zone, the portion of the organ closer to the pelvic urethra, had lobules with nearly circular diagrams, various epithelial folds, covering the lumen and encompassing

fibromuscular tissues. The fringe zone, speaking to the portion of the organ farther from the urethra, had lobules with a wide lumen and a moderately littler sum of encompassing fibromuscular tissue [42].

In mice, the epithelium of all prostate lobes consists of secretory epithelial cells, basal cells with minimal cytoplasm located beneath the secretory layer, and a small population of neuroendocrine cells, similar to the human prostate. Each lobe is enclosed by a thin mesothelial layer that also contains adipose tissue, nerves, and blood vessels[89]. These findings are fully consistent with the observations reported by D. Oliveira et al.. [110] "Each lobe of the mouse prostate is made up of individual tubuloalveolar glands and a network of branching ducts that empty separately into the urethra. The acini are divided by fibromuscular stroma" [92, 138].

"Each lobe of the mouse prostate consists of distinct tubuloalveolar glands interconnected by a branching ductal system, with each duct opening independently into the urethra. The acini are separated by a fibromuscular stromal framework" [92, 138]. 12 Like the human prostate, the mouse prostate is composed of acinar glands and ducts, whose epithelium includes columnar luminal secretory cells, basal cells, and a small population of neuroendocrine cells[121]. 6 13 The foremost eminent histological contrast between the prostates of both species is the stromal component, which is exceptionally well created in people as an front fibromuscular locale, while in mice it is inadequate with negligible smooth muscle cells [129]. The epithelial lining of the agouti prostate gland is pseudocolumnar [105]. But in the guinea pig it is simple columnar [60]. In the Tarabula gerbil, the lobes of the prostate gland consist of a folded mucous membrane with secretory epithelial cells forming tubular units and a thin fibromuscular stroma. The stroma consisted of a subepithelial region and a layer of smooth muscle cells surrounding the tubules [91]. In the Mongolian gerbil, with the exception of the dorsal lobe, which has a tubular-acinar organization, all other lobes demonstrate a tubular organization and variable branching of the ducts [120]. These data are not consistent with the results of the studies of Campos S.G.P. et al. [57], who argue that the ventral prostate of the Mongolian gerbil under

morphologically and functionally normal conditions corresponds to a group of tubuloacinar structures formed by simple epithelium surrounded by fibromuscular stroma. According to Rochel S. S. et al. [120], the dorsolateral and ventral lobes have equal relative volumes between the epithelial and stromal sections, together occupying approximately 40% of the entire organ. This result indicates that these lobes are more closely related to the peripheral zone of the human prostate gland in accordance with the zonal model of ductal architecture described by McNeal [101], whose stromal and epithelial structures occupy approximately half of the gland. In the giant anteater, the prostate gland is enclosed by a histological capsule composed of loose connective tissue, blood vessels, nerve ganglia, and muscle bundles. The central zone contains fibromuscular stroma, lined with epithelial cells of the prostatic ducts and urethra featuring transitional epithelium. In the peripheral zone, the stroma consists of fibrous connective tissue with fibroblasts, arterioles, and venules adjacent to the acini, which are lined by pseudostratified columnar epithelium. In the peripheral zone, young anteaters had 50% fewer acini and ducts of the prostate gland than adults. Interestingly, the prostate gland of the giant anteater has a continuous basal cell layer, similar to that of humans [106]. 11 It ought to be famous that the stroma of the prostate organ of mammoth insect eating animals has striated muscle bundles, more often than not the prostate in warm blooded creatures is spoken to as it were by smooth muscle filaments. The nearness of striated muscles within the central zone affirms the speculation of conceivable independent control of ejaculation of prostatic fluid, as was watched within the prostate organ of people and mutts [100]. Akmal Yusrizal [43] inspected the adornment organs of a male pangolin and came to the conclusion that the prostate organ includes a lobular structure, separated by thick connective tissue into projections and lobules, the acinar cells were of the mucous sort. In cold foxes and foxes, the prostate capsule is generally lean and is spoken to by connective tissue strands. In minks and sables, it is thicker and smooth muscle strands prevail in it. The parenchyma of the organ in hide creatures includes a tubular-alveolar structure. The sizes of acini in cold fox and ruddy fox are littler than those in sable and mink. The greatest thickness of the

epithelium of the secretory segments is found in mink, normal- in ice fox and ruddy fox, the littlest- in sable [31]. Theinterdependence of the epithelial and stromal elements of the prostate in the order of carnivores varies insignificantly. This correspondence of glandular and non glandular structures is due to the seasonality of reproduction and the absence of the bulbous gland and seminal vesicles [32]. In the rabbit, the prostate gland is the most developed of all the accessory glands, which is according to their year-round reproduction, and this requires constant tension in the function of the sex glands. They have a minimum area of glandular tissue, which is explained by the well-developed muscle tissue in the stromal elements of the organ. [32]. Anumber of authors indicate that in the rabbit, the capsule of the organs of the vesicoprostatic complex is represented mainly by smooth and striated muscle fibers. Between them there is an insignificant layer of elastic fibers, and the number of bundles of collagen fibers is negligible [67, 145]. The canine family has a thin capsule consisting of elastic and collagen fibers. The number of smooth muscle fibers in the capsule, which are collected in bundles, is extremely small. A similar structure of the fox capsule was observed by Batueva A. B. [4]. In individuals of the mustelid family, in contrast to canines, the capsule is more developed, it is mainly represented by bundles of smooth myocytes, between whichthere are collagen fibers. Circularly and transversely located bundles of elastic fibers are located superficially [32]. Investigate by Randazzo M., Grobholz R. [116] appeared that people of the canine family have septa comprising of smooth myocytes with an admixture of collagen strands. Flexible strands are primarily included within the arrangement of septal layers of halfway and inner lobules. In expansion, mustelids have a small number of myocytes within the septa, which is practically recharged by well developed layers of capsular myocytes, which is affirmed within the ponders of Zadonskaya V. Yu. [10]. Badluev E. B. [3] provides data in his studies that the histological structure of the septa of the submucosa of the prostate part of the urogenital canal in rabbits differs from representatives of carnivores. Both in the submucosa and in the septa, the presence of smooth muscle fibers with layers of elastic fibers is noted. Collagen fibers in the stroma are almost absent. Stefanov M.,

Martín-Alguacil N., Martín-Orti R. [126] identified the main, intermediate and internal groups of lobules in the secretory sections of the prostate gland parenchyma in individuals representing carnivores and lagomorphs.

The comes about of the ponder by V. N. Telenkov [32] concerning the histological structure of the organs of the vesicoprostatic complex in agents of the orders of carnivores and lagomorphs coincide with the information of a number of creators [3, 59, 67] concerning the alveolar-tubular structure of the organ in people and warm blooded animals. The acini of the prostate in agents of carnivores and lagomorphs are lined with a single-layer round and hollow epithelium. The stature of the epithelium can change from moo to tall columnar, this depends on the degree of filling of the lumen of the alveoli with glandular emission, which is affirmed within the thinks about of a number of creators [44, 109, 122] concerning a few creatures and people, Batuev A. B. [6] concerning the fox and Badluev E. B. [3] concerning the rabbit. Canids have prostate gland excretory ducts lined with multi-row (two to four) prismatic epithelium; in mustelids the number of rows in the epithelium varies up to five, in hares from one to four rows. Depending on the functional state of the gland, stretching with secretion, the epithelium can become low single-row, which is indicated in the studies of a number of authors [10, 34, 37, 119, 125] in relation to mammals. Having studied the morphology of the prostate of three species of phyllostomid bats, Fabiane F. M. et al. [72] came to the conclusion that the ventral region has an atypical epithelium without obvious cellular boundaries. The dorsolateral region of Carollia perspicillata and Phyllostomusdis color showed pseudostratified cuboidal morphology, and in Glossophagasoricina-columnar morphology. The dorsal region of the three species analyzed consists of pseudostratified columnar epithelium. In A. lituratus bats, each region of the prostate gland has unique and distinctive characteristics. The ventral region of the prostate gland has an epithelium with variable morphology due to its holocrine type of secretion. In contrast, the dorsal region has a typical cuboidal-columnar pseudostratified epithelium [117]. In the greater horseshoe bat, the prostate gland is lined by pseudostratified columnar epithelium, which can be classified as

transitional epithelium[90]. Histologically, the prostate gland in the three species of bats of the genus Sturnira is differentiated into two regions: ventral and dorsal. The dorsal region contains tubuloalveolar glands, and the ventral region contains alveolar glands. The prostate gland morphology of the three species is similar to that of other studied Stenodermatinae and Desmodontinae, but varies from other subfamilies of Phyllostomidae (Carolinae, Glossophaginae and Phyllostominae), such as Molossidae and Vespertilionidae [59].

The canine prostate is a morphologically homogeneous organ, not differentiated into regions like the human prostate, and includes mainly of secretory glandular tissue. Stromal projections divide the prostate gland into several lobes of glandular epithelium. This epithelium is mainly columnar, which is modified to cubic within the ductal structures. At the same time, the epithelium of the prostatic part of the urethra can be cubic or simple columnar or stratified [93].

In dogs, the lobes consist of abundant complex tubular-alveolar glands lined with columnar epithelium [71].

Morphologically, the canine prostate gland lacks differentiation into zones, it is a homogeneous parenchyma along its longitudinal axis [77]

Adistinctive feature is found in newborn puppies, in which several long main ducts diverge from the prostatic part of the urethra to the outer periphery of the gland. Some of these ducts have a lumen, while others are solid structures [94]. The prepubertal canine prostate gland is a lobulated gland and consists primarily of dense epithelial aggregates with no luminal structures surrounded by a thick proliferation of stromal tissue. After puberty, the fibrous connective tissue is replaced by prostatic epithelium under the control of androgens [95]. In the canine prostate, 15 lobules containing glandular secretory tissue are separated by stromal projections known as capsular trabeculae. The majority of the prostate gland consists of glandular secretory tissue lined by columnar epithelium [76, 134]. Comparable to the organ in men, typical canine prostatic epithelium comprises of three cell sorts: basal, secretory, and neuroendocrine [88]. Secretory cuboidal or columnar epithelial cells

make up the lion's share of the epithelial cells and straight tubuloalveolar organs are dispersed inside lobules that purge into little channels encompassing the urethra [127].

In domestic animals, the parenchyma of the prostate gland consists of tubular alveolar glands lined with a single layer of cuboidal or columnar epithelium. The stroma, which constitutes approximately one-quarter of the gland’s volume, is rich in connective tissue fibers and blood vessels. In boars, the secretory portions of the prostate are organized into multiple lobules separated by connective tissue, while the excretory ducts exhibit numerous folds. The acini are lined with pseudostratified epithelium composed of basal and columnar cells, with the ductal epithelium being notably lower in height than that of the secretory regions. In bulls, the glandular parenchyma of the prostate displays both secretory sections and excretory ducts, which differ in size and structural organization.

The ducts are covered with pseudo stratified epithelium, the basal cells are located between the columnar epithelial cells. The secretory alveolar sections are lined with simple epithelium of varying heights [37].

Mahmud Muhammad Abdullahi et al. [96] examined the accessory gonads of dromedary bulls, rams and Sokoto red bulls and concluded that the prostate gland of the dromedary has the greatest amount of interstitial connective tissue and is rich in striated muscles that surround the lobules. Fibromuscular trabeculae penetrate the parenchyma and are more pronounced in the dromedary than in the other two species. The number of secretory acini was greater in Sokoto red males than in the other two species

All Bengal goat guys have as it were a spread parcel of the prostate organ and are found within the submucosa of the dorsal divider of the pelvic urethra, the secretory units and intraglandular conduits of the prostate organ are lined with basic cuboidal or columnar epithelium [84].

The prostate organ of the barka goat (Capra hircus) was encompassed by a connective tissue capsule, lean dorsally and ventrally, thick along the side. The capsule was secured by a layer of smooth muscle, comparative to those detailed by a few creators [84, 113]. The prostatic acini were lined by basic cuboidal epithelium [45]. The human prostate gland is a single gland with distinct histological zones (peripheral, transitional, and central zones).

The peripheral zone makes up about 70% of the normal prostate tissue [112, 137]. The transitional zone is located adjacent to the prostatic urethra and is not noticeable in most young men, making up about 5% of the prostate. The central zone is a cone-shaped region with a wider portion at the base of the prostate and an apex at the spermatic cord surrounding the ejaculatory ducts [47]. Histologically, the human prostate gland consists of epithelial and stromal compartments. The epithelium contains three cell types: cuboidal columnar secretory cells, nonsecretory basal cells located along the basement membrane, and rare neuroendocrine cells [81, 130].

The epithelial-stromal proportion shifts among species, for case, in people and primates the number of cells within the two components is approximately the same, while within the prostate organ of an grown-up rodent their proportion is 5:1 [64]. The comes about of these considers are steady with the information of M. Randazzo, R. Grobholz [116], in whom the proportion of stroma and parenchyma within the human prostate organ was around the same.

The cellular composition of the prostate gland of humans and rodents differs: in humans the ratio of basal and luminal cells is 1:1, whereas in rodents the ratio is 1:7 [69]. The amount and thickness of the stroma in humans is also higher compared to rodents [135].

The function of basal cells in the prostate gland has long attracted significant interest among morphologists. These cells rest on the epithelial basement membrane and express specific differentiation markers that distinguish them from the luminal

secretory cells. In humans, basal epithelial cells form a continuous layer beneath the luminal cell population of the prostate gland[66].

The relatively higher proportion of basal epithelial cells in the human prostate compared to that in mice may have functional significance. The role of these basal cells in prostate carcinogenesis remains unclear, as existing data are contradictory. In both humans and rats[140], the loss of basal cells occurs early in the carcinogenic process; however, basal epithelial cells are also believed to play a regulatory role, suppressing the growth of human prostate cancer cells. [103].

The stroma of the prostate is fibromuscular, containing numerous smooth muscle cells interspersed with fibroblasts, blood vessels, and nerves. Evidence indicates that the smooth muscle layer plays a regulatory role in signaling between the mesenchyme and epithelium during prostate development in rats, thereby contributing to the mechanism controlling prostate induction [133].

The human prostate itself is heterogeneous, consisting of 70% glandular and 30% fibromuscular tissue, encapsulated by a thick fibrous capsule [97]. The prostate of newborn boys has a complex structure and is functionally similar to the body of an adult [8]. The decrease in the area of acini and the height of the epithelium found in their prostate correlate with the results of studies by Petko I. A., Usovich A.K.[24].Perhaps the reason lies in the decrease in the concentration of androgens in boys in the postpartum period [28]. The first wave of increasing secretory processes is observed in 13-year-old boys. The prostate of young men under 20 is a functionally formed organ. In the first period of mature age (22-35 years), the gland is in a functionally active state. After this period, due to reverse development, the number of functioning acini decreases. This process is possibly associated with stagnation of prostatic juice and the formation of concretions. Before puberty, the prostate gland, having insignificant dimensions, is represented mainly by connective tissue. The stroma formed between the secretory sections is represented by smooth muscle fibers. The formation of the gland in the period from 4 to 10 years is carried out at a slow pace. The glandular and non-glandular structures of the prostate reach

their maximum development at theages of 16-20,i.e. at puberty. In the period of 20-35 years, the glandular, muscular and elastic elements of the gland achieve the greatest morphofunctional progress. The number of normally functioning acini decreases after 40 years. These transformations progress every day and in old age cause fibrosis, which is due to involutional phenomena in the prostate gland [9]

1.2-§. Microscopic structure of the prostate gland under the influence of environmental factors

Each person is uncovered to natural variables, he cannot exist exterior the environment, they are interconnected and have an unrestricted impact on each other. Almost85%ofallillnesses within the present day world are related with unfavorable natural conditions caused by ordinary human mechanical movement. Natural components play a vital part within the event of regenerative dysfunctions [5, 22, 38, 58, 68, 143]. In connection with the widespread pathology of the prostate gland, morphofunctional transformations that begin in the organ under the influence of environmental factors deserve special attention [102, 131]. Zakharov A.A. [13] in the prostate gland of immature rats under the influence of the immunosuppressant-cyclophosphamide, observed a decrease in mass, a decrease in volumetric-linear parameters and flattening of the epithelial lining of the prostate acini.

Kashchenko S.A., Zakharov A.A.[15]noted statistically significant decrease in absolute and relative organ masses, micromorphometric indices of epithelial cells of the secretory sections of the gland, reliable deviations in linear and volumetric parameters of the organ during cyclophosphamide-induced immunosuppression in elderly rats. In experimental rats exposed to subzero temperatures, the prostate undergoes notable structural and functional changes. These include increased proliferative and secretory activity of the acinar epithelium, predominance of congestive processes such as venous stasis and dilation of the acinar lumens, as well as focal epithelial hyperplasia, diffuse connective tissue proliferation, and lymphocytic infiltration of the stroma. [26].

Hypokinetic stress induces circulatory disturbances in the microvascular network of the rat prostate. Prolonged exposure to a sedentary lifestyle leads to an expansion of the vascular area through compensatory mechanisms, which is reflected in the restoration of blood flow via vessel dilation and the formation of new capillaries[18].

In rats with prostatitis, the connective tissue stroma exhibited diffuse lymphocytic infiltration, stromal edema, and considerable variability in the shape and size of the glandular end sections. Secretory material was present in the lumens of approximately 70% of the glands, and localized hemorrhages were also observed[30].

Histological considers conducted on youthful rats with incessant prostatitis uncovered leukocyte penetration of the interlobar stroma, narrowing of the lumens of the acinuses, and atrophic marvels of the epithelial cover. Stagnation of discharge within the glandular sections caused an increment within the measure and distortion of the organ. Metaplasia of the secretory epithelium of the acini, their dystrophic changes, and neurotic expansion of connective tissue were watched [35]. In the prostate gland of rats with chronic autoimmune prostatitis, a morphological picture characteristic of chronic prostatitis was observed: atrophy of the epithelium of the acini, expansion of their lumen, diffuse fibrosis of the connective tissue stroma, lymphocytic infiltration. According to morphometric studies, in chronic prostatitis, an increase in the volume fraction of the inflammatory infiltrate, indicators of the volume fraction of acini not containing secretion, and the number of epithelial cells in the lumen of the acini were detected [36].

Neimark A.I. et al. [21] examined patients (agricultural machine operators) suffering from vibration disease and observed a decrease in the number and size of the main cells in prostate biopsies. In sections, the lumens of the acini had a predominantly folded appearance, with remnants of desquamative cells and amyloid bodies inside them. In places, focal atrophy of epithelial cells was detected, and fibrosis was noted everywhere around the acini.

When modeling liquor inebriation in rats, against the foundation of venous blockage within the pelvic organs, auxiliary changes are shaped, communicated in edema and disorganization of the prostate structure, enlargement of blood vessels. Inveterate liquor inebriation leads to extension of the lumens of the acini, amassing of secretion, an increment within the cross-sectional region of the hemocapillaries, a diminish within the zone of the parenchyma and an increment within the stroma [40]. In the prostate of mature men (31-40 years) with chronic alcohol intoxication, polymorphism of the glands, a decrease in the lumen diameter and the number of acini, the height of the acinar epithelium, and the percentage of glandular tissue were observed. An increase in the proportion of muscle and connective tissue in the prostate of alcoholic men was noted, single lymphoid infiltrates were determined in the stroma, and the walls of individual arteries were significantly thickened due to sclerosis [6]. Histological analysis of young rats with persistent prostatitis revealed leukocyte infiltration of the interlobular stroma, narrowing of the acinar lumens, and atrophic changes in the epithelial lining. Stagnation of secretions within the glandular compartments contributed to organ enlargement and deformation. Metaplastic alterations of the acinar secretory epithelium, dystrophic changes, and pronounced expansion of the connective tissue were also observed. In rats with chronic autoimmune prostatitis, the prostate exhibited classic morphological features of chronic inflammation, including epithelial atrophy of the acini, lumen dilation, diffuse stromal fibrosis, and lymphocytic infiltration. Morphometric studies further indicated an increased volume fraction of inflammatory infiltrates, a higher proportion of acini lacking secretions, and an elevated number of epithelial cells within the acinar lumens [36].

Neimark A.I. et al. [21] examined patients (agricultural machine operators) suffering from vibration disease and observed a decrease in the number and size of the main cells in prostate biopsies. In sections, the lumens of the acini had a predominantly folded appearance, with remnants of desquamative cells and amyloid bodies inside them. In places, focal atrophy of epithelial cells was detected, and fibrosis was noted everywhere around the acini.

When modeling liquor inebriation in rats, against the foundation of venous blockage within the pelvic organs, auxiliary changes are shaped, communicated in edema and disorganization of the prostate structure, enlargement of blood vessels. Inveterate liquor inebriation leads to extension of the lumens of the acini, amassing of secretion, an increment within the cross-sectional region of the hemocapillaries, a diminish within the zone of the parenchyma andanincrement within the stroma [40]. In the prostates of adult men aged 31–40 with chronic alcohol intoxication, glandular polymorphism was observed, along with reduced acinar lumen diameter, a decrease in the number of acini, diminished height of the acinar epithelium, and a lower proportion of glandular tissue. An increase in the proportion of muscle and connective tissue in the prostate of alcoholic men was noted, single lymphoid infiltrates were determined in the stroma, and the walls of individual arteries were significantly thickened due to sclerosis [6].

Favaro W.J., Cagnon V.H.A. [127] in 45-day-old rats and Candido E. M. et al. [58] in 3-month-old rats with alcohol and nicotine intoxication in the prostate observed inflammatory cells in the stroma of the organ, a decrease in secretion, the number of acini and the folding of the mucous membrane, a decrease in the amount of nuclear volume and stromal hypertrophy. In the epithelium, atrophy of columnar cells and prostatic intraepithelial neoplasia were noted. In adult mice subjected to chronic alcohol consumption, the prostate exhibited a reduced number of acini as well as a decrease in the number of mucosal folds. The secretory epithelium was sharply atrophied, a large amount of collagen was observed in the stroma [56].

Martinez F.E. et al. [99] in their thinks about appeared widened cisterns of the endoplasmic reticulum, uncommon microvilli and sporadically formed cores within the epithelium of the ventral flap of the prostate in rats subjected to long-term harming with 35% ethanol. Afterward, Cagnon et al. [54] famous that persistent utilization of sugar cane brandy diminishes the stature of epithelial cells and leads to decay of the cisterns of the endoplasmic reticulum within the secretory cells of the rodent coagulation organ. Ultrastructural examination of the sidelong and dorsal

flaps of the prostate organ of rats subjected to inveterate utilization of sugar cane brandy appeared dynamic decay of the glandular epithelium [55, 80]. Sattolo S. et al. [124] moreover affirmed characteristic morphological changes within the ventral prostate in rats of the alcoholic gather. Gomes I.C. et al. [83] In mice from the alcoholic bunch, a diminish in cell volume and changes within the secretory organelles of the seminal vesicles were watched.

CHAPTER II. DESIGN AND METHODOLOGY OF HISTOLOGICAL STUDY OF THE PROSTATE

2.1-§. Characteristics of experimental studies

The morphological study was conducted on 213 male white outbred rats, ranging from the neonatal period to 18 months of age, thus covering all stages of early and late postnatal ontogenesis to assess age-related morphological features of the rodent prostate. The collection of the examined specimens is presented in Table 2.1.1. The periods of think about of rats at the lactation arrange were chosen in agreement with the age periodization of research facility creatures (V.I. Zapadnyuk, 1971) and were based on the information of their physical improvement. On the 6th day, hair shows up and the ears open, on the 11th day, the incisors eject, on the 16th day they are totally secured with hair and the eyes open, on the 22nd day the creatures slither out of the settle. In addition, age gradation of laboratory animals, in particular rats, was applied (V.G. Makarov, M.N. Makarova, 2013), according to which the age of rats in late postnatal ontogenesis is distributed as follows: 1- month-old animals– infantile or immature age; 3-month-old– juvenile age; 6-9-month-old– young animals; 12-month-old– mature or adult animals; 18-month-old– old age. Laboratory animals were kept in standard recommended conditions (Zapadnyuk I.P., Zapadnyuk V.I., Zakharia E.A., 1983), in special cages installed on shelves. The date of birth and the beginning of the experiment, as well as the age of the experimental group, were indicated on the cage of the experimental animals.

Table 2.1.1

Distribution of rats by age and experimental period

group of animals	name of groups	age of animals											total number of animals
		early postnatal ontogenesis					late postnatal ontogenesis						
		newborns	6-day	11-day	16- day	21- day	1- month	3-month	6- month	9- month	12- month	18- month	
1	control	18	20	18	17	16	14	12	14	12	10	10	161
2	experimental	-	-	-	-	-	-	12	12	8	10	10	52
Total		18	20	18	17	16	14	24	26	20	20	20	213

The vivarium premises were cleaned daily in the morning hours. The bodies of animals that died during the experiment were buried in the ground, after being treated with a 20% solution of bleach. All stages of scientific research were carried out in compliance with the "European Convention for the Protection of Vertebrate Animals used for Experimental and other Scientific Purposes" [Directive 2010/63/EU].

All groups were formed simultaneously. The laboratory animals participating in the experiment were representative in age, weight, conditions of maintenance and feeding. Sixteen experimental groups were formed: 1st– newborns (n=18); 2nd– 6-day olds (n=20); 3rd– 11-day-olds (n=18); 4th– 16-day-olds (n=17); 5th– 21-day-olds (n=16); 6th– 1-month-olds (n=14); 7th– 3-month-olds, control (n=12); 8th– 6 month-olds, control (n=14); 9th– 9-month-olds, control (n=12); 10th– 12-month olds, control (n=10); 11th– 18-month-olds, control (n=10); 12th– 3-month-olds, experimental group (n=12); 13th– 6 months old, experimental group (n=12); 14th 9 months old, experimental group (n=8); 15th– 12 months old, experimental group (n=10); 16th– 18 months old, experimental group (n=10).

Rats in the control and experimental groups had free access to the main diet, which consisted mainly of root crops and grain forage. 2 In the experimental groups, chronic alcohol exposure was induced in animals using a 40% ethanol solution (Sidorov P.I., 2002). The solution was administered intragastrically via a metal tube once daily at a total dose of 7 g/kg body weight for one monthprior to the planned endpoint. Additionally, the experimental groups were subjected to a model of artificial polydipsia, in which drinking water was replaced with a 5% ethanol solution sweetened with sucrose (5 g per 100 ml of 5% ethanol) (Knyshova L.P., 2016). Control animals received equivalent volumes of 0.9% NaCl intragastrically. Rats were sacrificed by rapid decapitation under ether anesthesia in accordance with approved ethical guidelines (Sidorov P.I., 2002; Rybakova A.V., 2015; Koptyaeva K.E., 2018). Slaughter was performed on days 6, 11, 16, 21, and at the end of months 1, 3, 6, 9, 12, 18 of life of animals on an empty stomach, in the morning hours. When killing and dissecting laboratory animals, the rules of 1 biological safety and ethical principles of working with laboratory animals were observed.

2.2-§. Research methods used

Following macroscopic examination of the excised prostate, histological preparations were performed. Tissue samples were fixed in 10% buffered formalin for 24 hours, rinsed under running water for 3 hours, dehydrated through a graded ethanol series (70%, 80%, 96%, and 100%), cleared in xylene and a xylene–paraffin mixture, and subsequently embedded in paraffin (BIOVITRUM LLC, Russia). Paraffin blocks were sectioned into 3-μm slices using a microtome (Reichert-Jung 2040, Leica Corp., Wetzlar, Germany) and mounted onto glass slides (Standard Grade, Citotest Labware Manufacturing Co., Ltd., China). After deparaffinization, sections were stained with hematoxylin and eosin (H&E) following van Gieson's method, dehydrated through an ethanol series, cleared in xylene, and coverslipped.

Additionally, for histological analysis, some prostate samples were fixed in 10% neutral formalin and processed using a carousel-type processor STP 120 (Thermo Fisher, Germany), followed by paraffin embedding on a Histo Star embedding station (Thermo Fisher Scientific, USA). Sections of 3–4 μm thickness were obtained using a rotary microtome HM 325 (Thermo Fisher Scientific, USA).

For staining sections with hematoxylin and eosin, serial sections were dewaxed and dehydrated. After which they were kept for 2-5 minutes in a solution of Ehrlich hematoxylin. The sections were washed in distilled water, followed by histological examination on a direct microscope Axio Lab.A1 by Carl Zeiss (Germany). The staining was considered satisfactory if the nuclei had an intense red-violet color, nucleoli and chromatin clumps were visualized inside the nucleus, while the cytoplasm was not stained. Sections stained with hematoxylin and washed with water were transferred to distilled water for 3-5 minutes. To stain the cytoplasm of cells, sections were placed in an eosin solution for 0.5-2 minutes. The staining was considered successful if the section had a uniform yellowish-pink color, against which the blue-stained nuclei were clearly visualized. After staining in an eosin solution, sections were washed in distilled water, dehydrated with alcohol, clarified in xylene and embedded in a preservative medium.

For van Gieson recoloring, areas were deparaffinized in xylene and passed through alcohols of slipping concentration. Segments were recolored in Weigert's press hematoxylin for 3-10 minutes, at that point washed for 2-3 minutes in running water, set in picrofuchsin for 2-3 minutes, rapidly washed in refined water (3-10 seconds) and dried out in two parcels of 96% ethanol, one parcel of supreme ethanol, and clarified in two parcels of xylene. The segments were kept in each parcel for 1-2 minutes.

As a result, cell cores were recolored dark, collagen- ruddy, muscle filaments and erythrocytes- yellow. For immunohistochemical examination, serial areas 3 Î¼m thick were dewaxed, got dried out, unmasked, and after that recolored with antigens employing a specialized mechanized framework Ventana Seat Check XT, Roche (Switzerland). Polyclonal antibodies to CD3 and Ki67 (Ventana, Switzerland) were utilized in a weakening of 1:100, carried out on histological glasses with an cement coating (Ventana, Switzerland). Immunohistochemical responses were carried out in understanding with the convention of the counter acting agent producer. Segments were counterstained with Mayer's hematoxylin.

Finished histological preparations were studied under a binocular microscope CX40 (Soptop, China), which has a digital image transmission system of the microscope OD400UHW10 4 MP with a built-in morphometric program. When describing the epithelial-stromal structures of the rat prostate in the experiment, the International Nomenclature of Diagnostic Criteria for Proliferative and Non-Proliferative Lesions in Rats and Mice (INHAND project (2012)- a joint initiative of the Toxicological Pathology Society of Europe (ESTP), Great Britain (BSTP), Japan (JSTP) and North America (STP) was used.

At 70× magnification (7×10), the following parameters were evaluated in the sections:

the shape of the glandular lumens, the number of terminal glandular segments within the field of view, the proportion of acini with and without secretions, the

number of acini containing desquamated epithelial cells, and the count of intra-organ vessels within the intralobular stroma for each field of observation.

In the preparations, at 280× magnification (7×40) using an ocular micrometer, measurements were made of the glandular lumen diameter, epithelial height, and the internal diameter and wall thickness of arterioles, capillaries, and venules. The thickness and distribution of collagen fibers within the glandular tissue were also evaluated. Additionally, the extent of lymphocytic infiltration in the glandular tissue was assessed at 7×40 magnification. Classification was performed following the criteria established by the North American Chronic Prostatitis Collaborative Research Network and the According to the International Prostatitis Collaborative Network [9], lymphocytic infiltration is classified as follows:

1. Mild — individual lymphocytes scattered with clearly defined intervening zones.

2. Moderate — confluent lymphocyte areas without evidence of tissue destruction or formation of lymphoid nodules.

3. Severe — confluent lymphocyte areas accompanied by tissue damage and the development of lymphoid nodules.

To assess the extent of connective tissue proliferation (fibrosis), the thickness of the stromal layers between the glands was measured using an ocular micrometer at ×40 objective and ×7 ocular magnification. The degree of stromal compaction was evaluated according to the method described by Gorbunova E.N., Davydova D.A., and Krupin V.N. (2011) as follows:

1. Mild — stromal septa thickened up to twofold in 2–4 out of 10 fields of view.

2. Moderate—stromalsepta thickened up to twofold in more than 4 fields of view, or marked thickening exceeding threefold observed in 1–2 fields of view.

3. Severe — stromal septa thickened threefold or more in 7–10 fields of view.

To further elucidate the relationship between the glandular and stromal components, their volume fractions (%) were determined. Using G.G. Avtandilova's morphometric grid with 100 intersection points at 100× magnification, intersections corresponding to glandular and stromal elements in prostate sections were counted.

Statistical analysis was performed using Microsoft Excel 7.0 and the Statistica 6.0 software package. Mean (M) and relative (P) values, along with their standard errors (m), were calculated. Both parametric and nonparametric methods were applied, and the Student's t-test was used to determine the significance of differences. Differences were considered statistically significant at $p \leq 0.05$.

CHAPTER III. DEVELOPMENT AND MORPHOLOGICAL STRUCTURE OF THE PROSTATE OF RATS OF THE CONTROL GROUP IN POSTNATAL ONTOGENESIS

3.1-§. Microscopic structure of the prostate gland of rats in early postnatal ontogenesis

The ponder found that in study microscopy of infant rats, the prostate does not have the samestructure in all cases. In a few cases, shaped secretory conclusion segments of the organs are uncovered, in others-epithelial strands, demonstrating continuous separation of the organ. Within the to begin with case, the secretory segments are spoken to by ordinary alveolar-tubular organs with a sofnowshaped lobules, their epithelium islined withasingle-layer mookaleidoscopic epitheliumwith

out epithelial folds(Fig.3.3.1).

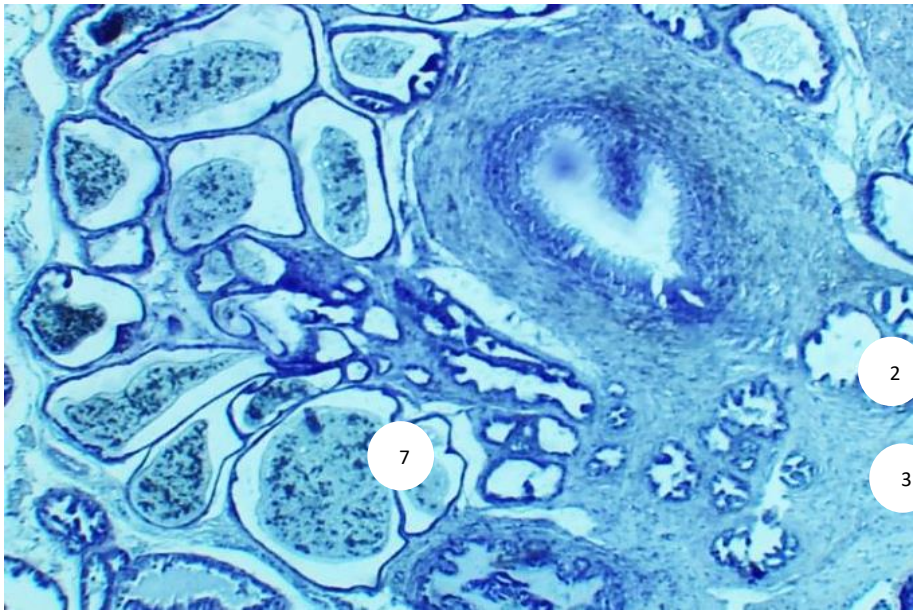

Fig. 3.3.1. Prostate of a newborn rat. Hematoxylin and eosin staining. 1-prostatic urethra, 2-ejaculatory ducts, 3-glandular ducts, 4-oval and rounded secretory sections, 5-acini with flocculent, fine-grained secretion, 6-interglandular stroma, 7-single-layer low-prismatic epithelium. Approx. 10 x vol. 20.

In the second case, epithelial (compact) cords are determined in the gland, which are round or oval formations limited by the basal membrane, filled with epithelial cells (Fig. 3.3.2). In this case, the epithelial cells have large nuclei that are not polarized with respect to the basal membrane. In some acini, the epithelium is loosely located, the cell boundaries are unclear, multi-row and polymorphism of the cells are noted. Cells exhibiting large, multiple nucleoli and mitotic figures were identified. (Fig. 3.3.3).

In the mature acini, the epithelial lining thickness ranges from 4.2 to 8.4 μm, with an average of 6.3 ± 0.21 μm. The acini are oval or round in shape. The glandular lumen diameter ranges from 50.4 to 197.4 μm, averaging 116.8 ± 5.9 μm. The number of acini per field of view varies from 23 to 37, with an average of 29.7 ± 0.8. Most acini contain vesicular, fine-granular secretions. (Fig. 3.3.1).

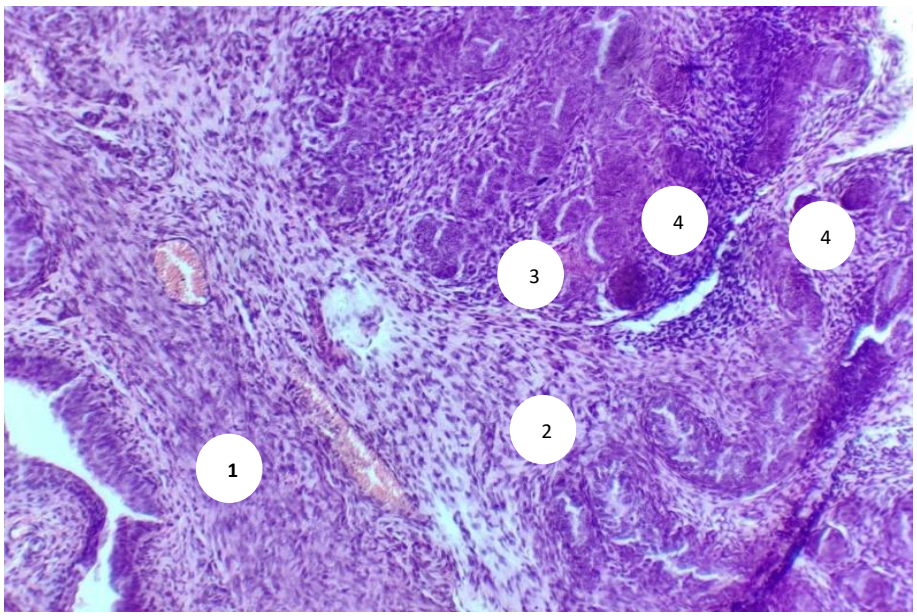

Fig.3.3.2. Prostate of a newborn rat. Hematoxylin and eosin staining. 1-prostatic urethra, 2-stromal vessels, 3-forming glandular ducts, 4-epithelial strands without signs of canalization.

Oc. 10 x ob. 10.

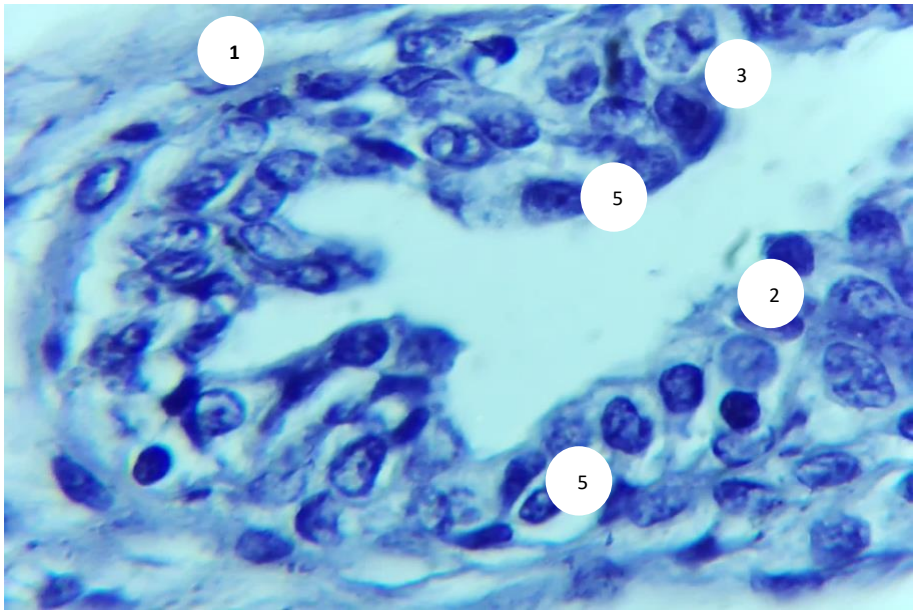

4

Fig.3.3.3. Prostate of a newborn rat. Hematoxylin and eosin staining. 1-interglandular stroma, 2-acinus lumen, 3-epithelial lining of the acinus (multi-row

and polymorphic cells are noted), 4-cells with large and multiple nucleoli, 5-mitotic cells. Approx. 10 x vol. 40.

The volume fraction of acini containing secretions ranges from 70% to 94%, with a mean value of 82.7 ± 1.3%. The proportion of acini lacking secretions varies between 6% and 30%, averaging 17.3 ± 1.3%. In the lumens of certain acini, desquamated epithelial cells were observed. The number of acini exhibiting epithelial desquamation ranges from 4 to 8 per field of view, with a mean of 6.5 ± 0.2. In the periglandular stroma, isolated lymphocytes separated by distinct gaps were identified, numbering between 2 and 4 per field of view, with a mean of 3.0 ± 0.1. The thickness of stromal septa between the acini ranges from 16.8 to 50.4 μm, with an average measurement of 28.6 ± 1.7 μm.

The number of stromal vessels per field of view ranges from 3 to 5, with a mean of 3.6 ± 0.1. The walls of the venules are composed of a single layer of spindle-shaped endothelial cells oriented longitudinally relative to the vessel lumen. The internal diameter of the venules ranges from 8.4 to 12.6 μm, averaging 10.5 ± 0.21 μm, while their wall thickness varies from 2.1 to 4.2 μm, with a mean of 3.0 ± 0.13 μm. The capillary wall consists of a single layer of elongated endothelial cells arranged perpendicular to the lumen. Capillary diameters range from 4.2 to 8.4 μm, with an average of 4.8 ± 0.21 μm. The wall thickness ranges from 2.1 to 4.2 μm, with a mean value of 2.4 ± 0.13 μm. The wall of the arterioles consists of three layers: an inner endothelial layer, a middle muscular layer, and an outer connective tissue layer composed of thin bundles of connective tissue fibers. The internal diameter of the arterioles ranges from 4.2 to 8.4 μm, with a mean of 5.6 ± 0.21 μm. The wall thickness varies between 4.2 and 8.4 μm, averaging 4.5 ± 0.21 μm. The wall of the arterioles consists of an inner endothelial layer, a middle muscular layer, and an outer connective tissue layer composed of thin bundles of connective tissue fibers. Their internal diameter ranges from 4.2 to 8.4 μm, with a mean of 5.6 ± 0.21 μm, while the wall thickness varies between 4.2 and 8.4 μm, averaging 4.5 ± 0.21 μm.kness of their wall varies from 4.2 to 8.4 μm, on average 4.5 ± 0.21 ± μm.

The volume fraction of glandular tissue ranges from 60% to 89%, with a mean of 72.2 ± 1.6%. The proportion of stromal tissue varies between 11% and 40%, averaging 27.8 ± 1.6%.

Collagen fibers in the prostate stroma form a fine-meshed network, with most fibers located beneath the epithelium and encircling the prostatic acini. The collagen fiber layers separating the secretory sections are not expanded (Fig. 3.3.4). The thickness of collagen fiber bundles ranges from 2.1 to 4.2 μm, with a mean of 3.15 ± 0.13 μm.

The study demonstrated that in 6-day-old rats, the prostate consists of glandular segments and connective tissue stroma containing bundles of smooth muscle cells and blood vessels.

Microscopic examination revealed that the acini lack papillary structures, and the terminal secretory portions are lined with a single layer of columnar epithelium, displaying distinct cytoplasmic and nuclear boundaries. In some preparations, isolated epithelial strands without signs of canalization were observed. The epithelial height ranges from 8.4 to 12.6 μm, with a mean of 8.4 ± 0.42 μm.

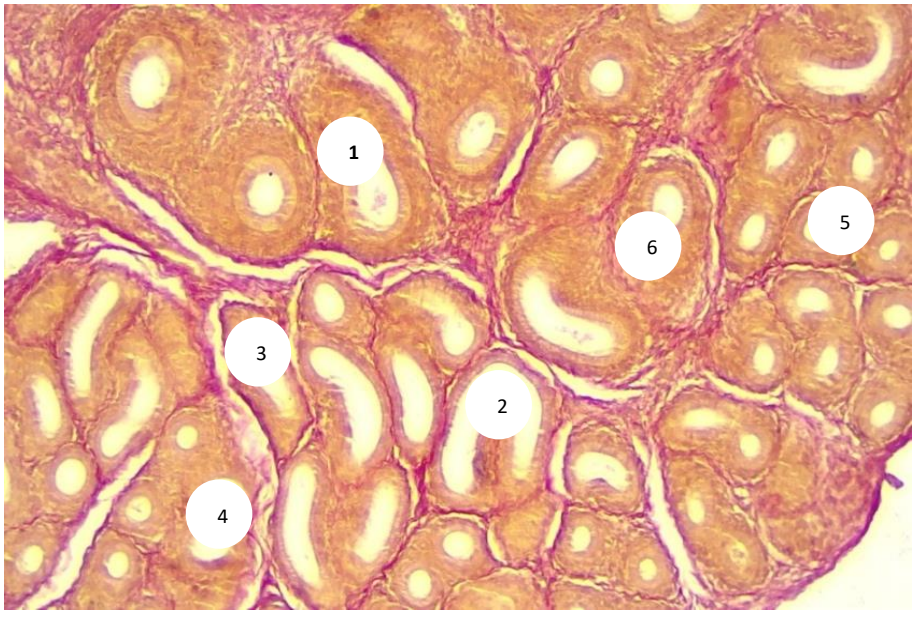

Fig.3.3.4. Prostate of a newborn rat. Van Gieson staining.

1-round acini, 2-oval acini, 3-glandular lobule, 4-interlobular septum, 5-collagen fiber bundles around the secretory sections, 6-stromal fine-mesh network formed by collagen fiber bundles. Approx. 10 x vol. 20.

The acini are oval or round in shape (Fig. 3.3.5). The glandular lumen diameter ranges from 29.4 to 54.6 μm, with a mean of 37.8 ± 1.05 μm. The number of secretory sections per field of view varies from 40 to 55, averaging 47.5 ± 0.8.

The lumens of the acini are predominantly empty and, in 100% of cases, lack secretory material. The number of acini exhibiting epithelial desquamation ranges from 4 to 8 per field of view, with a mean of 6.5 ± 0.2.

In the periglandular stroma, isolated lymph 4 es separated by distinct gaps were observed. Their numb7r per field of view ranges from 3 to 5, with a mean of 3.8 ± 0.1. The thickness of the stromal septa between 2 ni 3 es from 12.6 to 33.6 μm, averaging 24.8 ± 1.3 μm.

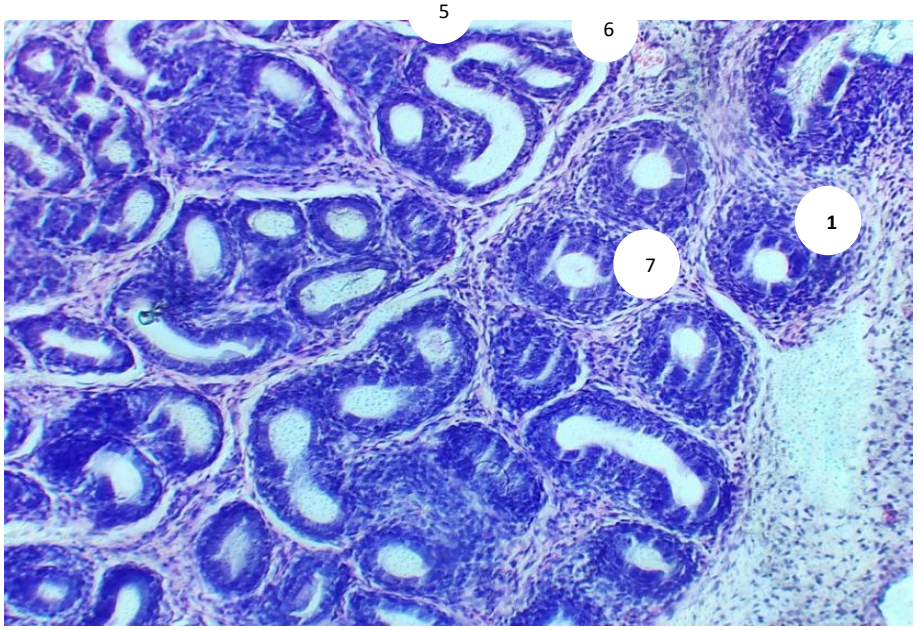

Fig.3.3.5. Prostate of a 6-day-old rat. Hematoxylin and eosin staining.

1-oval acinus, 2-round acinus, 3-interglandular stroma, 4-stromal vessels, 5-formed lobule, 6-interlobular septa, 7-epithelial cords. Approx. 10 x vol. 10.

The number of stromal vessels per field of view ranges from 3 to 6, with a mean value of 3.9 ± 0.2. The walls of the venules are composed of a single layer of spindle-

shaped endothelial cells oriented longitudinally in relation to the vessel lumen. The internal diameter of the venules ranges from 12.6 to 16.8 μm, with an average of 12.9 ± 0.21 μm. Their wall thickness varies between 2.1 and 4.2 μm, averaging 3.2 ± 0.13 μm. The capillary wall consists of a single layer of elongated endothelial cells oriented perpendicular to the vessel lumen. The internal diameter of the capillaries ranges from 4.2 to 8.4 μm, with a mean value of 5.4 ± 0.21 μm. Their wall thickness varies from 2.1 to 4.2 μm, with an average of 2.7 ± 0.13 μm. Arterioles have an internal – endothelial, middle – muscular and external membranes. Endothelial cells have an elongated shape. The middle membrane is formed by smooth myocytes circularly located in 1-2 layers. The outer adventitial membrane is composed of loose fibrous connective tissue. The internal diameter of the arterioles ranges from 4.2 to 8.4 μm, with a mean value of 6.3 ± 0.21 μm. The wall thickness varies between 4.2 and 8.4 μm, averaging 4.8 ± 0.21 μm.

The volume fraction of glandular tissue ranges from 68% to 80%, with an average of 73.1 ± 0.6%. The proportion of stromal tissue varies between 20% and 32%, averaging 26.9 ± 0.6%.

Collagen fibers, forming rims around the secretory sections, create a fine-mesh network within the stroma. The thickness of the collagen fiber bundles ranges from 4.2 to 8.4 μm, with an average of 4.54 ± 0.21 μm.

It was found that in 11-day-old rats, the prostate is composed of alveolar-tubular glands and connective tissue stroma containing bundles of smooth myocytes and blood vessels.

During general microscopy, the acini do not exhibit papillary structures. The terminal secretory sections are lined with cylindrical epithelium showing distinct cytoplasmic and nuclear boundaries (Fig. 3.3.6). The epithelial height ranges from 8.4 to 12.6 μm, averaging 11.3 ± 0.21 μm. In addition to the fully formed epithelial lining of the acini, some preparations reveal epithelial cords without signs of canalization (Fig. 3.3.7). The acini are oval or rounded in shape. The lumen diameter of the glands ranges from 16.8 to 29.4 μm, with an average of 23.1 ± 0.5 μm. The

number of acini observed within the field of vision varies between 65 and 85, averaging 77.0 ± 1.1. In all cases (100%), the terminal secretory sections are empty and contain no secretion. The number of acini with epithelial desquamation ranges from 5 to 8 per field of vision, averaging 7.0 ± 0.16.

In the periglandular stroma, individual lymphocytes are observed, separated by distinct intercellular spaces. Their number per field of vision ranges from 3 to 5, averaging 4.0 ± 0.1. The thickness of the stromal septa between the acini varies from 8.4 to 16.8 μm, with an average of 13.9 ± 0.42 μm.

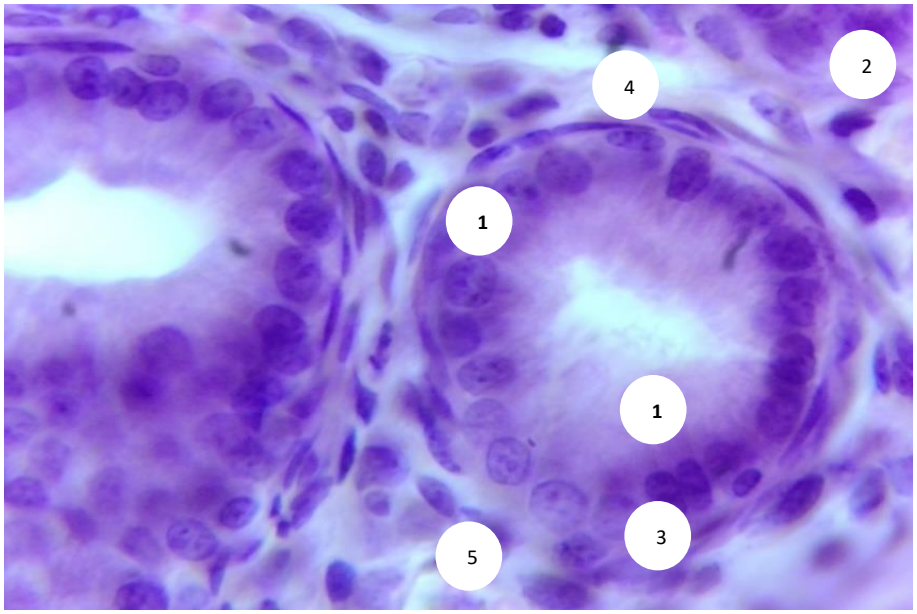

Fig.3.3.6. Prostate of an 11-day-old rat. Hematoxylin and eosin staining.

1-highly prismatic epithelium of acini, 2-interglandular stroma,

3-bundles of smooth myocytes, 4-connective tissue cells,

5-lymphocytes. Approx. 10 x ob. 40.

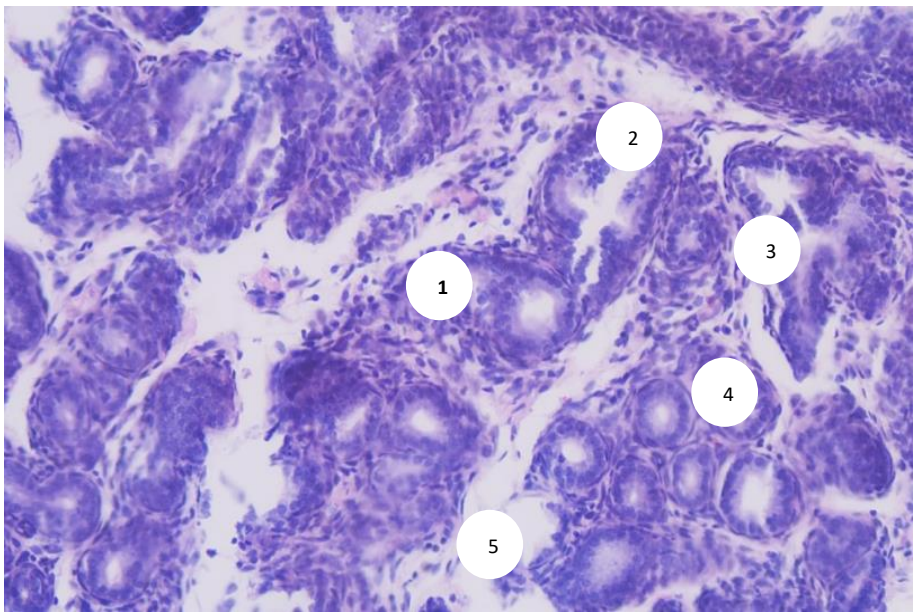

5

Fig.3.3.7. Prostate of an 11-day-old rat. Hematoxylin and eosin staining.

1-interglandular stroma, 2-stromal vessels, 3-acinus with formed lumen, 4-interlobular septa, 5-epithelial cords without lumen. Approx. 10 x vol. 20.

The number of stromal vessels in the field of vision ranges from 3 to 6, with an average of 4.4 ± 0.2. The walls of the venules are composed of a single layer of spindle-shaped endothelial cells oriented longitudinally to the vessel lumen. The internal diameter of the venules varies from 12.6 to 16.8 μm, averaging 14.5 ± 0.21 μm. The wall thickness ranges from 2.1 to 6.3 μm, with an average of 3.7 ± 0.21 μm. The divider of the capillaries is spoken to by a single layer of stretched endothelial cells coordinated opposite to the lumen of the vessel. Their inside distance across changes from 4.2 to 8.4 Î¼m, averaging 6.3Â±0.21 Î¼m. The divider thickness ranges from 2.1-4.2 Î¼m, averaging 3.0Â±0.13 Î¼m. The walls of the arterioles consist of three layers: an inner endothelial layer, a middle muscular layer, and an outer connective tissue layer composed of thin bundles of connective tissue fibers. The internal diameter of the arterioles ranges from 4.2 to 12.6 μm, with a mean of 8.4 ± 0.42 μm. The wall thickness varies from 4.2 to 8.4 μm, averaging 5.4 ± 0.21 μm.

The volume fraction of glandular tissue ranges from 54% to 75%, with a mean of 64.7 ± 1.1%. The proportion of stromal tissue varies between 25% and 46%, averaging 35.3 ± 1.1%. Collagen fibers within the prostate stroma form a fine-meshed network, with most fibers located beneath the epithelium and surrounding the prostatic acini (Fig. 3.3.8). The thickness of the collagen fiber bundles ranges from 4.2 to 8.4 μm, with a mean of 4.75 ± 0.21 μm.

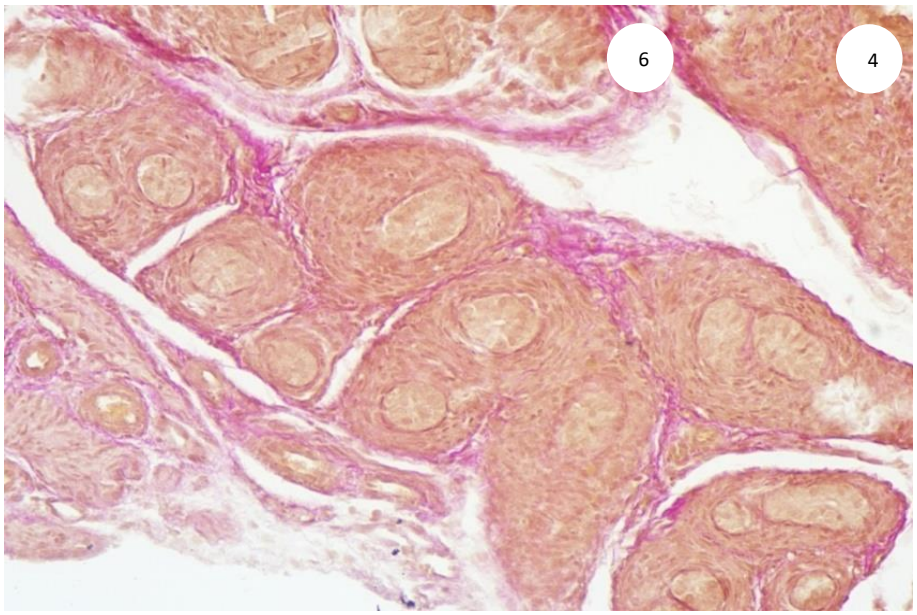

Fig.3.3.8. Prostate of an 11-day-old rat. Van Gieson staining. 1- glandular lobule, 2-interlobular septum, 3-fibromuscular stroma, 4-collagen fiber bundles around the secretory sections, 5-stromal fine-mesh network formed by collagen fibers, 6-acini without lumen (epithelial cords). Approx. 10 x vol. 20.

It has been demonstrated that in 16-day-old rats, each lobe of the prostate is composed of individual glands (acini) and excretory ducts that independently empty into the urethra. The acini are separated by a thin layer of loose connective tissue containing stromal cells, smooth muscle cells, blood vessels, and nerves. Under light microscopy, the acini generally do not exhibit stromal outgrowths, and the terminal secretory portions are lined by cylindrical epithelium (Fig. 3.3.9). The epithelial layer thickness ranges from 8.4 to 16.8 μm, with a mean of 12.6 ± 0.42 μm. In some preparations, single epithelial cords are occasionally observed. The acini display oval to round shapes (Fig. 3.3.10). The luminal diameter of the glands varies from

21.0 to 63.0 μm, with an average of 37.0 ± 1.7 μm. The number of acini within a single field of view ranges from 60 to 80, averaging 73.2 ± 1.1. In all cases (100%), the secretory portions are empty and lack secretion. The number of acini exhibiting epithelial desquamation ranges from 5 to 8 per field, with a mean of 6.7 ± 0.2.

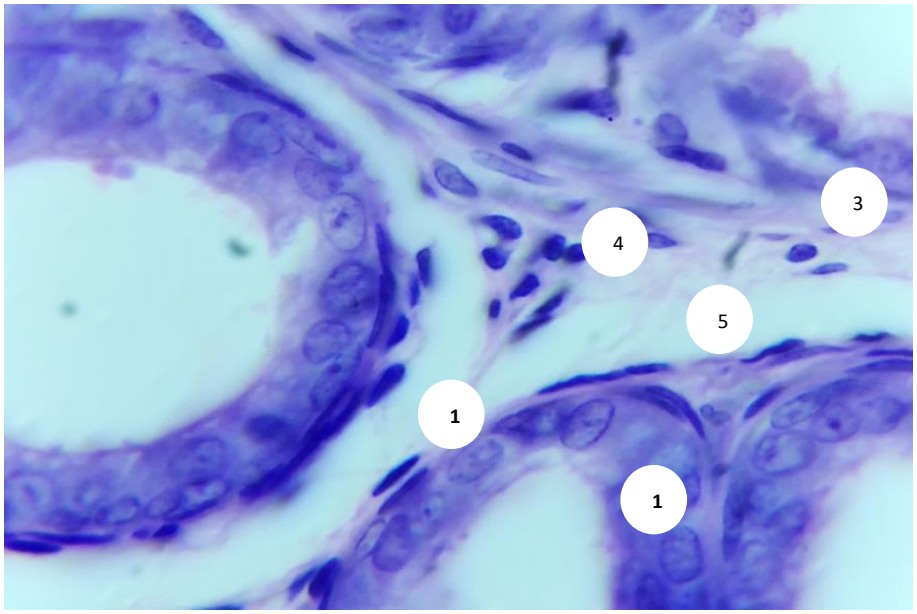

Fig.3.3.9. Prostate of a 16-day-old rat. Hematoxylin and eosin staining.

1-columnar epithelium of acini, 2-interglandular stroma,

3-smooth muscle cells, 4-connective tissue cells,

5-lymphocytes. Approx. 10 x ob. 40.

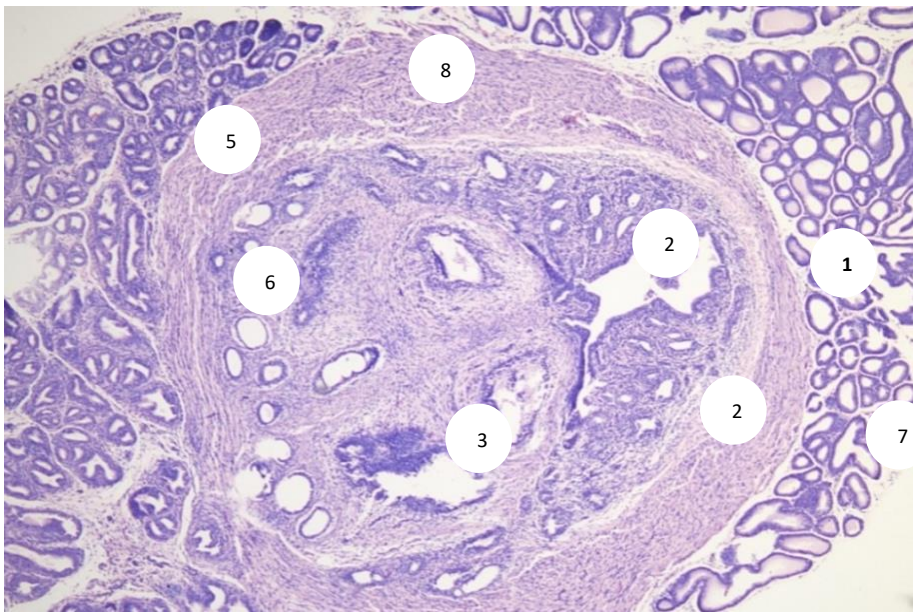

Fig.3.3.10. Prostate of a 16-day-old rat. Hematoxylin and eosin staining. 1-prostatic urethra, 2-ejaculatory ducts, 3-excretory ducts, 4-oval and round secretory sections, 5-formed lobule, 6-interlobular septa, 7-muscle fiber bundles, 8-epithelial cords. Approx. 10 x vol. 10.

In the periglandular stroma, individual lymphocytes are observed, separated by clear spaces. Their number per field of view ranges from 4 to 6, with a mean of 4.7 ± 0.1. The thickness of the stromal septa between the acini varies from 8.4 to 21.0 μm, averaging 14.7 ± 0.7 μm. The number of stromal vessels within the visual field ranges from 3 to 6, with an average of 4.5 ± 0.2.

The walls of the venules consist of a single layer of spindle-shaped endothelial cells oriented longitudinally along the lumen. The internal diameter of the venules ranges from 12.6 to 21.0 μm, with a mean of 16.8 ± 0.42 μm, while their wall thickness varies from 2.1 to 6.3 μm, averaging 4.2 ± 0.21 μm. The capillary walls are composed of a single layer of elongated endothelial cells oriented perpendicular to the lumen. Capillary diameters fluctuate between 4.2 and 8.4 μm, with a mean of 6.3 ± 0.21 μm, and wall thickness ranges from 2.1 to 4.2 μm, averaging 2.9 ± 0.13 μm. Arterioles have an inside - endothelial, center - strong and outside films. Endothelial cells have a spindle-shaped shape. The center film comprises of 1-2 layers of smooth myocytes found circularly. The adventitia is spoken to by bundles

of collagen strands. The inner distance across of arterioles varies between 8.4 and 12.6 Î¼m, on normal - 9.24Â±0.21 Î¼m. Their wall thickness ranges from 4.2 to 8.4 μm, with a mean of 5.8 ± 0.21 μm.

The volumetric fraction of glandular tissue ranges from 64 to 84%, with a mean of 73.1 ± 1.1%. The proportion of stromal tissue fluctuates between 16 and 36%, averaging 26.9 ± 1.1%. Collagen fibers are located within the prostatic stroma, forming a fine-mesh network, with most fibers situated beneath the epithelium and surrounding the prostatic acini (Fig. 3.3.11). The thickness of collagen fiber bundles varies from 4.2 to 8.4 μm, with a mean of 5.04 ± 0.21 μm.

Fig.3.3.11. Prostate of a 16-day-old rat. Van Gieson staining. 1-collagen fiber bundles around the secretory sections, 2-muscle fiber bundles, 3-thick collagen fiber bundles around the ejaculatory ducts, 4-prostatic urethra, 5-interlobular collagen fiber bundles, 6-gland capsule. Approx. 10 x vol. 10.

It was found that the prostate of 21-day-old rats consists of numerous alveolar tubular glands and a fibromuscular stroma composed of loose fibrous connective tissue, bundles of smooth muscle cells, and blood vessels.

At survey microscopy, the acini do not have papillary folds, the terminal secretory sections are represented by a single-layer cylindrical, in places cubic

epithelium. Both formed acini and acini without lumen are found in the preparations (Fig. 3.3.12). The height of the epithelial layer ranges from 8.4 to 16.8 μm, with a mean of 14.0 ± 0.42 μm. The acini exhibit oval to round shape and in some preparations, compact epithelial strands can be observed (Fig. 3.3.13). The luminal diameter of the glands varies from 25.2 to 105.0 μm, averaging 55.4 ± 3.4 μm. The number of acini per field of view ranges from 75 to 110, with a mean of 92.5 ± 1.9. In all cases (100%), the terminal secretory sections lack secretion (see Appendix 1). The number of acini showing epithelial desquamation ranges from 2 to 5 per field, with an average of 3.6 ± 0.2.

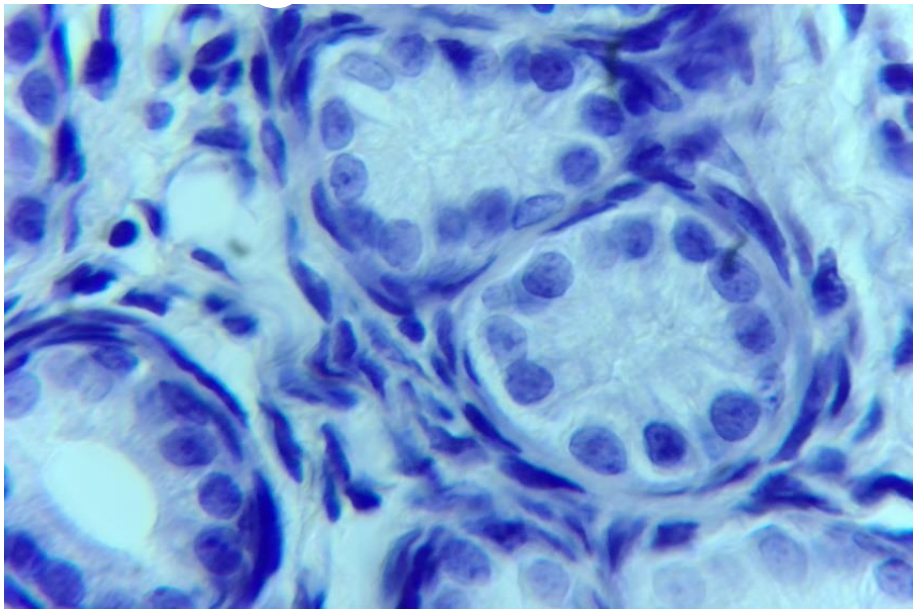

Fig.3.3.12. Prostate of a 21-day-old rat. Hematoxylin and eosin staining. 1-acinus with formed lumen, 2-acinus with closed lumen, 3-columnar epithelium, 4-interglandular stroma, 5-bundles of smooth muscle cells, 6-fibroblasts, 7-lymphocytes. Approx. 10 x vol. 40.

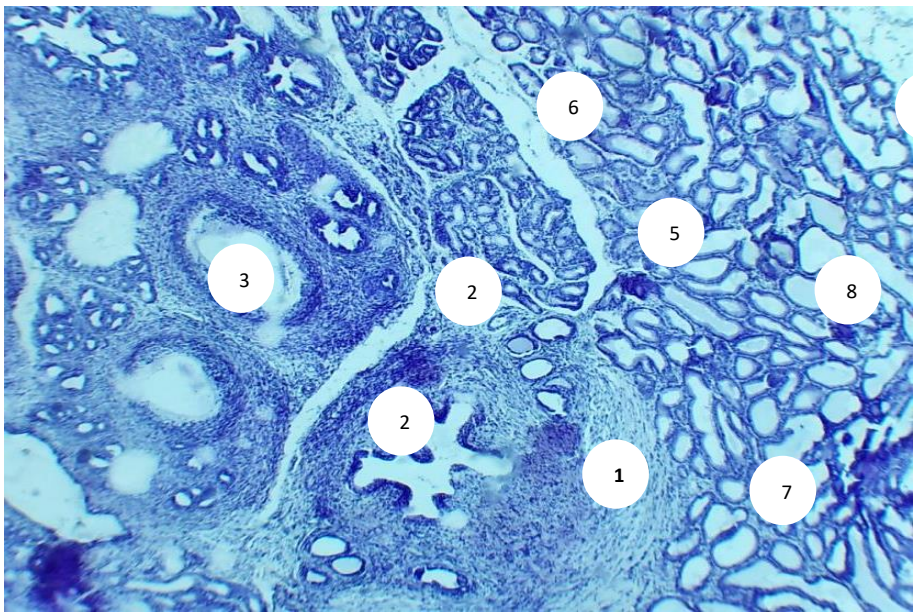

Fig.3.3.13. Prostate of a 21-day-old rat. Hematoxylin and eosin staining. 1-prostatic urethra, 2-ejaculatory ducts, 3-excretory ducts, 4-oval and round secretory sections, 5-formed lobule, 6-interlobular septa, 7-muscle fiber bundles, 8-single epithelial strands. Approx. 10 x ob. 10.

In the periglandular stroma, individual lymphocytes are observed, separated by clear spaces. Their number per field of view ranges from 4 to 6, with a mean of 5.0 ± 0.1. The thickness of the stromal septa between the acini varies from 4.2 to 16.8 μm, averaging 9.5 ± 0.7 μm. The number of stromal vessels within the field of view ranges from 4 to 7, with a mean of 4.6 ± 0.2. The walls of the venules are composed of a single layer of flat endothelial cells oriented longitudinally relative to the vessel lumen. The internal diameter of the venules ranges from 12.6 to 25.2 μm, with a mean of 18.0 ± 0.67 μm, and their wall thickness varies from 4.2 to 8.4 μm, averaging 4.8 ± 0.21 μm. The capillary wall is represented by a single layer of oval-shaped endothelial cells directed perpendicularly to the lumen of the vessel. The diameter of the capillaries ranges from 4.2 to 12.6 μm, with a mean of 7.4 ± 0.42 μm. Their wall thickness varies between 2.1 and 4.2 μm, averaging 3.2 ± 0.13 μm. The wall of the arterioles consists of an inner endothelial layer, a middle muscular layer, and an outer connective tissue layer composed of thin bundles of connective tissue fibers. The internal diameter of the arterioles ranges from 8.4 to 12.6 μm, with

a mean of 10.5 ± 0.21 μm. The thickness of the arteriolar wall varies from 4.2 to 8.4 μm, averaging 6.3 ± 0.21 μm (see Appendix 2). The volumetric fraction of glandular tissue ranges from 59 to 85%, with a mean of 70.6 ± 1.4%. The proportion of stromal tissue fluctuates within 15-41%, with an average of 29.4±1.4% (see Appendix 3).

Collagen fibers are present within the prostatic stroma, forming a fine-mesh network, with most fibers situated beneath the epithelium and surrounding the prostatic acini. The thickness of the collagen fiber bundles ranges from 4.2 to 8.4 μm, with a mean of 5.46 ± 0.21 μm.

3.2-§. Histological characteristics of the rat prostate in late postnatal ontogenesis

The study demonstrated that in 1-month-old rats, the prostate is fully differentiated and comprises numerous alveolar-tubular glands along with a muscular-elastic stroma, consisting of loose fibrous connective tissue, bundles of smooth muscle cells, and blood vessels.

Under light microscopy, the terminal secretory portions, or acini, exhibit epithelial folds in 50% of cases. The acini are lined by a single layer of highly prismatic epithelium. The epithelial cells are polarized relative to the basement membrane and form a single cellular layer. The height of the epithelial layer ranges from 8.4 to 16.8 μm, with a mean of 14.87 ± 0.42 μm. The acini are oval to round in shape (Fig. 3.4.1). The luminal diameter of the glands varies from 63.0 to 168.0 μm, averaging 108.4 ± 4.2 μm. The number of acini per field of view ranges from 60 to 90, with a mean of 78.1 ± 1.6. The volumetric fraction of acini containing secretion ranges from 15 to 30%, with an average of 22.1 ± 0.8%, whereas the proportion of

acini without secretion ranges from 70 to 85%, averaging 77.9 ± 0.8%. The number of acini exhibiting desquamated epithelial cells within the lumen ranges from 3 to 6 per field of view, with a mean of 4.6 ± 0.2.

In the periglandular stroma, individual lymphocytes are observed, separated by clear spaces. Their number per field of view ranges from 4 to 6, with a mean of 5.2 ± 0.1. The thickness of the stromal septa between the acini varies from 4.2 to 16.8 μm, averaging 12.6 ± 0.67 μm. The number of stromal vessels per field of view ranges from 3 to 7, with a mean of 4.7 ± 0.2. The walls of the venules are composed of a single layer of elongated endothelial cells oriented longitudinally relative to the vessel lumen. The internal diameter of the venules ranges from 12.6 to 25.2 μm, with a mean of 18.9 ± 0.67 μm, and their wall thickness varies from 4.2 to 8.4 μm, averaging 5.0 ± 0.21 μm. The capillary wall is represented by a single layer of oval-shaped endothelial cells directed perpendicular to the lumen of the vessel. The diameter of the capillaries ranges from 4.2 to 12.6 μm, with a mean of 8.4 ± 0.42 μm. Their wall thickness varies between 2.1 and 4.2 μm, averaging 4.0 ± 0.13 μm. The walls of the arterioles consist of an inner endothelial layer, a middle muscular layer, and an outer connective tissue layer composed of thin bundles of connective tissue fibers. The internal diameter of the arterioles ranges from 8.4 to 16.8 μm, with a mean of 12.6 ± 0.42 μm, while their wall thickness varies from 4.2 to 8.4 μm, averaging 7.0 ± 0.21 μm.

The volume fraction of glandular tissue is 82-90%, on average 86.5±1.0%. The fraction of stromal tissue fluctuates within 10-18%, on average 13.5±1.0%. Collagen fibers are located in the stroma of the prostate, forming a fine-mesh network, most of the fibers lie under the epithelium and surround the prostatic acini (Fig. 3.4.2). The thickness of the collagen fiber bundles varies from 4.2 to 8.4 μm, on average 6.3±0.21 μm.

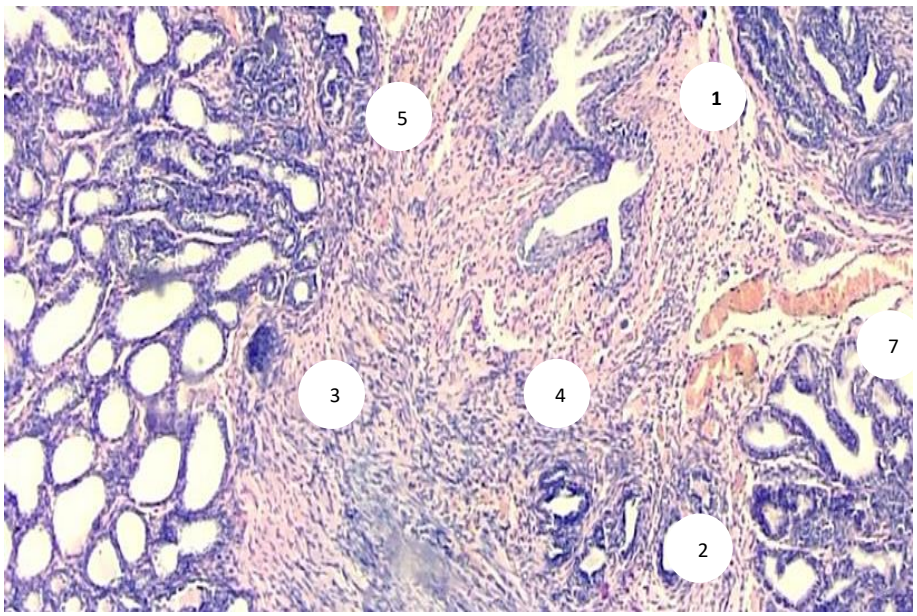

Fig.3.4.1. Prostate of a 1-month-old rat. Hematoxylin and eosin staining.

1-prostatic urethra, 2-excretory ducts, 3-oval and round secretory sections, 4-myocyte bundles, 5-intralobular stroma, 6-interlobular septa, 7-stromal vessels. Approx. 10 x ob. 20.

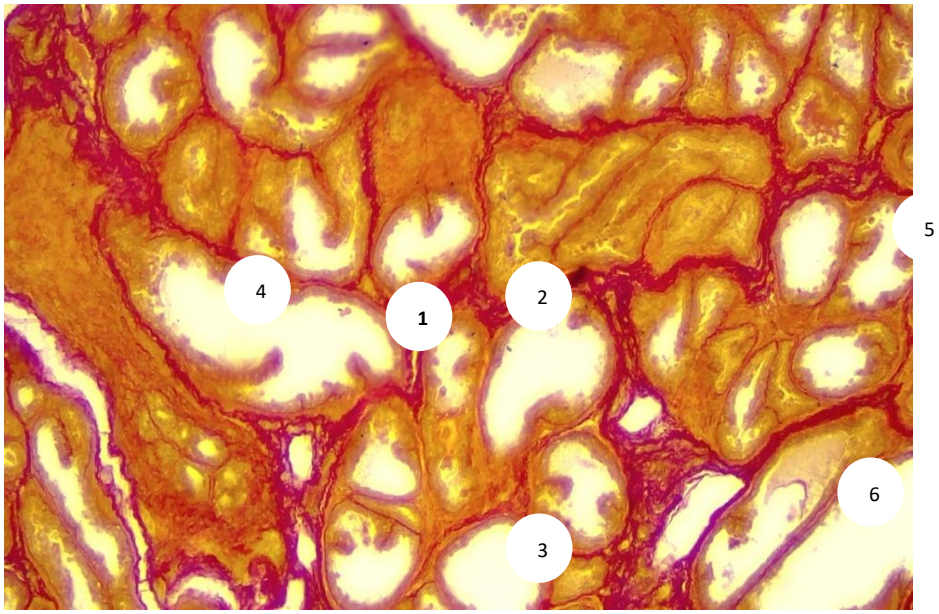

Fig. 3.4.2. Prostate of a 1-month-old rat. Van Gieson staining. 1-oval acinus, 2-columnar epithelium, 3-round acinus,

4-fibromuscular stroma, 5-collagen fiber bundles around the secretory sections, 6-stromal fine-mesh network formed by collagen fibers. Approx. 10 x vol. 20.

The study demonstrated that in 3-month-old rats, the prostate exhibits a normal structural organization and comprises numerous alveolar-tubular glands along with a muscular-elastic stroma, consisting of loose fibrous connective tissue, bundles of smooth muscle cells, and blood vessels.

Under light microscopy, the terminal secretory portions, or acini, exhibit a folded appearance in most cases (70%), and are lined by highly prismatic epithelium composed of tall columnar and basal cells resting on a clearly visible basement membrane. The height of the epithelial layer ranges from 8.4 to 21.0 μm, with a mean of 16.5 ± 0.6 μm. The acini are oval to round in shape (Fig. 3.4.3). The luminal diameter of the glands varies from 105.0 to 298.2 μm, averaging 198.7 ± 8.0 μm. The number of acini per field of view ranges from 38 to 66, with a mean of 51.8 ± 1.5. The volumetric fraction of acini containing secretion ranges from 70 to 100%, averaging 83.5 ± 1.6%, whereas the proportion of acini without secretion ranges from 8 to 30%, with a mean of 16.5 ± 1.2%.

The number of acini containing desquamated epithelial cells within the lumen ranges up to 4 per field of view, with a mean of 1.7 ± 0.2.

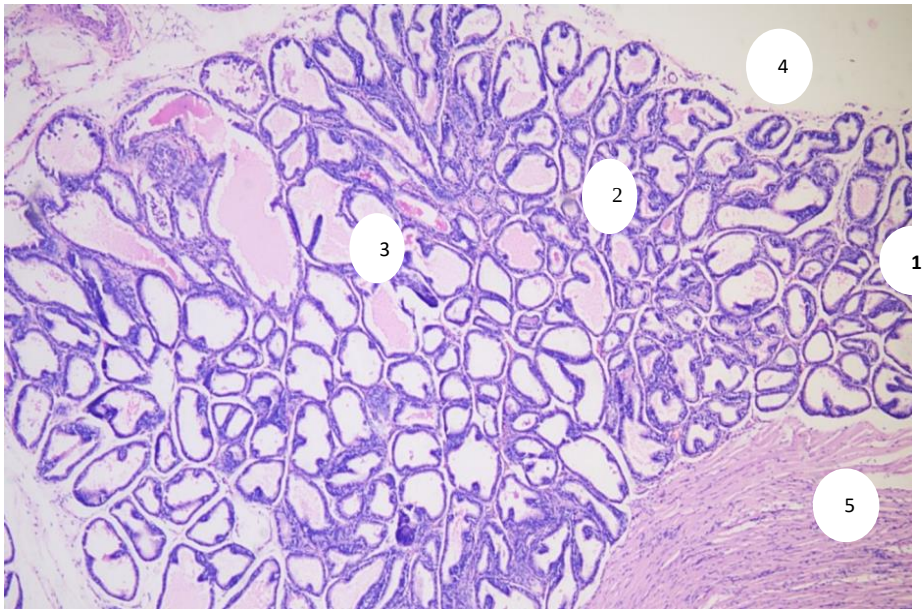

Fig.3.4.3. Prostate of a 3-month-old rat. Hematoxylin and eosin staining. 1-secretory terminal sections (acini), 2-intralobular stroma, 3-acini with intraluminal secretion, 4-gland capsule, 5-bundles of smooth myocytes. Approx. 10 x ob. 10.

In the periglandular stroma, individual lymphocytes are observed, separated by clear gaps. Their number per field of view ranges from 4 to 9, with a mean of 5.7 ± 0.3. The thickness of the stromal septa between the acini varies from 8.4 to 25.2 μm, averaging 15.5 ± 0.9 μm. The number of stromal vessels per field of view ranges from 3 to 8, with a mean of 5.0 ± 0.3. The walls of the venules consist of one layer of spindle-shaped endothelial cells located in the longitudinal direction. The internal diameter of the venules ranges from 16.8 to 19.4 μm, with a mean of 20.6 ± 0.67 μm. Their wall thickness varies from 4.2 to 8.4 μm, averaging 4.7 ± 0.21 μm. The capillary wall is represented by a single layer of oval-shaped endothelial cells directed perpendicular to the lumen of the vessel. The diameter of the capillaries ranges from 8.4 to 12.6 μm, with a mean of 9.6 ± 0.21 μm. Their wall thickness varies between 2.1 and 4.2 μm, averaging 2.9 ± 0.13 μm. The walls of the arterioles consist of an inner endothelial layer, a middle muscular layer, and an outer connective tissue layer composed of thin bundles of connective tissue fibers. The internal diameter of the arterioles ranges from 8.2 to 16.4 μm, with a mean of 13.8 ± 0.46 μm, and their wall thickness varies from 4.2 to 8.4 μm, averaging 7.5 ± 0.21 μm.

The volumetric fraction of glandular tissue ranges from 62 to 80%, with a mean of 71.0 ± 1.0%. The proportion of stromal tissue fluctuates between 20 and 38%, averaging 29.0 ± 1.0%. Collagen fibers are present within the prostatic stroma, forming a fine-mesh network, with most fibers situated beneath the epithelium and surrounding the prostatic acini. The thickness of collagen fiber bundles varies from 4.2 to 12.6 μm, with a mean of 8.2 ± 0.46 μm. The study demonstrated that in 6-month-old rats, the prostate comprises numerous individual alveolar-tubular glands and a muscular-elastic stroma, composed of loose fibrous connective tissue, bundles of smooth muscle cells, and blood vessels. In 75% of cases, light microscopy reveals epithelial-stromal outgrowths within the acini. The terminal sections are lined by a single layer of highly prismatic, and in some areas low prismatic, epithelium composed of tall columnar and basal cells. The height of the epithelial layer ranges from 12.6 to 21.0 μm, with a mean of 17.8 ± 0.38 μm. The acini are oval to round in

shape (Fig. 3.4.4). The luminal diameter of the glands varies from 210.0 to 441.0 μm, averaging 330.5 ± 9.7 μm. The number of acini per field of view ranges from 18 to 28, with a mean of 22.0 ± 0.5. The volumetric fraction of acini containing secretion ranges from 90 to 100%, with a mean of 93.3 ± 0.5%, while the proportion of acini without secretion ranges from 0 to 10%, averaging 6.7 ± 0.5%. Acini containing desquamated epithelial cells were not observed in any preparations.

In the periglandular stroma, isolated lymphocytes are observed, separated by clear gaps. Their number per field of view ranges from 8 to 12, with a mean of 10.0 ± 0.22. The stroma is thin in most preparations, and the acini are often arranged end-to-end. The thickness of the stromal septa between the acini varies from 12.6 to 33.6 μm, averaging 23.1 ± 1.13 μm. The number of stromal vessels per field of view ranges from 4 to 9, with a mean of 7.0 ± 0.3. The walls of the venules consist of a single layer of flat endothelial cells oriented longitudinally relative to the vessel lumen. The internal diameter of the venules ranges from 21.0 to 29.4 μm, with a mean of 24.8 ± 0.42 μm.

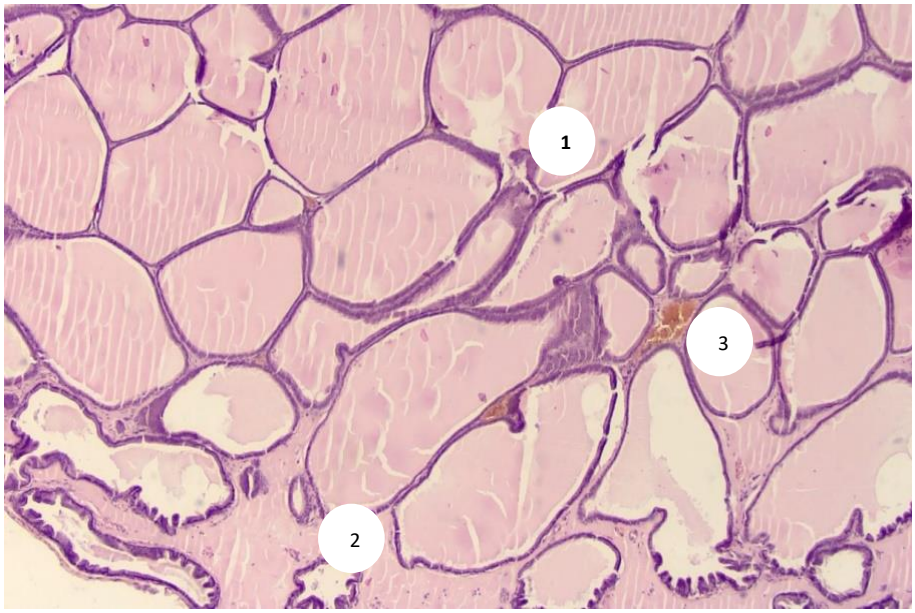

Fig.3.4.4. Prostate of a 6-month-old rat. Hematoxylin and eosin staining. 1-round and oval acini with intraluminal homogeneous secretion, 2-interlobular stroma, 3-vessels of the intralobular stroma. Approx. 10 x vol. 20.

The wall thickness of the venules ranges from 4.2 to 8.4 μm, with a mean of 5.8 ± 0.21 μm. Capillary walls consist of a single layer of spindle-shaped endothelial cells oriented perpendicular to the vessel lumen. The diameter of the capillaries varies from 8.4 to 16.8 μm, averaging 13.1 ± 0.42 μm, and their wall thickness ranges from 2.1 to 4.2 μm, with a mean of 4.1 ± 0.13 μm. The walls of the arterioles are composed of an inner endothelial layer, a middle muscular layer, and an outer connective tissue layer represented by thin bundles of connective tissue fibers. The internal diameter of the arterioles ranges from 12.6 to 16.8 μm, with a mean of 14.7 ± 0.21 μm, and their wall thickness varies from 4.2 to 8.4 μm, averaging 7.7 ± 0.21 μm.

The volumetric fraction of glandular tissue ranges from 77.0 to 90.0%, with a mean of 82.5 ± 0.7%. The proportion of stromal tissue varies between 10.0 and 23.0%, averaging 17.5 ± 0.7%.

Collagen fibers surround the terminal sections of the glands, with most fibers located beneath the epithelium. Within the stroma, they form a fine-mesh network. The thickness of collagen fiber bundles ranges from 4.2 to 12.6 μm, with a mean of 10.0 ± 0.21 μm.

The study demonstrated that the prostate of 9-month-old rats comprises terminal glandular sections and a muscular-elastic stroma.

S Light microscopy reveals papillary outgrowths in 60–80% of acini. The terminal sections are lined by a single layer of highly prismatic, and in some areas low-prismatic, epithelium. The height of the epithelial layer ranges from 16.8 to 21.0 μm, with a mean of 19.74 ± 0.21 μm. The acini are predominantly oval to round in shape (Fig. 3.4.5). The luminal diameter of the glands varies from 336.0 to 840.0 μm, averaging 531.7 ± 20.6 μm. The number of acini per field of view ranges from 10 to 21, with a mean of 14.9 ± 0.6. Survey microscopy reveals papillary outgrowths in 60-80% of cases in the acini, the terminal sections are represented by a single-layer highly prismatic, and in places low-prismatic epithelium. The thickness of the epithelial lining varies from 16.8 to 21.0 μm, with an average of 19.74±0.21 μm.

The acini are predominantly oval and rounded (Fig. 3.4.5). The lumen diameter of the glands varies fr 6 336.0 to 840.0 μm, with an average of 531.7±20.6 μm. The number of acini in the field of vi 2 varies from 10 to 2 5 with an average of 14.9±0.6. The volu 4 ic fraction of acini containing secretion ranges from 85 to 100%, with a mean of 92.0 ± 0.8%. The propo 1 of acini without secretion varies from 0 to 15%, averaging 8.0 ± 0.8%. Acini containing desquamated epithelial cells were not observed in any preparations.

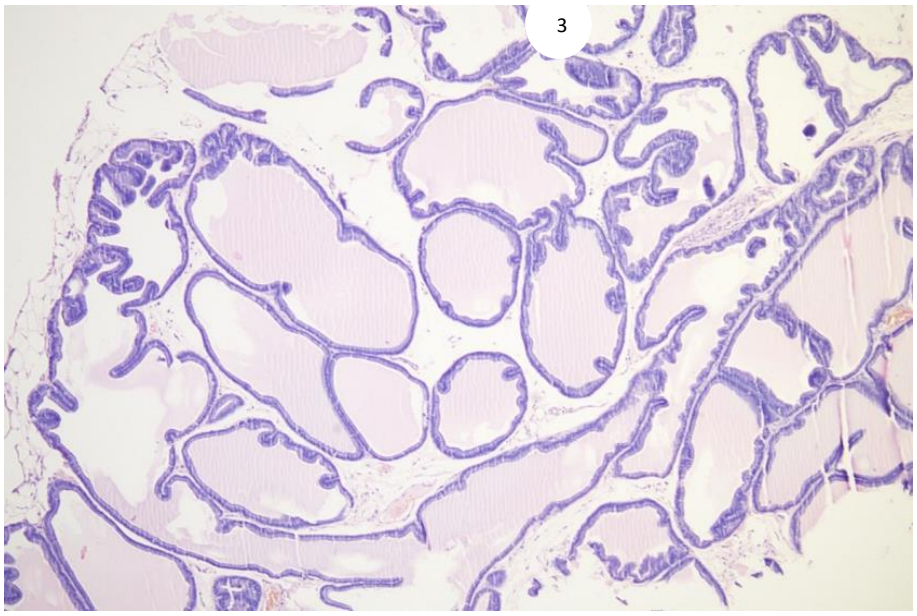

Fig.3.4.5. Prostate of a 9-month-old rat. Hematoxylin and eosin staining. 1-round and oval acini with intraluminal homogeneous secretion, 2-intralobular stroma, 3-vessels of the intralobular stroma, 4-epithelial-stromal outgrowths, 5-bundles of smooth myocytes, 6-glandular capsule. Approx. 10 x vol. 20.

In the periglandular stroma, isolated lymphocytes are observed, separated by clear intervals. Their number per field of view ranges from 9 to 14, with a mean of 12.5 ± 0.3. The stroma is thin, and the thickness of the stromal septa between the acini varies from 42.0 to 71.4 μm, averaging 53.3 ± 1.7 μm. The number of stromal vessels per field of view ranges from 7 to 10, with a mean of 9.0 ± 0.2. The walls of the venules consist of a single layer of spindle-shaped endothelial cells oriented longitudinally. The internal diameter of the venules ranges from 21.0 to 33.6 μm,

with a mean of 29.8 ± 0.67 μm.The thickness of their walls varies from 4.2 to 8.4 μm, averaging 7.5±0.21 μm. The wall of the capillaries is represented by one layer of elongated endothelial cells directed perpendicular to the lumen of the vessel. The diameter of the capillaries ranges from 12.6 to 16.8 μm, with a mean of 15.2 ± 0.21 μm. Their wall thickness varies between 4.2 and 8.4 μm, averaging 5.0 ± 0.21 μm. Arterioles have an internal - endothelial, middle - muscular and external membranes. Endothelial cells have a spindle-shaped form. The middle membrane is represented by smooth myocytes lying circularly in one layer. The outer adventitia is formed by bundles of loose fibrous connective tissue. The internal diameter of the arterioles ranges from 12.6 to 16.8 μm, with a mean of 15.1 ± 0.21 μm. Their wall thickness varies from 4.2 to 8.4 μm, averaging 8.0 ± 0.21 μm.

The volumetric fraction of glandular tissue ranges from 85 to 91%, with a mean of 88.2 ± 0.3%, while the proportion of stromal tissue varies between 9 and 15%, averaging 11.8 ± 0.3%.

Collagen fibers surround the terminal sections of the glands, with most fibers located beneath the epithelium, forming a fine-mesh network within the stroma. The thickness of the collagen fiber bundles ranges from 8.4 to 12.6 μm, with a mean of 11.6 ± 0.21 μm.

The study demonstrated that in one-year-old rats, the prostate comprises individual alveolar-tubular glands and a fibromuscular stroma.

In all cases (100%), light microscopy reveals that the acinar lining exhibits a scalloped or finely villous configuration. The acini are lined by highly prismatic, and occasionally cubic, epithelium. The height of the epithelial layer ranges from 4.2 to 12.6 μm, with a mean of 9.37 ± 0.38 μm. The acini are oval to round in shape (Fig. 3.4.6). The luminal diameter of the glands varies from 147.0 to 252.0 μm, averaging 191.9 ± 4.2 μm. The number of acini per field of view ranges from 16 to 26, with a mean of 20.1 ± 0.5. All acini (100%) contain homogeneous or finely granular secretion (Fig. 3.4.6). The number of acini with desquamated epithelial cells ranges from 3 to 6 per field of view, with a mean of 4.4 ± 0.2.

In the periglandular stroma, isolated lymphocytes are observed, separated by clear layers. In some areas, they are located around blood vessels and within the fibromuscular stroma. Their number per field of view ranges from 16 to 25, with a mean of 18.5 ± 0.5. The thickness of the stromal septa between the acini varies from 37.8 to 84.0 μm, averaging 64.7 ± 2.5 μm.

The number of stromal vessels per field of view ranges from 8 to 12, with a mean of 10.2 ± 0.2. The walls of the venules consist of a single layer of spindle-shaped endothelial cells or[5]ed longitudinally. The int[7]l diameter of the venules varies from 21.0 to 33.6 μm, averaging 29.7 ± 0.67 μm, and their wall thickness ranges from 4.2 t[2].4 μm, with a n[1]n of 7.7 ± 0.21 μm.

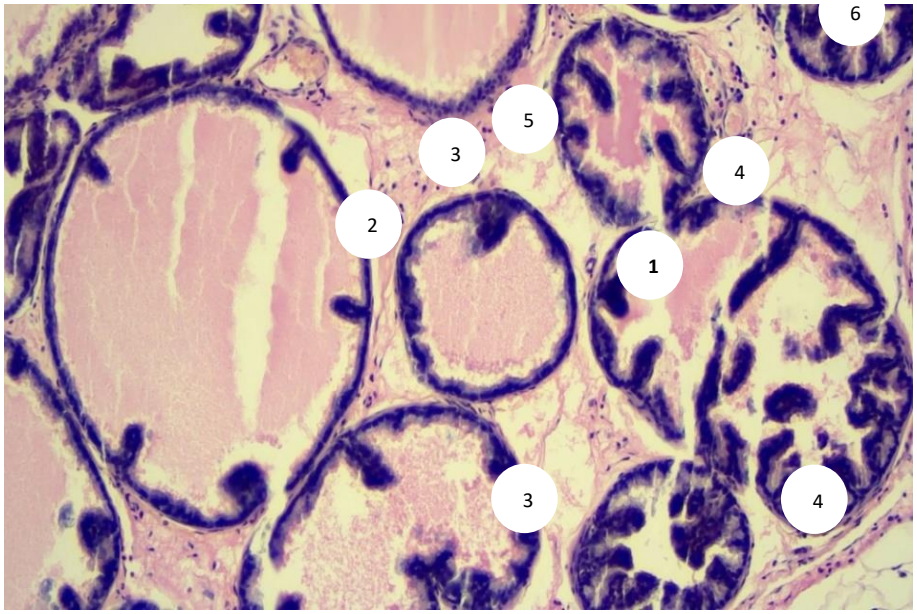

7

6

Fig.3.4.6. Prostate of a 12-month-old rat. Hematoxylin and eosin staining. 1-round acinus with intraluminal homogeneous secretion, 2-oval acinus, 3-acinus with fine-grained secretion, 4-folded structures of the terminal sections, 5-stromal vessels and single lymphocytes around them, 6-desquamated epithelial cells, 7-interglandular stroma. Approx. 10 x vol. 20.

The walls of the capillaries consist of a single layer of elongated endothelial cells oriented perpendicular to the vessel lumen. The diameter of the capillaries ranges from 12.6 to 16.8 μm, with a mean of 15.9 ± 0.21 μm, and their wall thickness varies from 4.2 to 8.4 μm, averaging 6.1 ± 0.21 μm. The walls of the arterioles are

composed of an inner endothelial layer, a middle muscular layer, and an outer connective tissue layer represented by thin bundles of connective tissue fibers. The internal diameter of the arterioles fluctuates from 12.6 to 16.8 μm, with a mean of 15.5 ± 0.21 μm, and their wall thickness ranges from 4.2 to 8.4 μm, averaging 8.2 ± 0.21 μm.

The volumetric fraction of glandular tissue ranges from 60.0 to 85.0%, with a mean of 70.3 ± 1.4%, while the pro ı ion of stromal tissue varies between 15.0 and 40.0%, averaging 29.7 ± 1.4%. Collagen fibers surround the terminal sections of the glands, with most ³ ers located beneath ⁴ epithelium. Within the stroma, they form a fine-meshed network (Fig. 3.4.7). The thickness of th. ⁵ ollagen fiber bundles ranges from 12.6 to 16.8 μm, with a mean of 13.31 ± 0.21 μm.

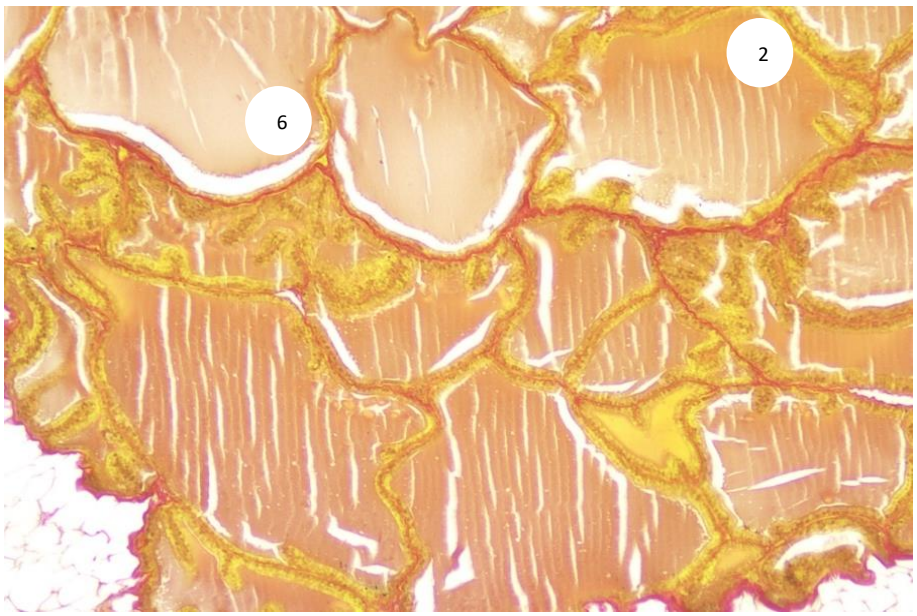

Fig. 3.4.7. Prostate of a 12-month-old rat. Van Gieson staining.

1-end secretory sections, 2-low-prismatic epithelium, 3-fibromuscular stroma, 4-collagen fiber bundles around the secretory sections, 5-stromal fine-mesh network formed by collagen fibers, 6-capsule of the gland. Approx. 10 x vol. 20.

The study found that in one-and-a-half-year-old rats, the prostate comprises terminal secretory sections and a connective tissue stroma, which includes bundles of smooth myocytes and blood vessels.

Under light microscopy, the acini display an irregular to oval shape, with epithelial-stromal outgrowths observed in 100% of cases. The epithelial lining of the terminal secretory sections consists of cuboidal, and less frequently, highly prismatic epithelium (Fig. 3.4.8). The height of the epithelial layer ranges from 4.2 to 12.6 μm, with a mean of 8.4 ± 0.42 μm. In some preparations, areas of cellular expansion are evident within the epithelium of the secretory segments, appearing dull in color due to the increased epithelial thickness; a similar pattern is noted in the epithelium of the prostatic urethra and excretory ducts. Focal cystic degeneration is observed in hyperplastic regions. (Fig. 3.4.10).

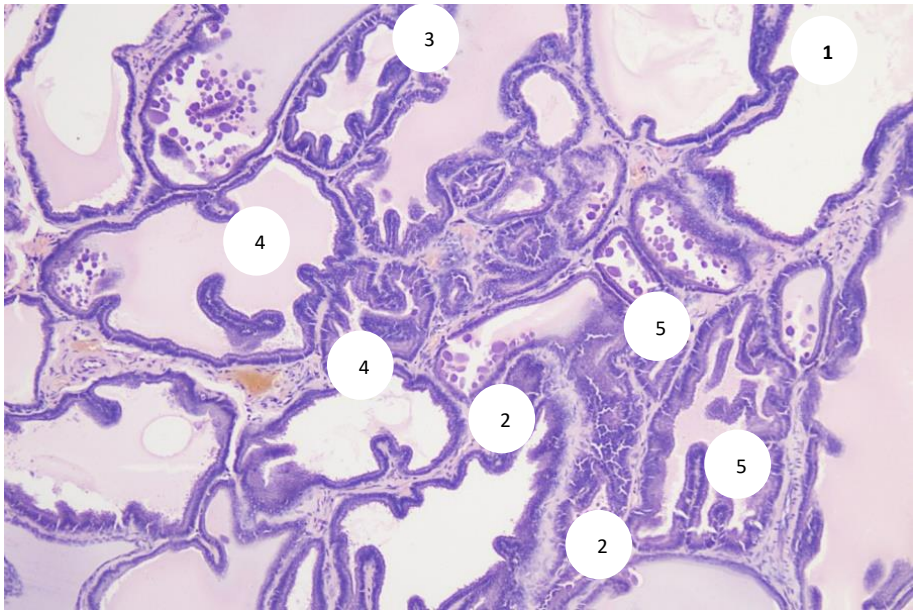

Fig.3.4.8. Prostate of an 18-month-old rat. Hematoxylin and eosin staining. 1-oval acinus with intraluminal secretion, 2-irregular acinus, 3-concretions inside the secretory sections, 4-stromal vessels with plethora, 5-diffuse lymphocyte accumulations in the stroma. Approx. 10 x vol. 20.

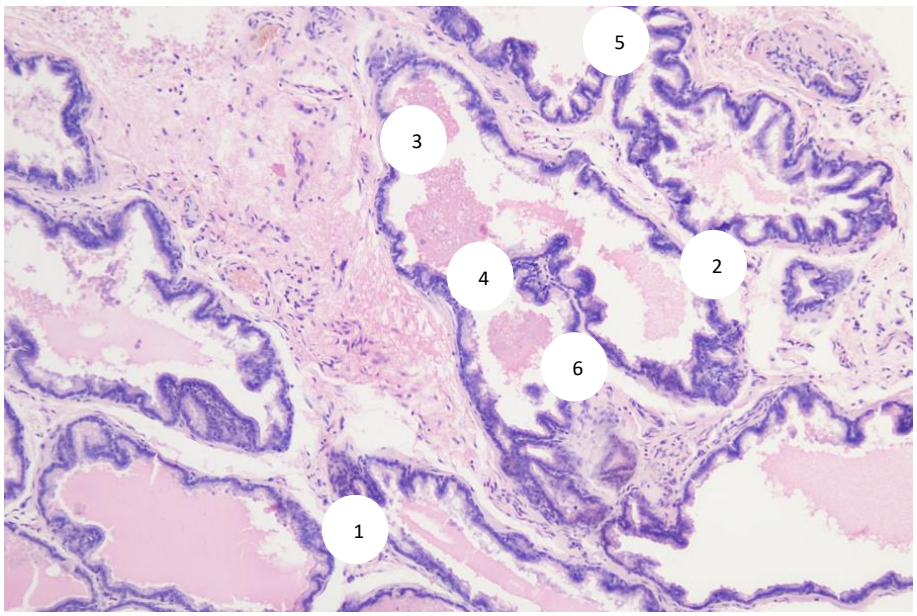

Fig.3.4.9. Prostate of an 18-month-old rat. Hematoxylin and eosin staining. 1-oval acinus with intraluminal secretion, 2-irregular acinus with unevenly filled secretion, 3-dilated stromal septa, 4-stromal vessels with congestion, 5-diffuse lymphocyte clusters in the stroma, 6-lymphocyte clusters around stromal vessels. Approx. 10 x vol. 20.

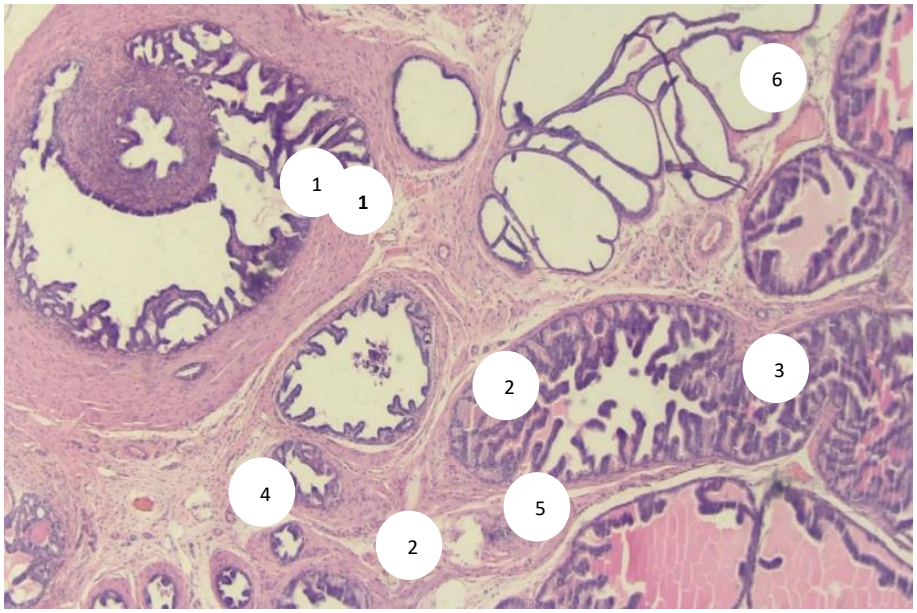

Fig.3.4.10. Prostate of 18-month-old rat of the experimental group. Hematoxylin and eosin staining. 1-prostatic urethra with proliferating epithelium, 2-glandular ducts, 3-areas of cellular proliferation in the epithelium of acini, 4-intraorgan vessels with plethora, 5-areas of connective tissue proliferation, 6-cystic atrophy in hyperplastic adenomatous nodes. Approx. 10 x 20 ob.

The luminal diameter of the glands ranges from 252.0 to 504.0 μm, with a mean of 381.8 ± 10.5 μm. The number of acini per field of view varies from 18 to 34, averaging 25.9 ± 0.9. The volumetric fraction of acini containing secretion ranges from 90 to 100%, with a mean of 95.0 ± 0.5%, whereas the proportion of acini without secretion is up to 10%, averaging 5.0 ± 0.5% (see Appendix 4). In 50% of cases, small concretions measuring 5–15 μm are observed within the acini, while in some preparations, larger concretions are detected. Focal ruptures and disruptions of the epithelial lining are noted in certain areas. (Fig. 3.4.11).

In the periglandular stroma, diffuse clusters of lymphocytes are observed, merging without evidence of tissue destruction or lymphoid nodular formation; in some areas, lymphocytes are localized around stromal vessels (Fig. 3.4.9). The number of lymphocytes per field of view ranges from 20 to 35, with a mean of 29.3 ± 0.8. In the central regions of the gland, acinar expansion brings the secretory sections into close proximity, leaving minimal stroma; consequently, the thickness of the stromal septa varies between 4 and 12 μm. In the subcapsular zone, the stroma is expanded, with the septal thickness between acini ranging from 50.4 to 168.0 μm, averaging 108.8 ± 6.3 μm.

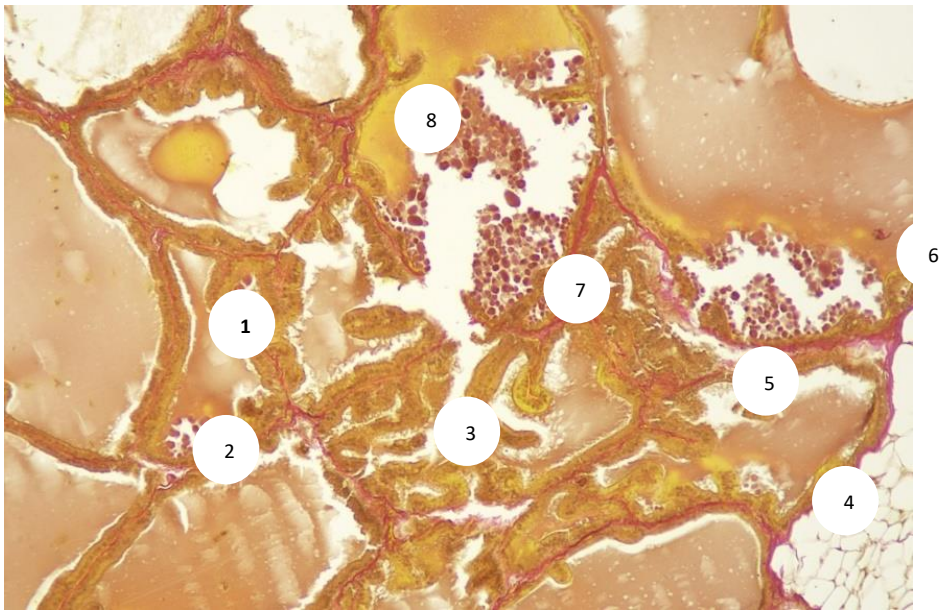

Fig.3.4.11. Prostate of an 18-month-old rat. Van Gieson staining.

1-terminal secretory sections with signs of congestion, 2-low-prismatic epithelium, 3-fibromuscular stroma, 4-collagen fiber bundles around the secretory sections, 5-stromal fine-mesh network formed by collagen fibers, 6-intraacinar concretions, 7-ruptures in the epithelial lining of the acini, 8-large concrement inside the secretory section. Approx. 10 x vol. 20.

The number of stromal vessels per field of view ranges from 11 to 15, with a mean of 13.0 ± 0.2. Most preparations show blood-filled lumens in nearly all vessels, particularly in venules. Lymphocyte clusters infiltrating the vessel walls are observed around the vessels (Fig. 3.4.9). The internal diameter of the venules varies from 25.2 to 33.6 μm, averaging 30.7 ± 0.42 μm, with wall thickness ranging from 4.2 to 8.4 μm, mean 7.9 ± 0.21 μm. The diameter of capillaries ranges from 12.6 to 16.8 μm, with a mean of 16.3 ± 0.21 μm, and wall thickness varies between 4.2 and 8.4 μm, averaging 6.5 ± 0.21 μm. The internal diameter of arterioles fluctuates from 12.6 to 16.8 μm, with a mean of 15.8 ± 0.21 μm, and their wall thickness ranges from 4.2 to 12.3 μm, averaging 8.4 ± 0.42 μm. (see Appendix 2).

The volumetric fraction of glandular tissue ranges from 45.0 to 75.0%, with a mean of 61.3 ± 1.6%, while the proportion of stromal tissue varies between 25.0 and 55.0%, averaging 38.7 ± 1.6% (see Appendix 5). Collagen fibers surround the terminal sections of the glands, with most fibers located beneath the epithelium. Within the stroma, they form a fine-meshed network, although interruptions and disruptions of the epithelial lining are observed in some areas. (Fig. 3.4.11). The thickness of collagen fiber bundles varies from 4.2 to 12.3 μm, averaging 10.5±0.42 μm.

3.3-§. Age-related immunohistochemical characteristics of the rat prostate gland

Immunohistochemical analysis using the Ki67 proliferation marker demonstrated that newborn rats exhibit pronounced proliferative activity within both the stromal layer and the parenchymal structures at birth (Fig. 3.5.1).

In 6-day-old animals, high expression of the proliferative marker is determined; the stroma and epithelial strands contain reaction products in the form of brownish precipitates (Fig. 3.5.2).

In rat pups on the 11th day of development, high reaction activity is observed in the connective tissue stroma and epithelium of the acini (Fig. 3.5.3).

In 16-day-old animals, immunohistochemical staining with antibodies to Ki67 shows pronounced expression of the marker in the epithelium of the terminal sections and stromal structures (Fig. 3.5.4).

In rat pups on the 21st day of development, high proliferative activity is determined. The reaction products in the form of brownish precipitates are present in the epithelium and singly in the stroma (Fig. 3.5.5).

In 1-month-old rats, weak activity of the reaction is observed in the glandular epithelium of the acini and structures of the stromal layer (Fig. 3.5.6). In 3-month-old rats of the control group, weak expression of the marker is observed in the glandular epithelium and structures of the stromal layer (Fig. 3.5.7).

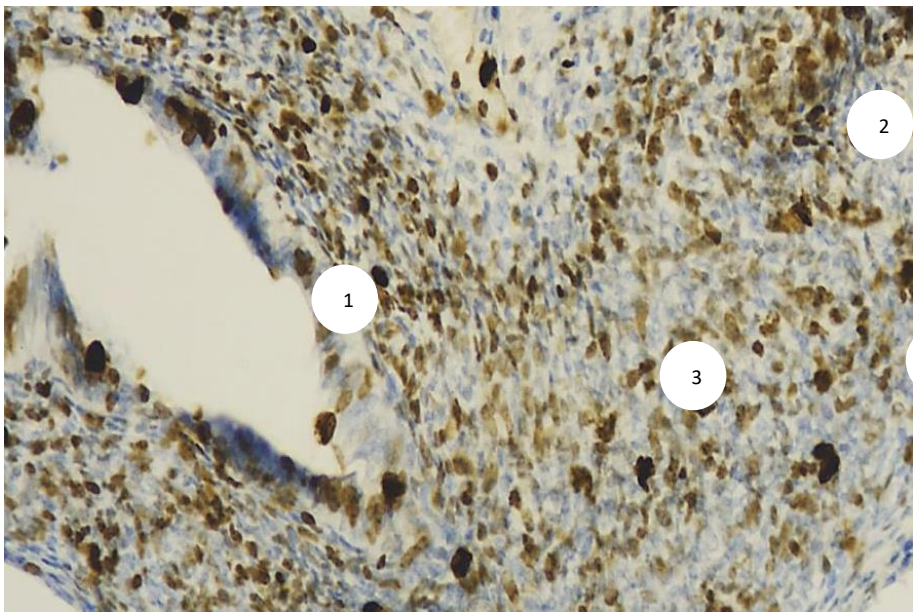

Fig.3.5.1. Prostate of a newborn rat. Immunohistochemical staining with antibodies to Ki67, chromogen diaminobenzidine, counterstaining with Mayer's hematoxylin. Increased expression of the marker in the structures of the prostate gland. 1-prostatic urethra, 2- epithelial cords, 3-connective tissue stroma. Approx. 10 x vol. 20.

In 6-month-old rats of the control group, immunohistochemical staining with antibodies to Ki67 revealed extremely weak expression of the marker in the glandular epithelium and stroma (Fig. 3.5.8).

In 9-month-old animals from the control group, weak expression of the Ki67 marker was observed in the glandular epithelium and stromal structures. (Fig. 3.5.9).

In 12-month-old rats, immunohistochemical staining with antibodies to Ki67 revealed extremely low expression of the marker in the structures of the prostate gland (Fig. 3.5.10).

In 18-month-old animals of the control group, extremely low reaction activity was determined in the epithelium and stroma (Fig. 3.5.11).

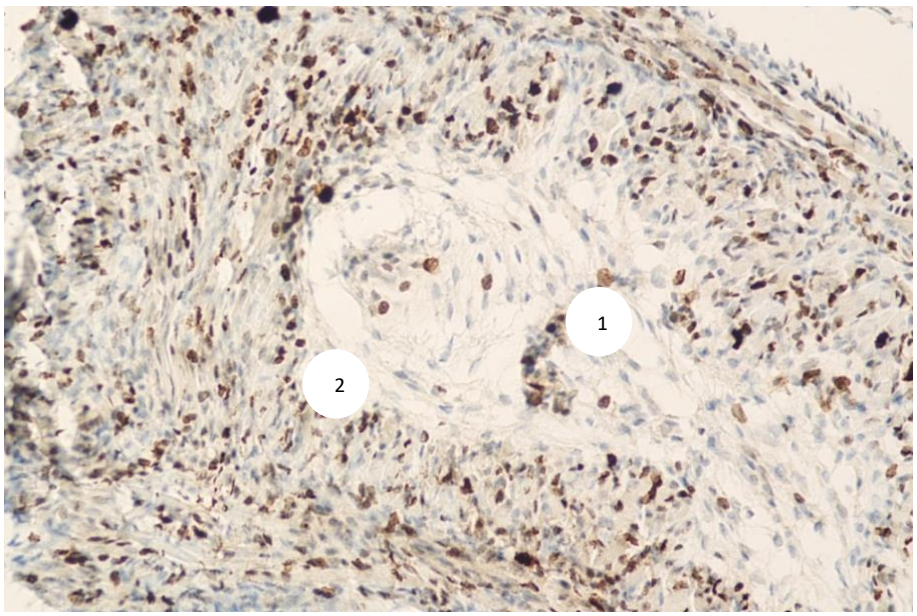

Fig.3.5.2. Prostate of a 6-day-old rat. Immunohistochemical staining with antibodies to Ki67, chromogen diaminobenzidine, counterstaining with Mayer's hematoxylin. High proliferative activity. Reaction products in the form of brown precipitates are present in the stroma and epithelial cords. 1- epithelial cords, 2- fibroelastic stroma, 3- capsule of the gland. Approx. 10 x vol. 20.

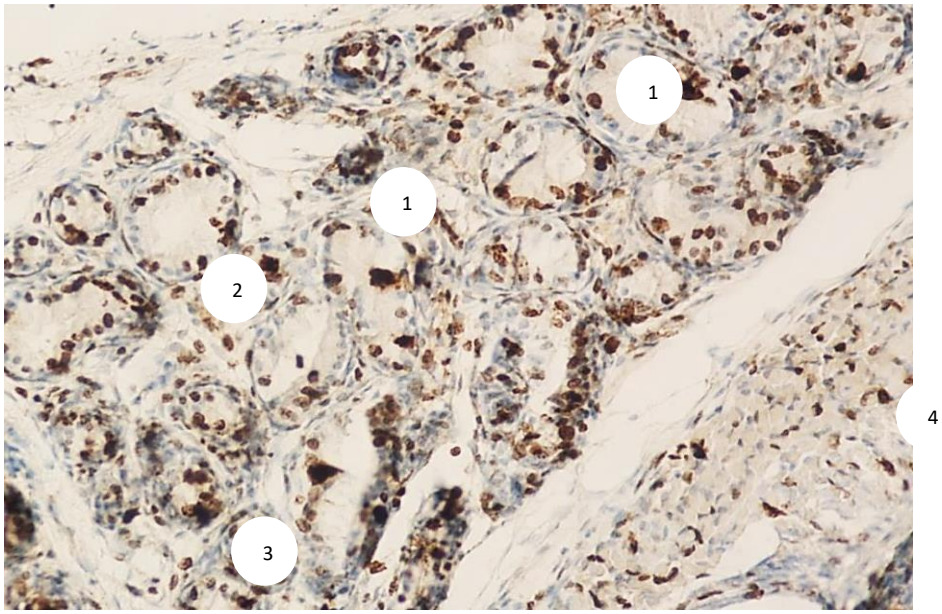

Fig.3.5.3. Prostate of an 11-day-old rat. Immunohistochemical staining with antibodies to Ki67, chromogen diaminobenzidine, counterstaining with Mayer's

hematoxylin. Strong expression of the marker in stromal structures and in the epithelium of the terminal sections. 1-acini, 2-epithelium of the terminal sections, 3-interlobar stroma, 4-bundles of myocytes. Approx. 10 x vol. 20.

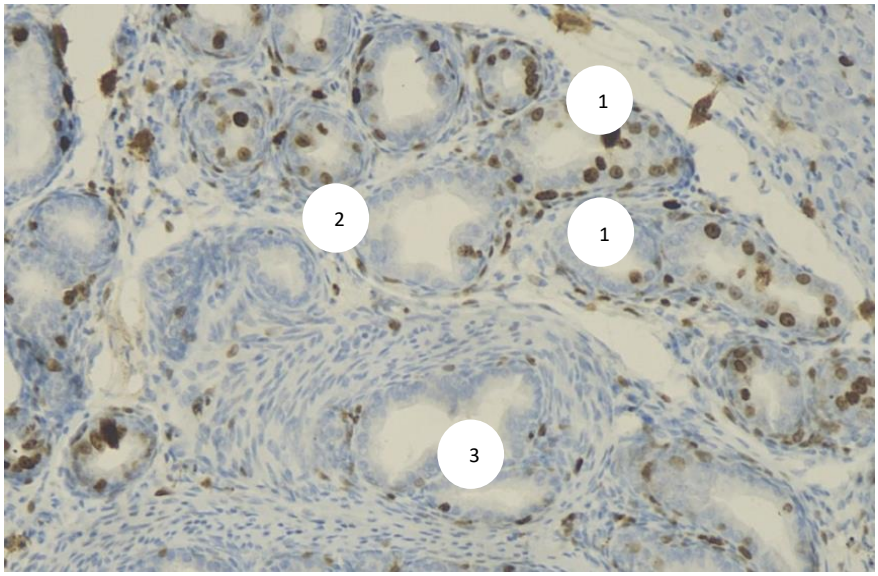

Fig.3.5.4. Prostate of a 16-day-old rat. Immunohistochemical staining with antibodies to Ki67, chromogen diaminobenzidine, counterstaining with Mayer's hematoxylin. High expression level. Epithelium and stroma contain brown reaction products.

1-secretory sections, 2-connective tissue stroma, 3-bundles of smooth myocytes. Approx. 10 x vol. 20.

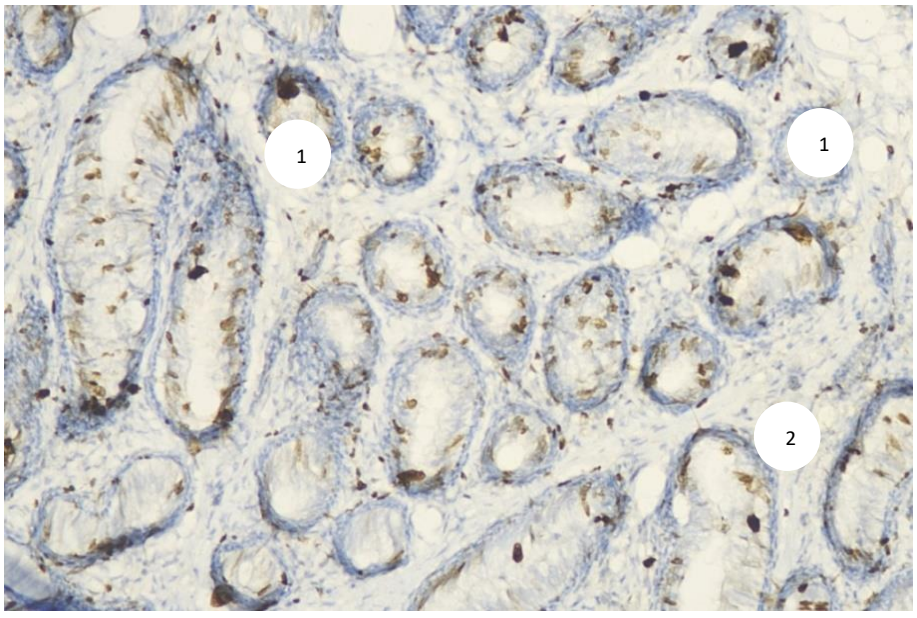

Fig.3.5.5. Prostate of a 21-day-old rat. Immunohistochemical staining with antibodies to Ki67, chromogen diaminobenzidine, counterstaining with Mayer's hematoxylin. High proliferative activity. Reaction products in the form of brown precipitates are present in the epithelium and singly in the stroma. 1-terminal secretory sections, 2-fibroelastic stroma. Approx. 10 x vol. 20.

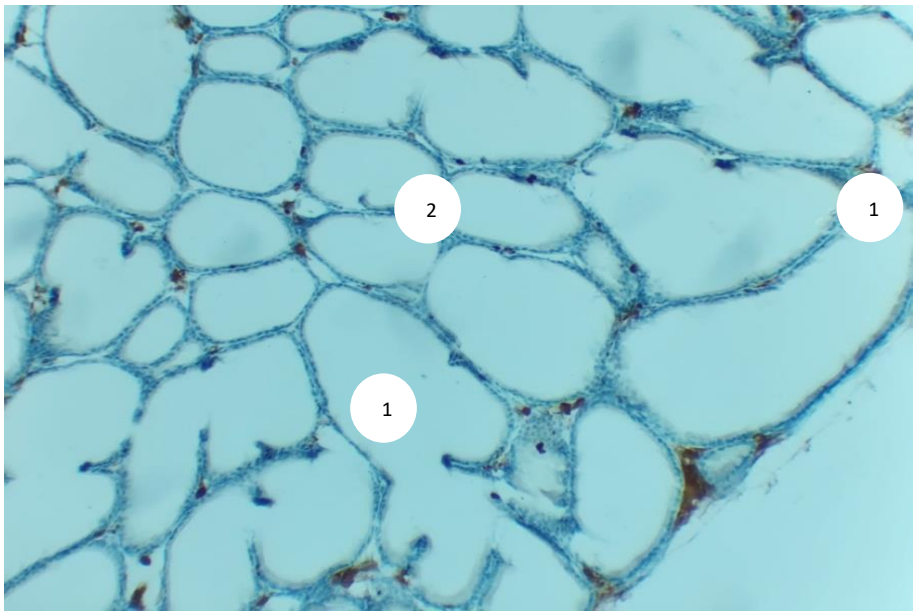

3

Fig.3.5.6. Prostate of a 1-month-old rat. Immunohistochemical staining with antibodies to Ki67, chromogen diaminobenzidine, counterstaining with Mayer's hematoxylin. Weak proliferative activity in the epithelium and structures of the stromal layer. 1-acini, 2-connective tissue stroma, 3-organ capsule. Approx. 10 x vol. 20.

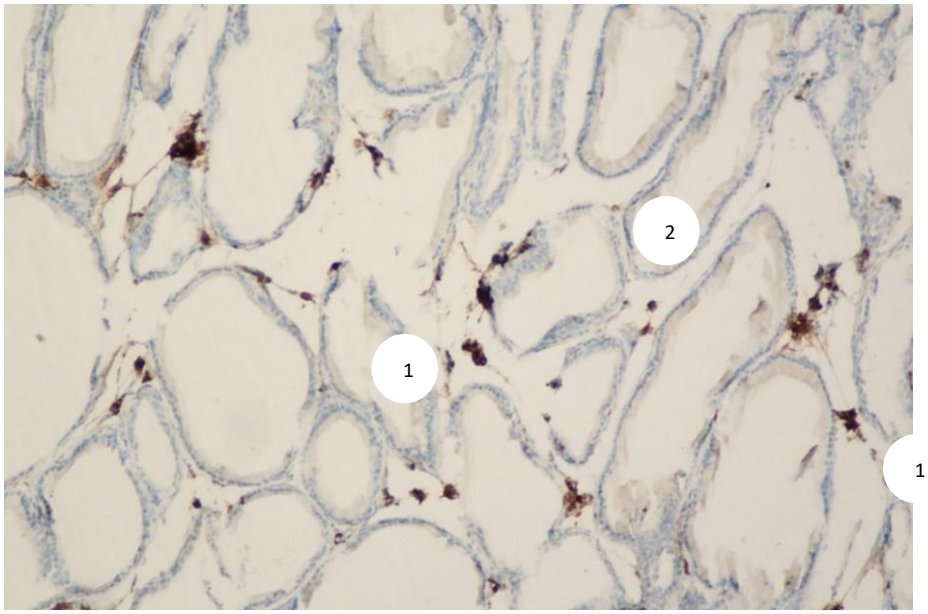

Fig.3.5.7. Prostate of a 3-month-old rat from the control group. Immunohistochemical staining with antibodies to Ki67, chromogen diaminobenzidine, counterstaining with Mayer's hematoxylin. Weak expression of the marker in the epithelium of the acini and structures of the stromal layer.

1-terminal secretory sections, 2-periglandular stroma. Approx. 10 x vol. 20.

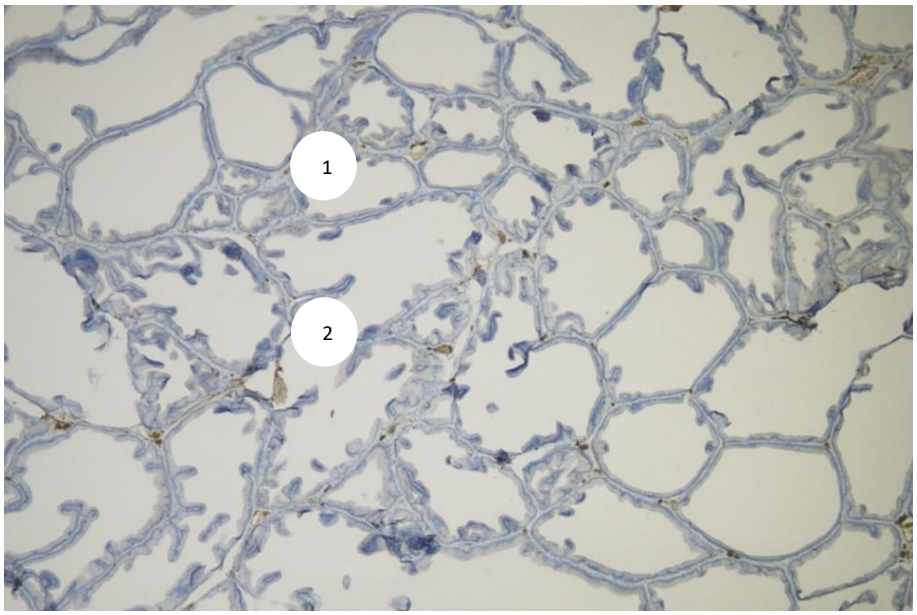

Fig.3.5.8. Prostate of a 6-month-old rat from the control group. Immunohistochemical staining with antibodies to Ki67, chromogen diaminobenzidine, counterstaining with Mayer's hematoxylin. The reaction activity

in the glandular epithelium and stroma is extremely weak. 1-terminal secretory sections, 2-folded structures of the acinus. Approx. 10 x vol. 20.

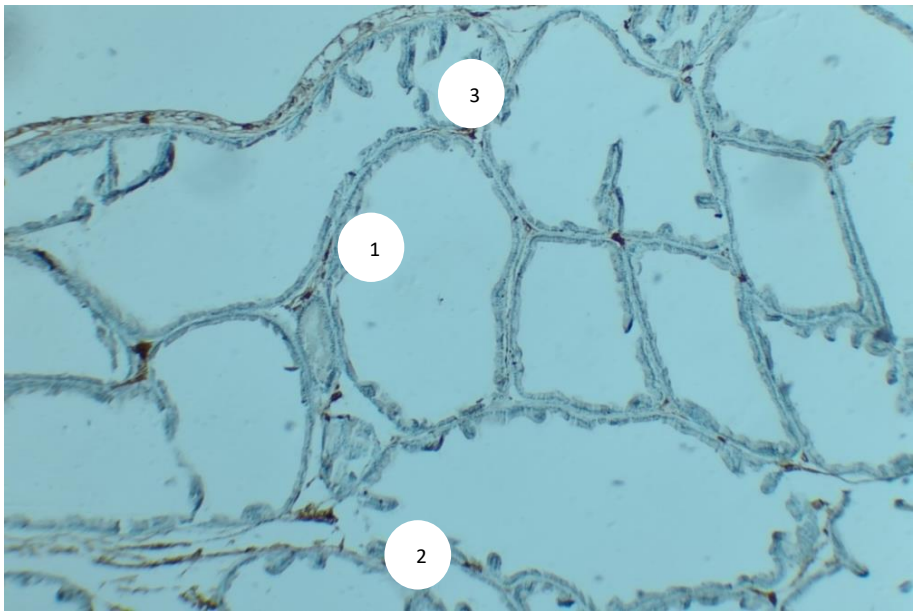

1

Fig.3.5.9. Prostate of a 9-month-old rat of the control group. Immunohistochemical staining with antibodies to Ki67, chromogen diaminobenzidine, counterstaining with Mayer's hematoxylin. Extremely low reaction activity in the epithelium and structures of the stromal layer.

1-glandular parts of the organ, 2-intralobular stroma, 3-gland capsule. Approx. 10 x vol. 20.

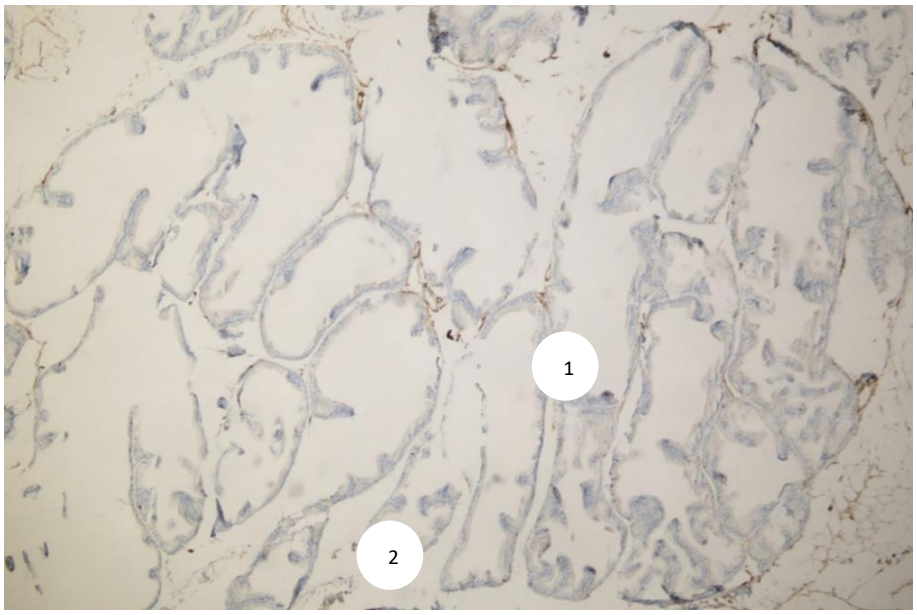

1

Fig.3.5.10. Prostate of a 12-month-old rat from the control group. Immunohistochemical staining with antibodies to Ki67, chromogen diaminobenzidine, counterstaining with Mayer's hematoxylin. Extremely low reaction activity. 1-terminal secretory sections, 2-fibromuscular stroma. Approx. 10 x vol. 20.

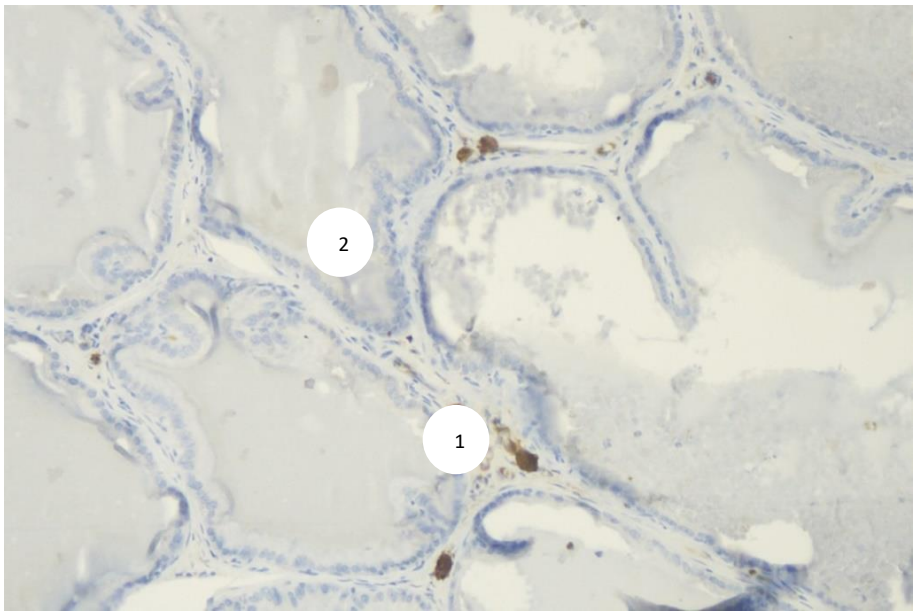

1

Fig. 3.5.11. Prostate of 18-month-old rat of the control group. Immunohistochemical staining with antibodies to Ki67, chromogen diaminobenzidine, counterstaining with Mayer's hematoxylin. The reaction activity in the glandular epithelium and stroma is extremely weak. 1-acini,

2-periglandular stroma. Approx. 10 x vol. 20.

Immunohistochemical analysis using the CD3 marker revealed weak expression of T-lymphocytes in the stromal structures and epithelial cords of newborn rats (Fig. 3.5.12).

In 6-day-old rats, weak activity of the T-lymphocyte reaction to the CD3 marker is observed in the structures of the prostate gland (Fig. 3.5.13).

In 11-day-old rats, an extremely low level of T-lymphocyte expression is observed in the structures of the stromal layer and secretory sections (Fig. 3.5.14).

In 16-day-old rats, weak activity of the T-lymphocyte reaction is determined in the structures of the prostate gland when stained with the CD3 marker (Fig. 3.5.15).

In 21-day-old rats, a moo level of T-lymphocyte response is watched within the epithelium of the secretory areas, while the response items within the frame of black-brown accelerates are show within the epithelium of the secretory segments (Fig. 3.5.16).

Immunohistochemical study of 1-month-old rats with the CD3 marker revealed weak expression of T-lymphocytes in the structures of the prostate gland (Fig. 3.5.17).

In 3-month-old rats of the control group, immunohistochemical staining with the CD3 marker reveals a low level of marker expression in the stroma and epithelium of the secretory sections (Fig. 3.5.18).

In 6-month-old rats of the control group, weak activity of the T-lymphocyte reaction is observed in the tissue stromal structures (Fig. 3.5.19).

In 9-month-old rats of the control group, immunohistochemical staining with the CD3 marker revealed a low level of marker expression in the stroma and epithelium of the secretory sections (Fig. 3.5.20).

In 12-month-old animals from the control group, weak T-lymphocyte activity is observed within the stromal structures and the epithelium of the secretory sections.

(Fig. 3.5.21).

In 18-month-old rats of the control group, immunohistochemical staining with the CD3 marker revealed a low level of T-lymphocyte expression in tissue stromal structures (Fig. 3.5.22).

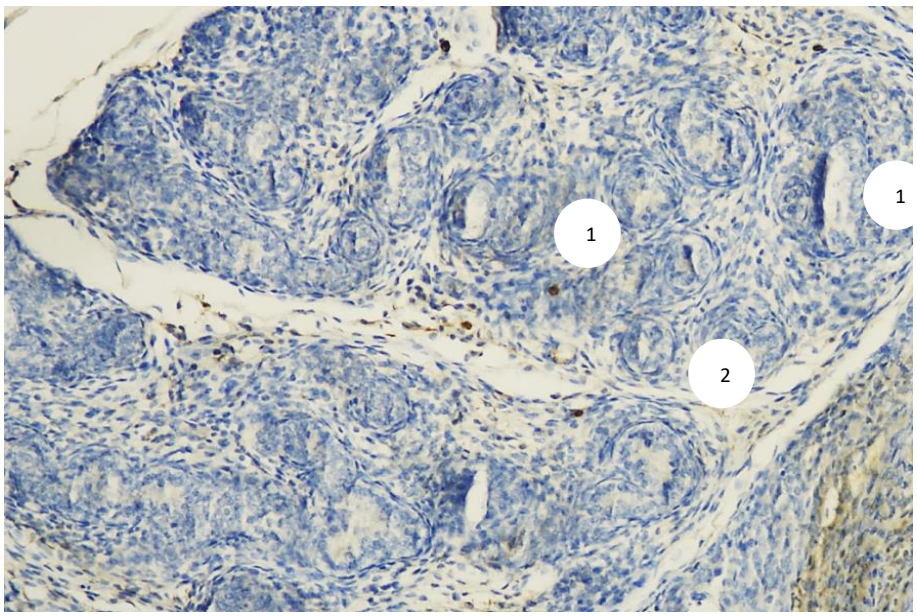

Fig.3.5.12. Prostate of a newborn rat. Immunohistochemical staining with the CD3 marker, chromogen diaminobenzidine. Low level of T-lymphocyte expression in the structures of the stromal layer and in the epithelial cords. 1-epithelial cords, 2-interlobular stroma.

Oc.10 x ob. 20.

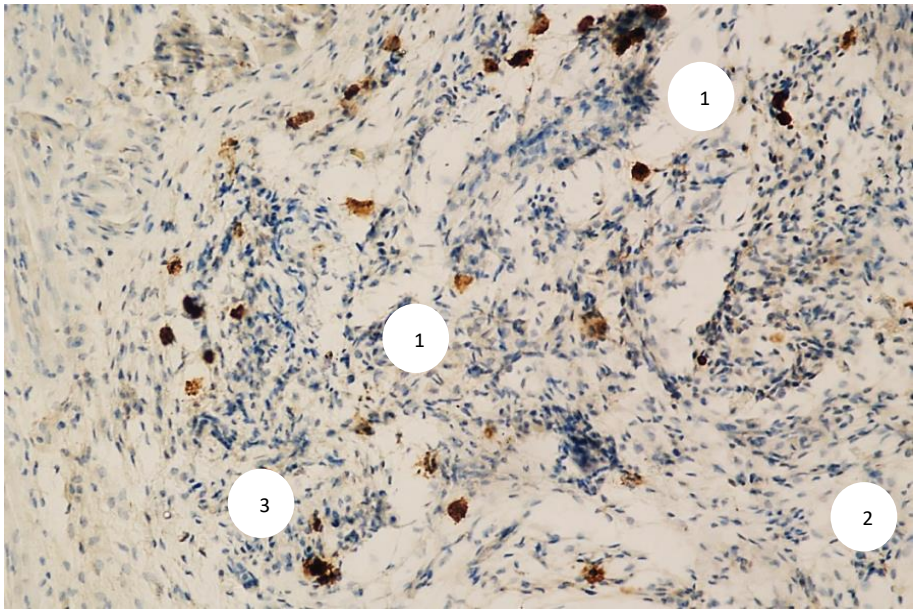

Fig. 3.5.13. Prostate of a 6-day-old rat. Immunohistochemical staining with the CD3 marker, chromogen diaminobenzidine. Low activity of T-lymphocyte reaction in the structures of the prostate gland.

1- epithelial strands, 2-connective tissue stroma, 3-bundles of smooth myocytes. Approx. 10 x vol. 20.

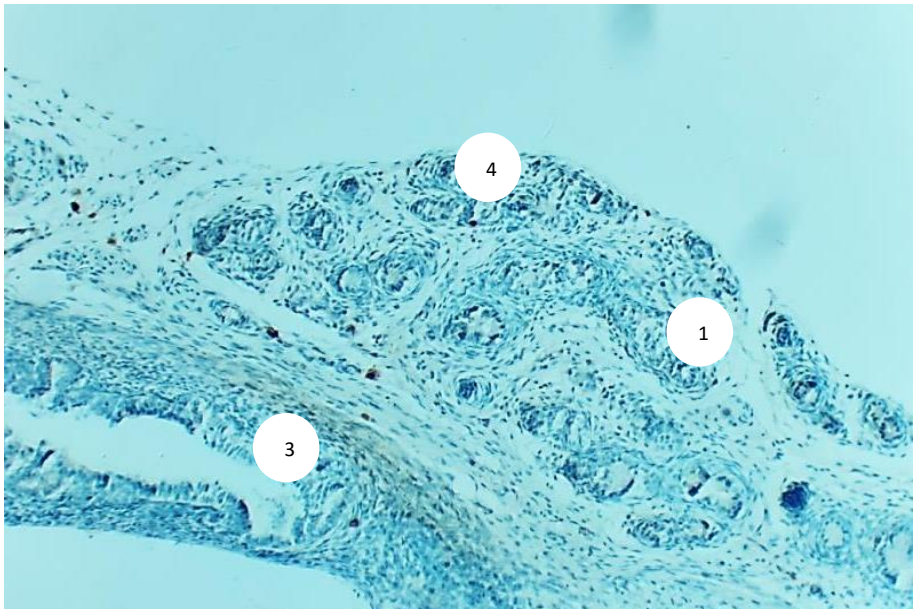

2

Fig.3.5.14. Prostate of an 11-day-old rat. Immunohistochemical staining with the CD3 marker, chromogen diaminobenzidine. Extremely low level of T-lymphocyte expression in tissue stromal structures and in the secretory sections. 1-glandular lobule, 2-interlobular stroma, 3-prostatic urethra, 4-gland capsule. Oc. 10 x ob. 10.

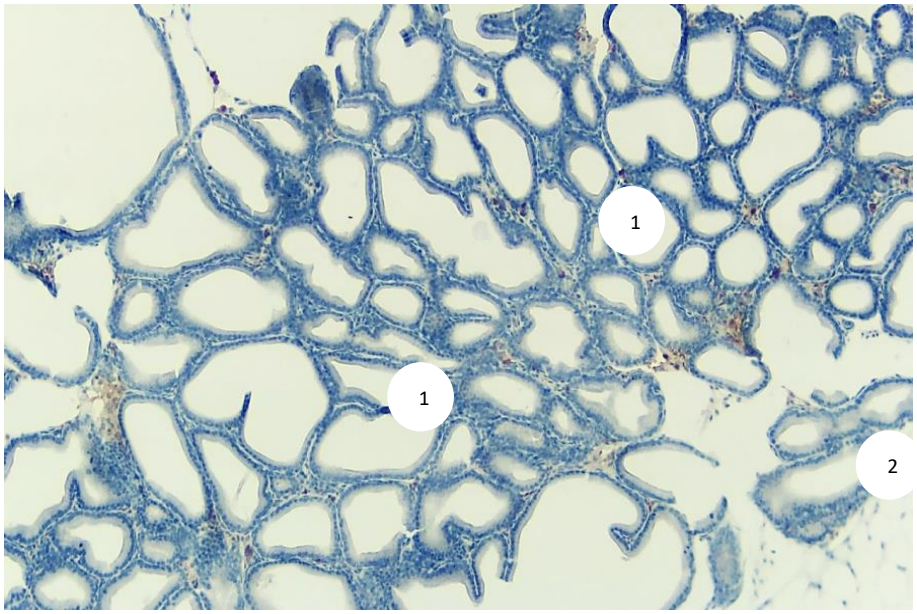

Fig. 3.5.15. Prostate of a 16-day-old rat. Immunohistochemical staining with the CD3 marker, chromogen diaminobenzidine. Weak activity of T-lymphocyte reaction in the structures of the prostate gland.

1-terminal secretory sections, 2-intralobular stroma. Approx. 10 x vol. 20.

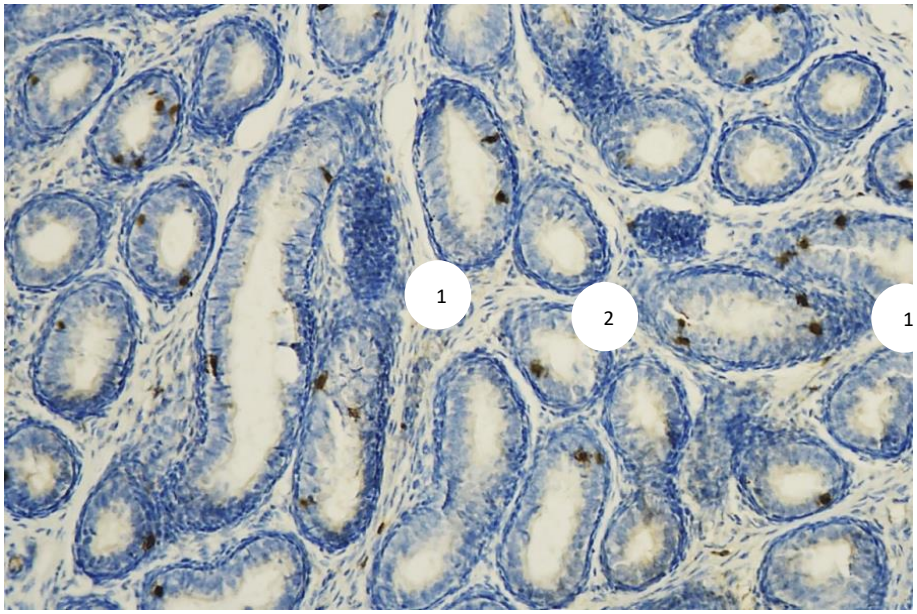

Fig. 3.5.16. Prostate of a 21-day-old rat. Immunohistochemical staining with the CD3 marker, chromogen diaminobenzidine. Weak expression of the T-

lymphocyte reaction in the epithelium of the secretory sections. 1-acini, 2-interlobular stroma. Oc. 10 x vol. 20.

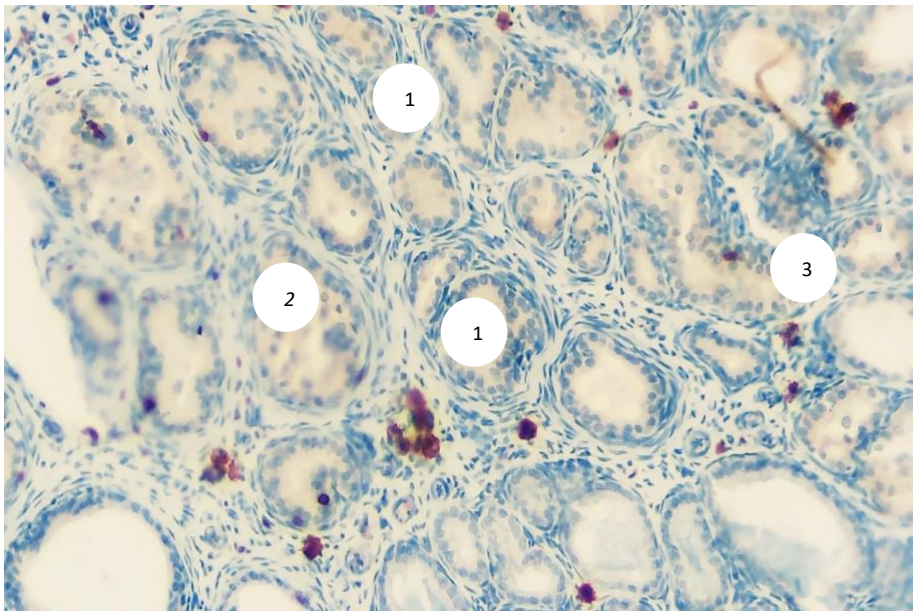

Fig. 3.5.17. Prostate of a 1-month-old rat. Immunohistochemical staining with the CD3 marker, chromogen diaminobenzidine. Weak activity of T-lymphocyte reaction in the structures of the prostate gland. 1-terminal secretory sections, 2-interglandular stroma, 3-bundles of smooth myocytes. Approx. 10 x vol. 20.

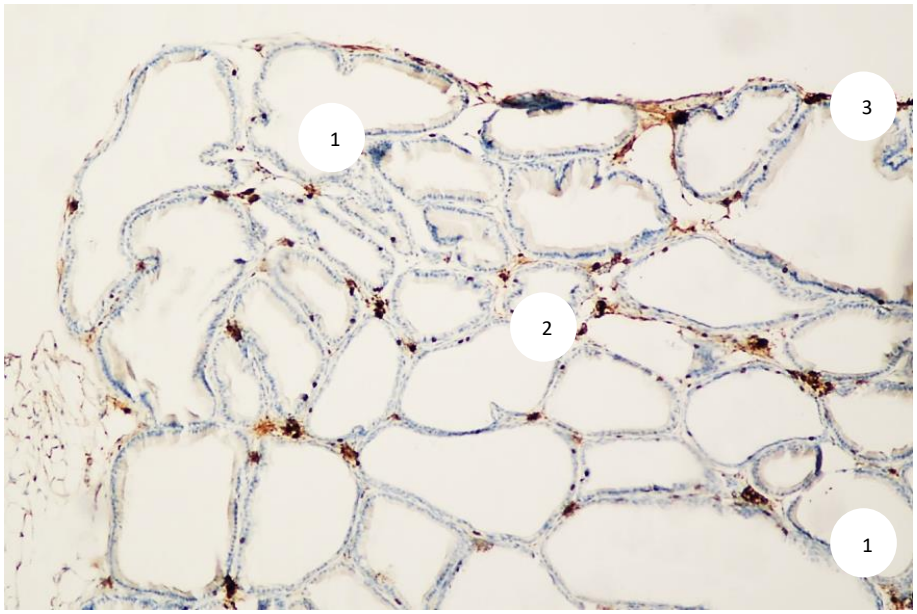

Fig.3.5.18. Prostate of a 3-month-old rat of the control group. Immunohistochemical staining with the CD3 marker, chromogen diaminobenzidine. Low level of marker expression in the stroma and epithelium of the secretory sections. 1-acini, 2-intralobular stroma, 3-capsule of the gland. Oc.10 x ob. 20.

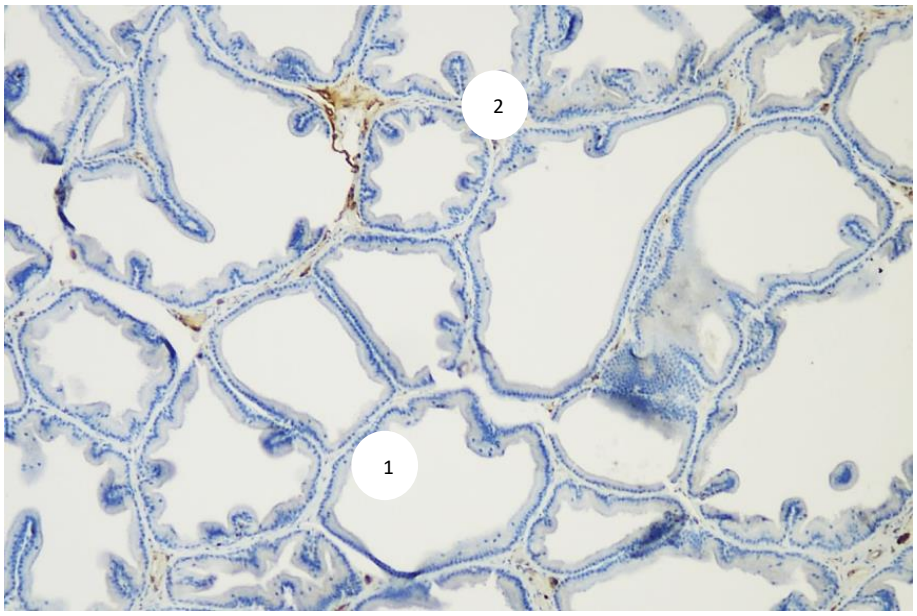

1

Fig.3.5.19. Prostate of a 6-month-old rat from the control group. Immunohistochemical staining with the CD3 marker, chromogen diaminobenzidine. Weak activity of T-lymphocyte reaction in tissue stromal structures. 1-terminal secretory sections, 2-interglandular stroma. Approx. 10 x vol. 20.

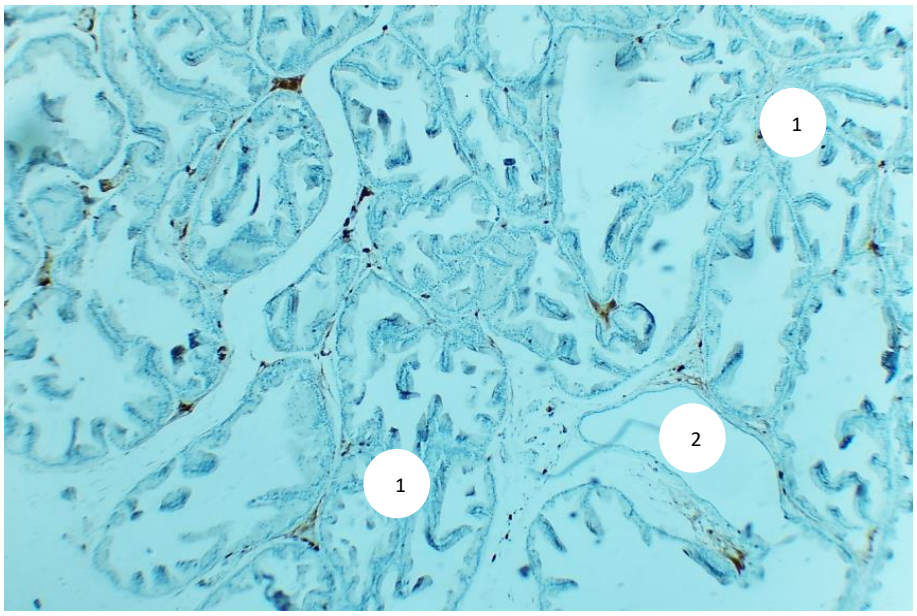

Fig.3.5.20. Prostate of a 9-month-old rat from the control group. Immunohistochemical staining with the CD3 marker, chromogen diaminobenzidine. Low level of marker expression in the stroma and epithelium of the secretory sections. 1-acini, 2-intralobular stroma. Oc.10 x vol.20.

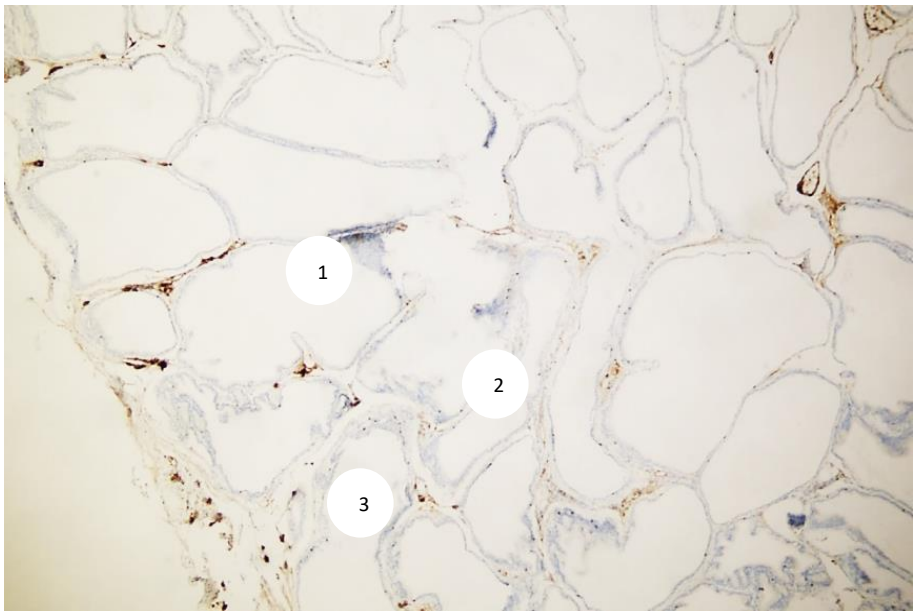

1

Fig.3.5.21. Prostate of a 12-month-old rat from the control group. Immunohistochemical staining with the CD3 marker, chromogen diaminobenzidine. Weak activity of T-lymphocyte reaction in the structures of the stromal layer and epithelium of the secretory sections. 1-terminal secretory sections, 2-interglandular stroma, 3-glandular capsule. Approx. 10 x vol. 20.

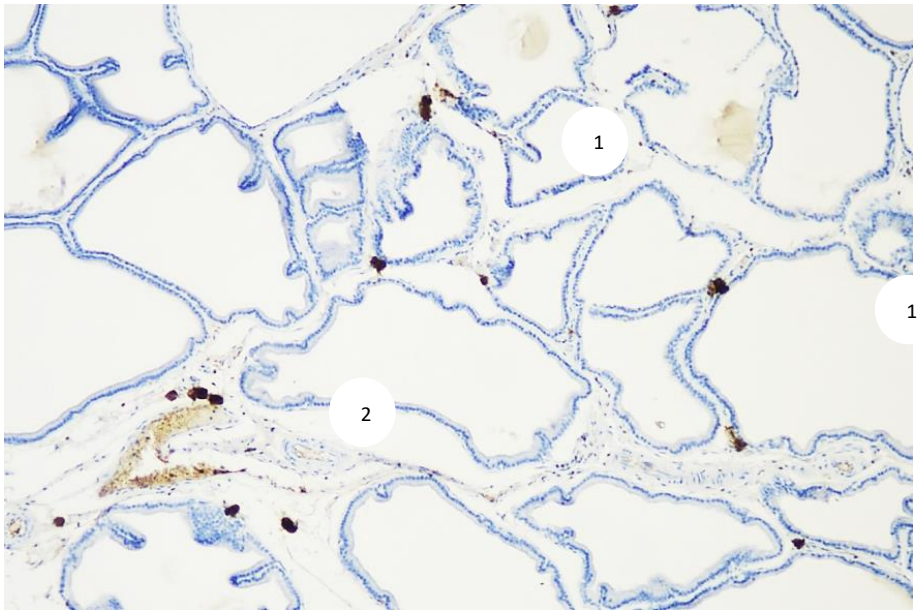

Fig.3.5.22. Prostate of 18-month-old rat of the control group. Immunohistochemical staining with CD3 marker, chromogen diaminobenzidine. Weak level of T-lymphocyte expression in tissue stromal structures. 1-acini, 2-periglandular stroma.

Oc.10 x vol.20.

CHAPTER IV. MORPHOLOGICAL STRUCTURE OF THE PROSTATE GLAND IN RATS OF THE EXPERIMENTAL GROUP

4.1-§. Microscopic structure of the prostate gland in rats suffering from chronic alcoholism

In 3-month-old rats of the experimental group, 50% of acini exhibit a folded morphology and are lined predominantly by a single-layer low-prismatic epithelium, with regions of highly prismatic epithelium also observed. The epithelial height ranges from 4.2 to 16.8 μm, averaging 9.1 ± 0.6 μm. Foci of epithelial stratification, indicative of prostatic intraepithelial neoplasia (PIN), are present in some areas. These regions display disrupted epithelial layering, cellular polymorphism, and nuclei with prominent, often multiple nucleoli (Fig. 4.2.1). The acini are polygonal in shape (Fig. 4.2.2). The luminal diameter of the glands ranges from 25.2 to 126.0 μm, with a mean of 75.2 ± 0.4 μm. The number of acini per field of view varies from 54 to 96, averaging 74.2 ± 2.3. Here's a polished, scientifically precise paraphrase of your text:

The acinar lumens are partially filled with homogeneous secretion. The volumetric fraction of acini containing secretion ranges from 15 to 46%, with a mean of 29.2 ± 1.7%, whereas acini without secretion constitute 54–85%, averaging 70.8 ± 1.7%. Within the lumens of certain acini, numerous exfoliated epithelial cells are observed, ranging from individual cells to small cell clusters (Fig. 4.2.3). Per field of view, the number of acini containing desquamated epithelium varies from 4 to 10, with a mean of 7.5 ± 0.3.

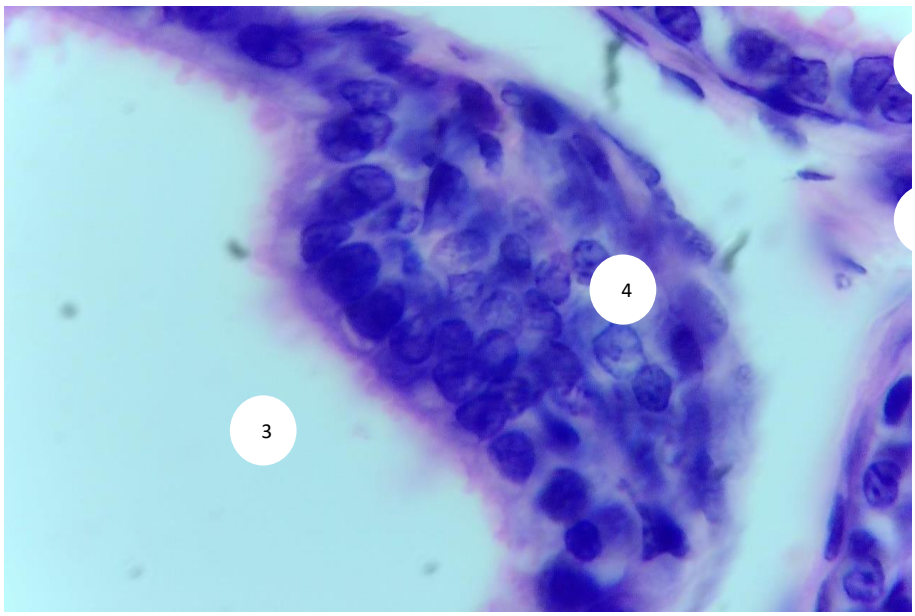

Fig.4.2.1. Prostate of a 3-month-old rat from the experimental group. Hematoxylin and eosin staining. 1-normal epithelial lining of acini, 2-interglandular stroma, 3-acinus lumen, 4-area of epithelial stratification (SES). Approx. 10 x vol. 40.

Here’s a polished, scientifically precise paraphrase of your text:

Within the interacinar stroma, isolated lymphocytes are occasionally observed. In most preparations, aggregations of lymphocytes are visualized, surrounding the terminal sections of the glands in circular or oval formations. In some areas, lymphocyte clusters are located within the acinar lumens and around vessels of the interlobular stroma, infiltrating the vessel walls. Despite these accumulations, the integrity of the epithelial lining is preserved, with no evidence of tissue destruction or formation of lymphoid nodules (Fig. 4.2.3). The number of lymphocytes per field of view ranges from 15 to 40, with an average of 26.0 ± 1.4. The thickness of the stromal septa between the glands is markedly increased in 1–2 fields of view out of 10, ranging from 21.0 to 75.6 μm, with a mean of 40.7 ± 2.94 μm.

Here’s a polished, scientifically precise paraphrase of your text:

The number of stromal vessels per field of view ranges from 6 to 12, with a mean of 9.1 ± 0.3. The walls of the venules consist of a single layer of endothelial cells oriented longitudinally relative to the vessel lumen. The internal diameter of the venules varies from 16.8 to 37.8 μm, averaging 25.2 ± 1.1 μm, while the wall thickness ranges from 2.1 to 4.2 μm, with a mean of 3.6 ± 0.13 μm. In capillaries, the endothelial cells are oriented perpendicularly to the lumen. Capillary diameters range from 8.4 to 16.8 μm, averaging 12.6 ± 0.46 μm, and their wall thickness varies between 2.1 and 4.2 μm, with a mean of 3.5 ± 0.13 μm. Arterioles have an internal, single-layer endothelial membrane of flat cells. The middle membrane is represented by one layer of circularly located smooth myocytes. The adventitia is formed by bundles of connective tissueIn many preparations, the walls of the arterioles are not clearly distinguishable. The internal diameter of the arterioles ranges from 12.6 to 21.0 μm, with a mean of 17.5 ± 0.46 μm, and their wall thickness varies from 4.2 to 8.4 μm, averaging 5.6 ± 0.21 μm.

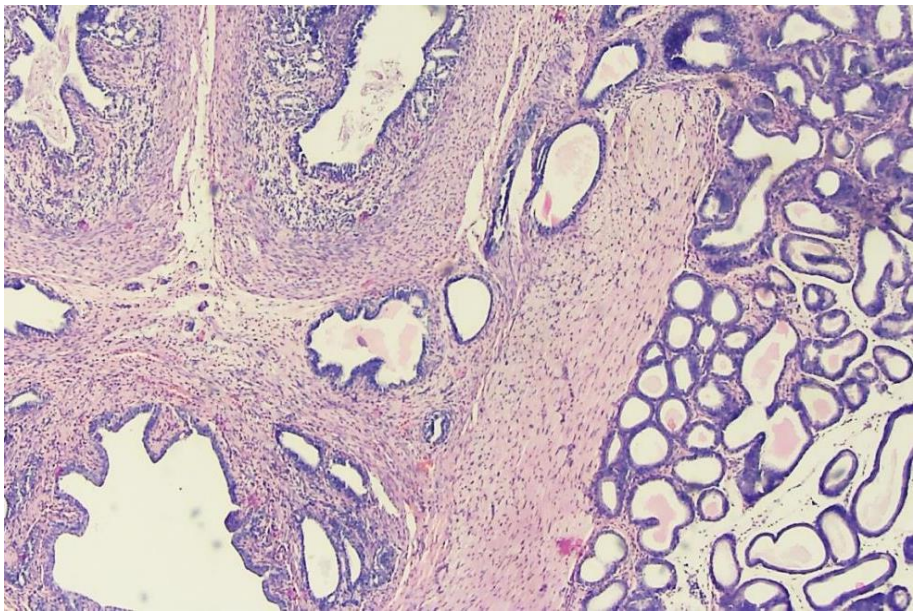

Fig.4.2.2. Prostate of a 3-month-old rat from the experimental group. Hematoxylin and eosin staining. 1-prostatic urethra, 2-ejaculatory ducts, 3-glandular ducts, 4-myocyte bundles, 5-polygonal acini, 6-interlobular stroma. Approx. 10 x ob. 10.

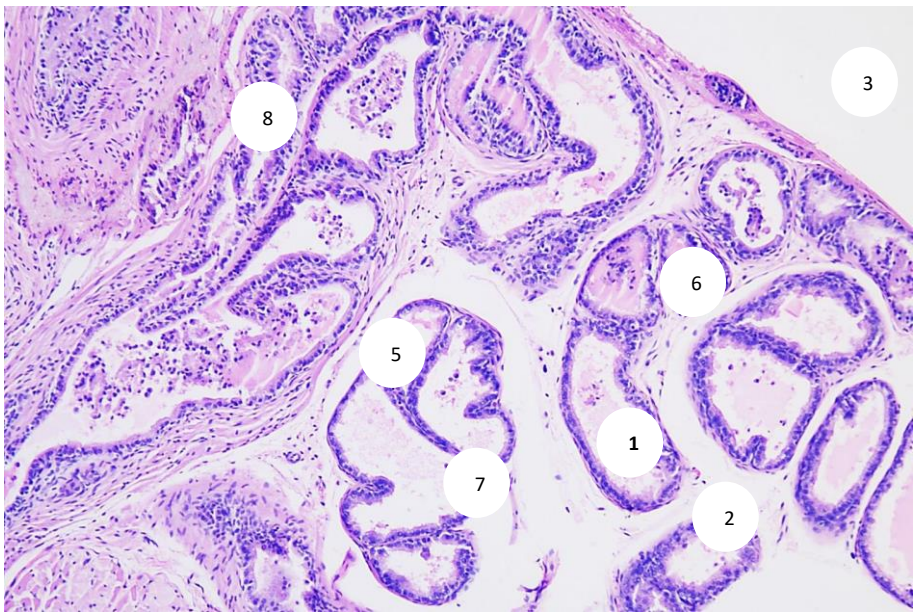

Fig.4.2.3. Prostate of a 3-month-old rat from the experimental group. Hematoxylin and eosin staining. 1-secretory terminal sections (acini), 2-expanded stromal septa, 3-glandular capsule, 4-intraluminal desquamated epithelial cells, 5-lymphocytes within the gland lumen, 6-diffuse lymphocyte clusters in the subepithelial layer of the stroma, 7-lymphocyte clusters around stromal vessels, 8-diffuse lymphocyte clusters in the interlobular stroma. Approx. 10 x 20 obv.

Morphometric analysis of the parenchyma-to-stroma ratio revealed that the relative area of parenchymal tissue ranges from 32 to 55%, with a mean of 40.6 ± 1.24%, while the proportion of stromal tissue varies from 45 to 68%, averaging 59.4 ± 1.24%. In the experimental group, numerous collagen fibers occupy all interepithelial regions of the stroma. They are observed surrounding the secretory sections and ducts of the gland, densely enveloping the smooth muscle cells of the stroma. In certain areas, a coarse network of collagen fibers is formed within the interacinar stroma. The thickness of collagen fiber bundles ranges from 4.2 to 8.4 μm, with an average of 6.13 ± 0.21 μm.

Morphometric analysis of the parenchyma-to-stroma ratio indicated that the relative area of parenchymal tissue ranges from 32 to 55%, with a mean of 40.6 ± 1.24%, while the proportion of stromal tissue varies between 45 and 68%, averaging 59.4 ±

1.24%. 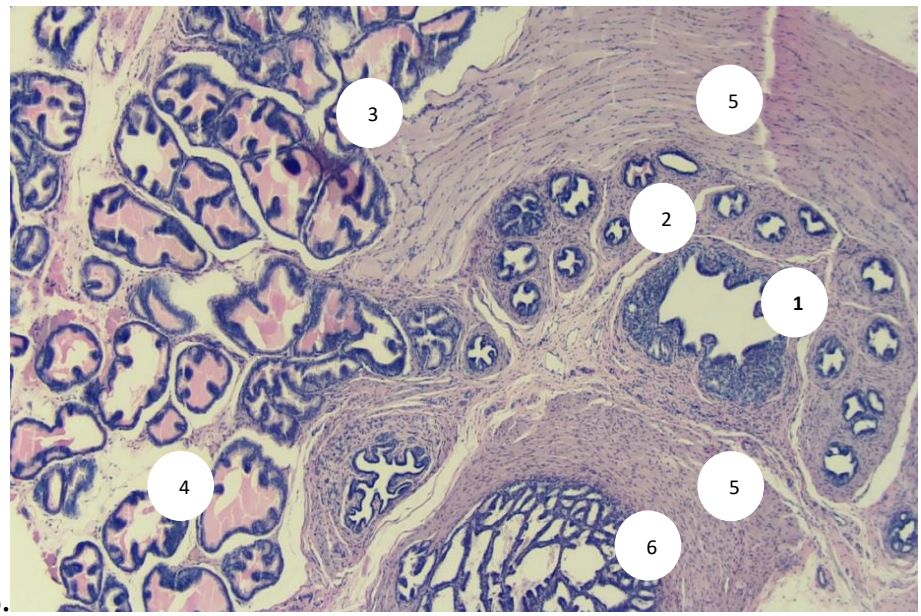

Fig.4.2.4. Prostate of a 6-month-old rat from the experimental group. Hematoxylin and eosin staining. 1-prostatic urethra, 2-glandular ducts, 3-secretory terminal sections (acini) of polygonal shape, 4-interglandular stroma, 5-areas of connective tissue proliferation, 6-areas of cellular proliferation. Approx. 10 x vol. 10.

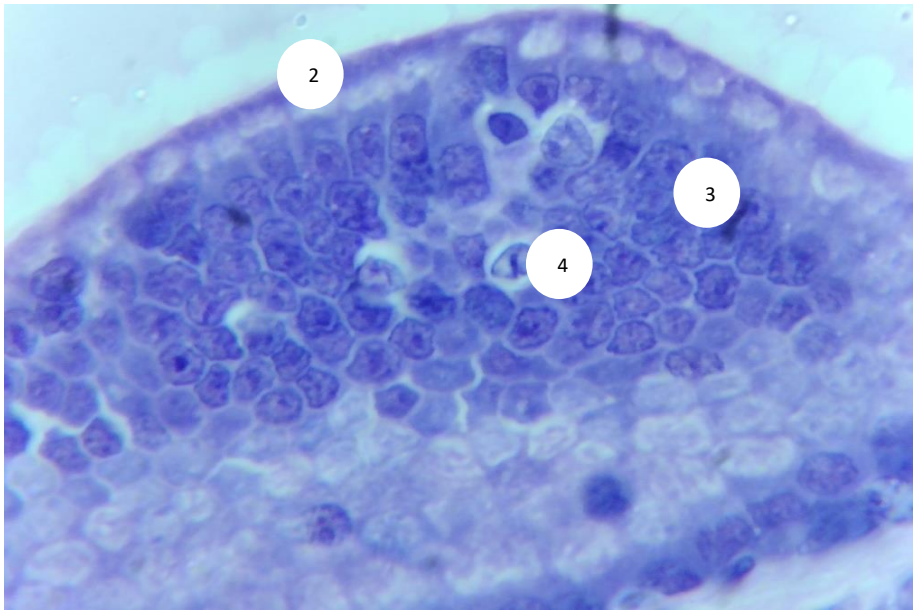

5

1

Fig.4.2.5. Prostate of a 6-month-old rat from the experimental group. Hematoxylin and eosin staining. 1-interglandular stroma, 2-acinus lumen, 3-focus of epithelial stratification (multi-row and polymorphism of cells are noted), 4-cells with large and

multiple nucleoli, 5-mitotic cells. Approx. 10 x vol. 40.

In the experimental group, numerous collagen fibers are present throughout all interepithelial regions of the stroma. They are observed surrounding the secretory sections and ducts of the gland, densely enveloping the smooth muscle cells of the stroma. In certain areas, a coarse network of collagen fibers is formed within the interacinar stroma. The thickness of collagen fiber bundles ranges from 4.2 to 8.4 μm, with a mean of 6.13 ± 0.21 μm. The study also demonstrated that in 6-month-old rats of the experimental group, 70–80% of the acini exhibit a folded morphology. (Fig. 4.2.4), The epithelium is predominantly cuboidal, with areas of highly prismatic epithelium observed in certain regions. The thickness of the epithelial lining ranges from 4.2 to 12.6 μm, averaging 9.8 ± 0.4 μm. In some preparations, regions of cellular proliferation are evident within the epithelium, characterized by a darker appearance due to the high density of epithelial cells (Fig. 4.2.4). Additionally, focal areas of epithelial stratification are observed, identified as prostatic intraepithelial neoplasia (PIN). In these regions, the normal organization of the epithelial layers is disrupted, with noticeable cellular polymorphism, enlarged and multiple nucleoli in the nuclei, and the presence of mitotic figures in certain areas.Fig. 4.2.5). The terminal sections of the glands are mostly irregular, with round and oval-shaped acini. The acinar lumens are convoluted, with diameters ranging from 105.0 to 327.6 μm, averaging 204.1 ± 9.2 μm. The number of acini per field of view ranges from 20 to 52, with an average of 35.9 ± 1.7. The lumens contain homogeneous secretion. The volume fraction of acini with secretion is 85–95%, averaging 87.8 ± 0.5%, while acini without secretion comprise 5–15%, averaging 12.2 ± 0.5%. Many fragments of exfoliated epithelial cells, sometimes forming complete cell conglomerates, partially fill the acinar lumens (Fig. 4.2.6). The number of acini containing desquamated epithelium per field of view ranges from 5 to 11, averaging 9.1 ± 0.3.

Numerous diffusely distributed lymphocytes are observed in the interacinar stroma. In most preparations, lymphocyte aggregates are seen encircling the terminal glandular areas in the form of follicle-like formations. Epithelial-stromal outgrowths are completely infiltrated by lymphocytes. Additionally, central lymphocyte clusters are present within the lumens of some acini, and individual lymphocytes are detected around intralobular stromal vessels, occasionally penetrating the vessel walls.

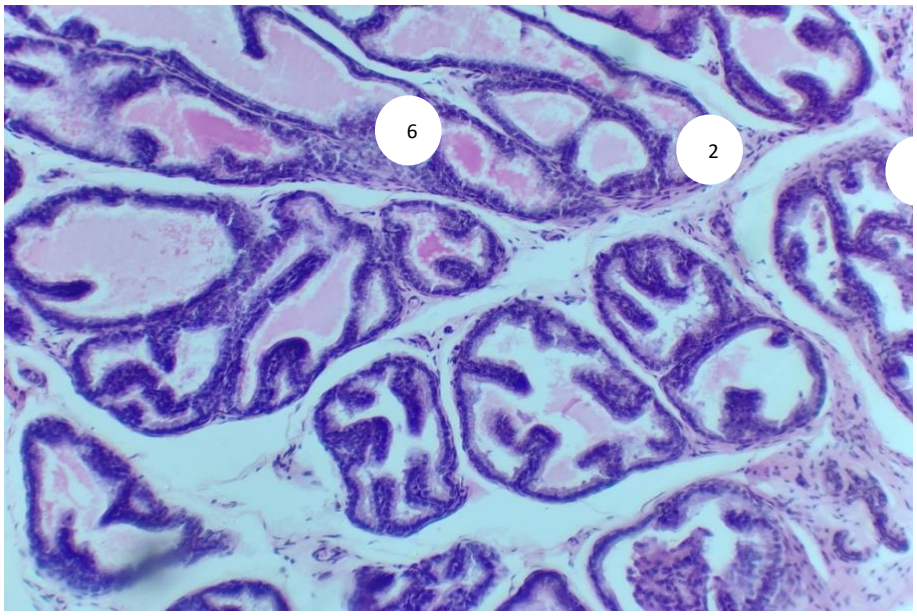

Fig.4.2.6. Prostate of a 6-month-old rat from the experimental group. Hematoxylin and eosin staining. 1-secretory terminal sections, 2-dilated stromal septa, 3-intraluminal desquamated epithelial cells, 4-lymphoid nodule within the lumen of the glands, 5-diffuse accumulation of lymphocytes in the subepithelial layer of the stroma, 6-accumulation of lymphocytes around stromal vessels, 7-diffuse accumulations of a large number of lymphocytes in the stroma, which destroy the epithelial lining of the acinus, 8- bundles of smooth myocytes. Approx. 10 x 20 rev.

In certain areas, the epithelial lining shows disrupted integrity (Fig. 4.2.6). The number of lymphocytes in the stroma per field of view ranges from 30 to 70, with an average of 46.0 ± 2.2. The thickness of the stromal layers between the secretory sections measures 12–30 μm in the central zone of the gland, while in the subcapsular zone it is markedly increased in 1–2 out of 10 fields of view, ranging from 75.6 to 201.6 μm, with an average of 122.6 ± 6.7 μm.

A large number of venules, capillaries and arterioles are determined in the interglandular stroma (Fig. 4.2.7). The number of stromal vessels in the field of vision is within 7-12, on average 9.9 ± 0.3. The venules of the interglandular stroma are dilated, formed elements of the blood are detected in their lumen. The internal diameter of the venules is within 25.2 to 33.6 μm, on average 29.8 ± 0.42 μm. The thickness of their wall fluctuates from 4.2 to 8.4 μm, on average 4.5 ± 0.21 μm. The wall of the capillaries is represented by a single layer of endothelial cells oriented perpendicular to its lumen, they are tightly adjacent to each other. Formed elements of the blood are often found in the lumen of the capillaries. The diameter of the capillaries varies from 12.6 to 16.8 μm, on average - 15.8 ± 0.21 μm. The thickness of their walls is within 2.1-4.2 μm, on average - 3.7 ± 0.13 μm. In the arterioles, the endothelial cells are located at a close distance from each other. In the middle layer, circular smooth myocytes occupy one layer. The adventitia is formed by bundles of connective tissue fibers. The internal diameter of the arterioles fluctuates from 12.6 to 21.0 μm, on average - 17.9 ± 0.42 μm. The thickness of their walls varies from 4.2 to 8.4 μm, on average - 6.1 ± 0.21 μm.

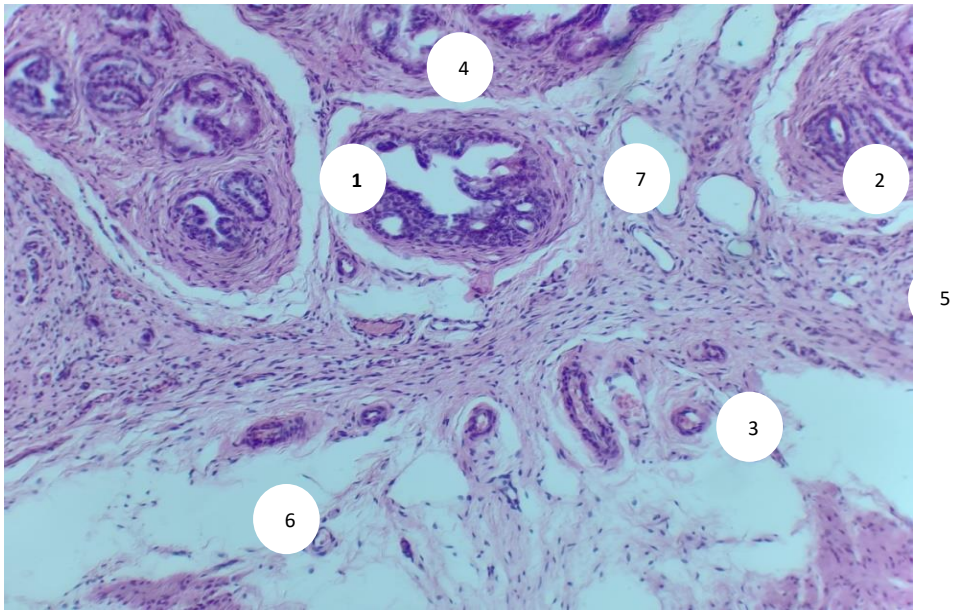

Fig.4.2.7. Prostate of 6-month-old rat of the experimental group. Hematoxylin and eosin staining. 1-glandular lobule, 2-glandular ducts, 3-vessels of the interlobular stroma, 4-interlobular septa, 5-areas of connective tissue proliferation,

6-bare area of stromal tissue, 7-areas of cellular proliferation in the epithelium of the acinus. Approx. 10 x vol. 20.

In 6-month-old rats from the experimental group, the stroma predominates over the glandular tissue. Morphometric analysis of the parenchyma-to-stroma ratio indicated that the relative ar f the parenchyma ranges from 37% 55%, with an average of 43.6 ± 0.1%, while the strc tissue proportion varies from 45% to 63%, averaging 56.4 ± 0.1%.

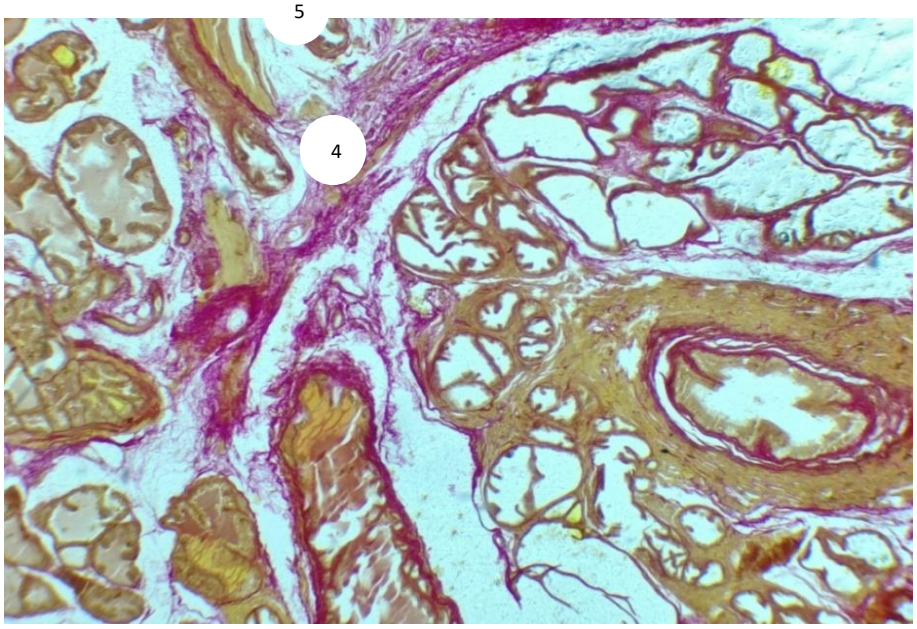

Fig. 4.2.8. Prostate of a 6-month-old rat from the experimental group. Van Gieson staining. 1-prostatic urethra, 2-excretory ducts, 3-acini, 4-fibromuscular stroma, 5-collagen fiber bundles around the secretory sections, 6-stromal coarse network formed by a large number of collagen fibers. Approx. 10 x vol. 20.

In the experiment, the number of thickened collagen fibers increased, they occupy all interepithelial areas of the stroma. They are also determined in the vicinity of the secretory sections, where they tightly cover the smooth muscle cells of the stroma. In places, a coarse network of collagen fibers is formed in the interacinar stroma (Fig. 4.2.8). The thickness of collagen fiber bundles varies from 4.2 to 8.4 μm, averaging 7.52±0.21 μm.

The study showed that in 9-month-old rats of the experimental group, acini in 50% of cases have a folded appearance, are represented mainly by flat epithelium,

in places cubic and highly prismatic epithelium are determined (Fig. 4.2.9). The height of the epithelium varies from 4.2 to 12.6 μm, on average - 7.56±0.38 μm.

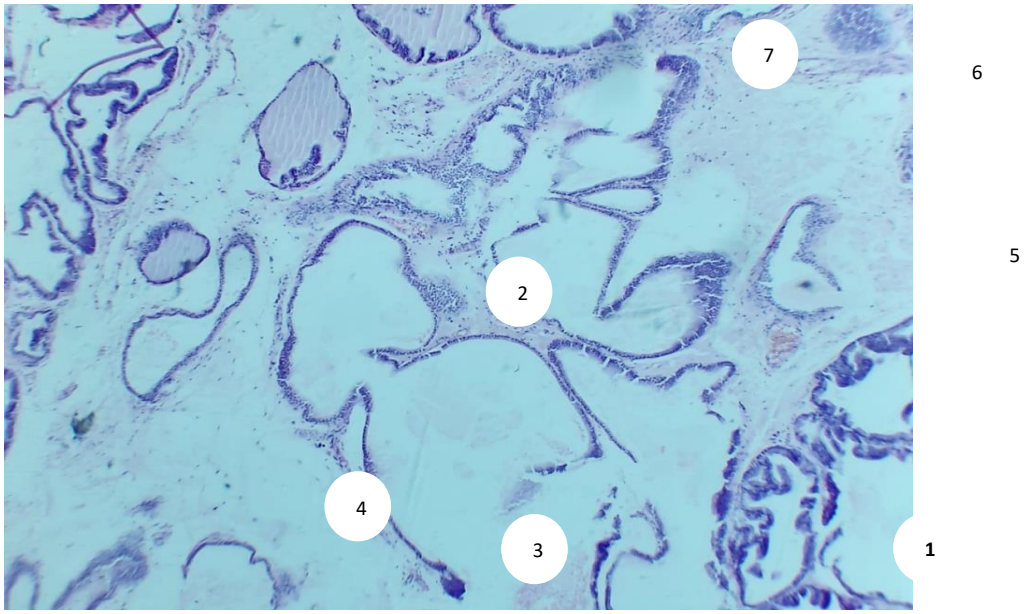

Fig.4.2.9. Prostate of a 9-month-old rat from the experimental group. Hematoxylin and eosin staining. 1-acinus with papillary structures, 2-acinus without papillary structures, 3-flat epithelium of the acinus, 4-expanded stromal septa, areas of exposure, the tissue structure of the gland disappears, 5-intraluminal desquamated epithelial cells, 6-lymphoid nodule of a rounded shape in the interglandular stroma, 7-diffuse accumulations of a large number of lymphocytes in the stroma, which destroy the epithelial lining of the acinus. Approx. 10 x vol. 20.

In some preparations, areas of cellular proliferation are observed in the epithelium, appearing darker due to the high density of epithelial cells (Fig. 4.2.10). In certain regions, foci of epithelial stratification are identified, with disruption of the normal layering, accompanied by cell polymorphism. The terminal sections of the glands are predominantly irregular in shape, with oval-shaped acini. The lumens of the acini are convoluted (Fig. 4.2.9). The diameter of the glandular lumens ranges from 231.0 to 483.0 μm, averaging 354.9 ± 10.5 μm. The number of acini in the field of vision varies from 12 to 34, with an average of 23.5 ± 1.2. The volume fraction of acini containing secretion ranges from 50% to 70%, averaging 58.8 ± 1.1%. The proportion of acini without secretion ranges from 30% to 50%, with an average of

41.2 ± 1.1%. In the lumens of individual acini, fragments of desquamated epithelial cells are observed. The number of acini containing desquamated epithelium in the field of view varies from 3 to 6, with an average of 5.1 ± 0.2. In the fibromuscular stroma, diffusely scattered clusters of lymphocytes are detected in the subepithelial layer. In some areas, there is disruption of the epithelial lining. Additionally, lymphocyte clusters are observed inside the acinar lumens and around the vessels of the intralobular stroma, where they infiltrate the vessel walls. The number of lymphocytes in the stroma is too high to be reliably counted in the field of view. In most preparations, focal accumulations of lymphocytes forming lymphoid nodules of round and oval shapes are observed in the stroma (Fig. 4.2.9, 4.2.10). The thickness of the stromal layers between the secretory sections in the central zone of the gland ranges from 40 to 80 μm. In the subcapsular zone, it is markedly increased in 7–8 fields of view out of 10, fluctuating between 252.0 and 462.0 μm, with an average of 326.3 ± 11.3 μm. In some areas, there is expansion between the acini, and the normal tissue structure of the gland is disrupted. (Fig. 4.2.9).

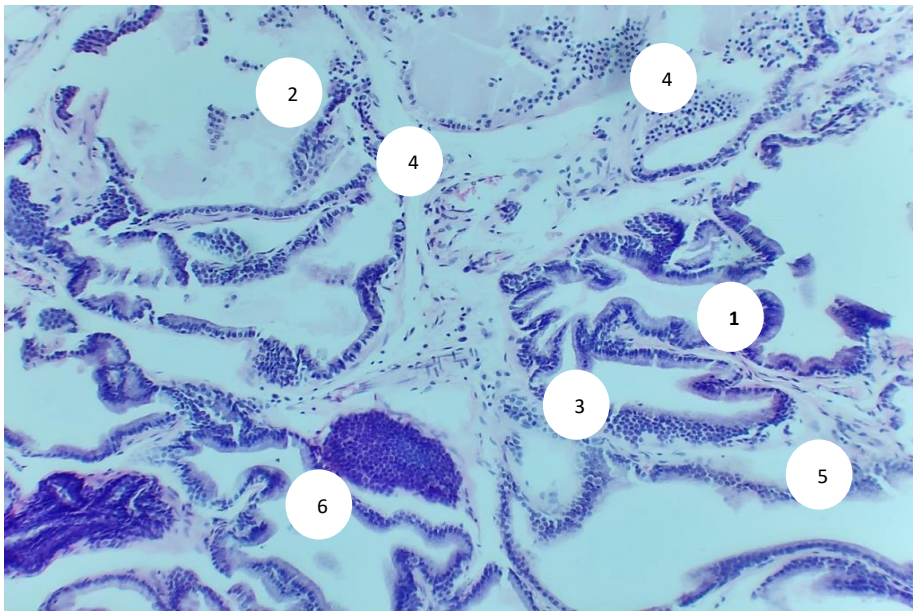

Fig.4.2.10. Prostate of a 9-month-old rat from the experimental group. Hematoxylin and eosin staining. 1-deformed, irregularly shaped acinus, 2-ruptures in the epithelial lining of the acini, 3-oval-shaped lymphoid nodule in the interglandular stroma, 4-

diffuse accumulations of lymphocytes inside the acini, 5-accumulations of lymphocytes in the subepithelial layer of the stroma, 6-areas of cellular proliferation. Approx. 10 x vol. 20.

In the interglandular stroma, a large number of venules, capillaries, and arterioles are observed. In nearly all vessels, stasis of formed blood elements occurs, accompanied by extensive areas of hemorrhage. The vessel lumens are markedly dilated, while their wall thickness is reduced (Fig. 4.2.11). The number of stromal vessels in the field of view ranges from 12 to 18, with an average of 15.4 ± 0.3. The walls of the venules consist of a single layer of endothelial cells, spaced 5–7 μm apart. The internal diameter of the venules varies from 25.2 to 37.8 μm, averaging 34.4 ± 0.67 μm, and the wall thickness ranges from 4.2 to 8.4 μm, averaging 6.3 ± 0.21 μm. Endothelial cells of the capillary walls are oriented perpendicular to the lumen. The diameter of the capillaries ranges from 12.6 to 21.0 μm, with an average of 17.6 ± 0.42 μm. The thickness of the capillary walls ranges from 2.1 to 4.2 μm, with an average of 3.7 ± 0.42 μm. Arterioles consist of an endothelial layer, a muscular layer represented by a single layer of smooth myocytes, and an adventitia formed by fibrous connective tissue. In many preparations, the arteriolar layers are not clearly distinguishable. The internal diameter of the arterioles varies from 12.6 to 21.0 μm, with an average of 17.7 ± 0.42 μm, and their wall thickness ranges from 4.2 to 8.4 μm, averaging 5.6 ± 0.21 μm.

In 9-month-old rats of the experimental group, the stroma exceeds the glandular tissue in volume. Morphometric analysis of the parenchyma-stromal ratio revealed that the relative area of the parenchyma varies from 17 to 52%, averaging 30.9 ± 1.9%, while the proportion of stromal tissue fluctuates between 60 and 83%, with an average of 69.1 ± 1.2%.

By the 9th month of the experiment, numerous strands of dense fibrous collagen fibers occupy all interglandular areas of the stroma, tightly enveloping the bundles of smooth muscle cells. In some regions of the interacinar stroma, a coarse network of collagen fibers is formed, displacing the network from the basal membrane of the

terminal sections. In certain areas, the fibers are torn and frayed. The thickness of the collagen fi[illegible]undles r[illegible]es from 4.2 to 8.4 μm, [illegible] an average of 7.35 ± 0.21 μm.

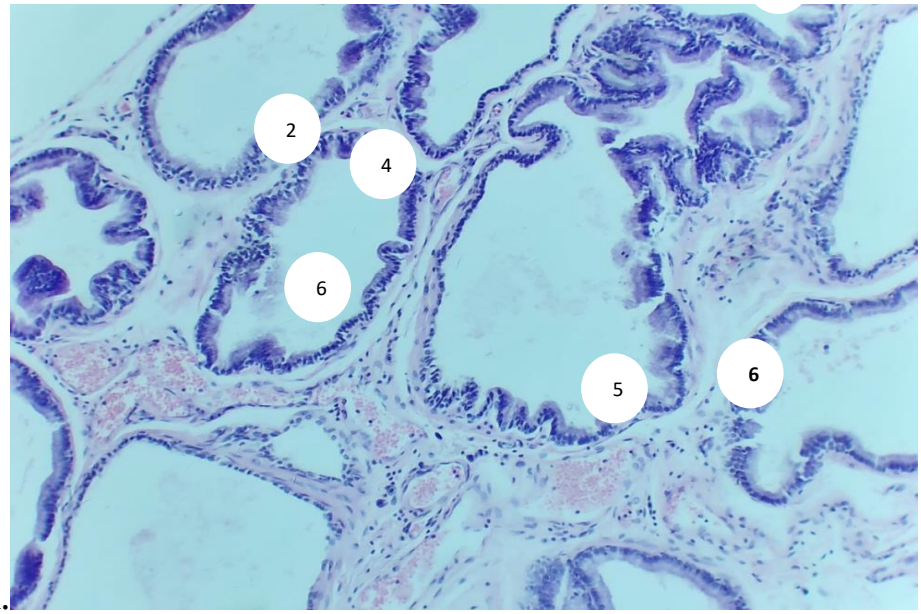

Fig.4.2.11. Prostate of a 9-month-old rat from the experimental group. Hematoxylin and eosin staining. 1-twisted, irregularly shaped acinus, 2-fibromuscular stroma, 3-acinus cavity, 4-diffuse lymphocyte clusters in the subepithelial layer of the stroma, 5-lymphocyte clusters around the stromal vessels, 6-phenomena of formed element stasis in the vessels with extensive areas of hemorrhage, 7-gland capsule. Approx. 10 x 20 ob.

The study demonstrated that in 12-month-old rats of the experimental group, the acini in 30% of cases exhibit a folded appearance. They are primarily lined by cuboidal epithelium, with areas of flattened epithelium observed in some regions. The epithelial thickness ranges from 4.2 to 8.4 μm, with an average of 7.7 ± 0.21 μm. In certain preparations, zones of cellular proliferation are detected in the epithelium, characterized by a darker color due to high epithelial cell density. Foci of epithelial stratification (FES) are also observed in some areas. The terminal sections of the glands are predominantly irregular and oval in shape, with convoluted lumens that are mostly stretched (Fig. 4.2.12).

The diameter of the glandular lumens ranges from 336.0 to 672.0 μm, with an average of 448.1 ± 13.9 μm. The number of acini in the field of view varies from 10

to 22, averaging 15.7 ± 0.6. All (100%) of the acinar lumens are filled with homogeneous or fine-grained secretion. In some acini, numerous fragments of exfoliated and desquamated epithelial cells are present, with total epithelial desquamation causing complete obstruction of the acinar lumen (Fig. 4.2.13). The number of acini with desquamated epithelium per field of view ranges from 8 to 20, averaging 13.7 ± 0.6.

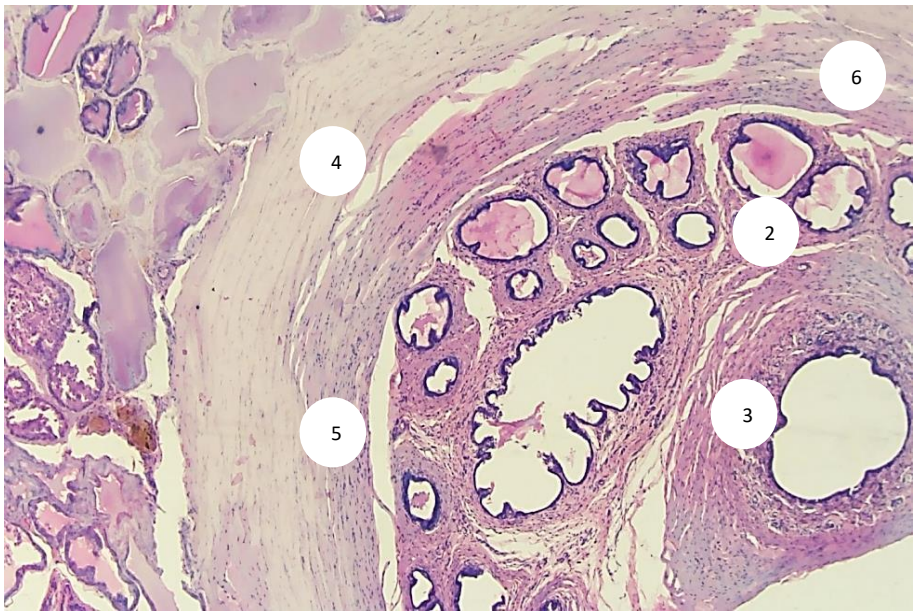

Fig.4.2.12 Prostate of a 12-month-old rat from the experimental group. Hematoxylin and eosin staining. 1-prostatic urethra, 2-glandular ducts, 3-ejaculatory ducts, 4-dilated polygonal acini filled with secretion, 5-interglandular stroma, 6-areas of connective tissue proliferation (fibrosis) with ruptures. Approx. 10 x vol. 20.

A large number of diffusely scattered lymphocytes are visualized in the interacinar stroma. In most preparations, confluent clusters of lymphocytes are observed, surrounding the terminal sections of the glands. Around the vessels of the intralobular stroma, diffuse accumulations of lymphocytes infiltrating the vessel walls are also noted. In some areas, tissue destruction of the stroma with disruption of the epithelial lining is observed (Fig. 4.2.13). The number of lymphocytes in the stroma per field of view ranges from 17 to 26, averaging 20.0 ± 0.5.

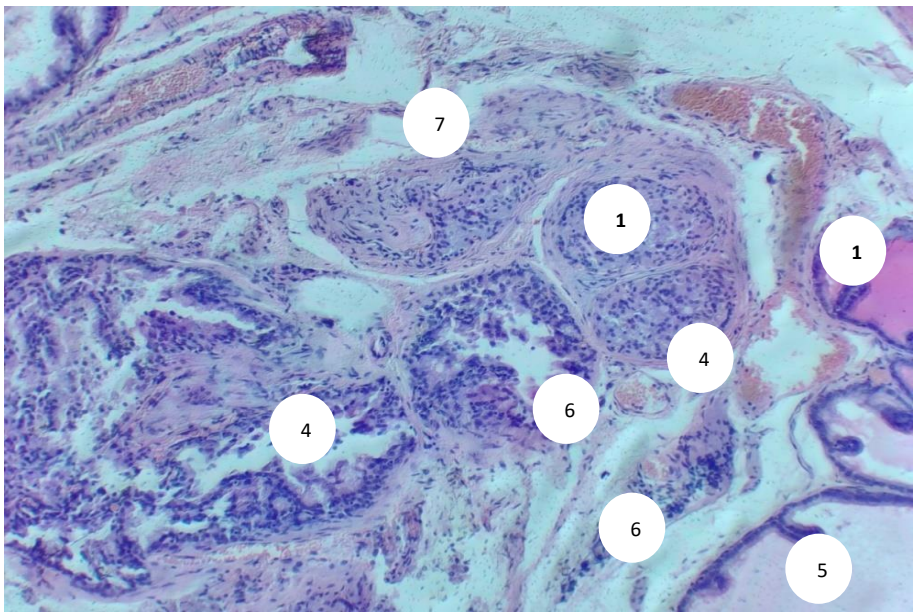

2

7

3

Fig.4.2.13. Prostate of a 12-month-old rat from the experimental group. Hematoxylin and eosin staining. 1-total desquamation of the acinar epithelium with complete obstruction of the acinar lumen, 2-expanded stromal septa with exposed areas, tissue structure of the organ is absent, 3-acinus with signs of congestion, 4-intraluminal desquamated epithelial cells with diffuse accumulations of lymphocytes, 5-diffuse accumulation of lymphocytes around the stromal vessels, 6-tissue destruction of the stroma with disruption of the integrity of the epithelium, 7-combination of stasis of formed elements in the vessels with extensive areas of hemorrhage. Approx. 10 x vol. 20.

In some places, exposed areas are found in the stroma, where the tissue structure of the organ is not visible. The thickness of the stromal layers between the secretory sections in the central zone of the gland is 40-100 μm, in the subcapsular zone it is sharply increased in 7-10 fields of view out of 10 and fluctuates from 151.2 to 252.0 μm, on average it is 189.4 ± 5.5 μm.

In the interglandular stroma, a large number of venules, capillaries, and arterioles are observed. Stasis of formed elements is evident in the vessels, accompanied by extensive areas of hemorrhage (Fig. 4.2.13). The number of stromal vessels per field of view ranges from 13 to 19, averaging 16.0 ± 0.3.

The internal diameter of venules ranges from 29.4 to 42.0 μm, averaging 38.1 ± 0.67 μm, and the thickness of their walls varies from 4.2 to 8.4 μm, averaging 6.0 ± 0.21 μm.

Capillaries are lined by a single layer of spindle-shaped endothelial cells oriented perpendicular to the lumen, fitting tightly together. Their diameter ranges from 12.6 to 21.0 μm, averaging 18.7 ± 0.42 μm, with wall thickness between 2.1 and 4.2 μm, averaging 3.8 ± 0.13 μm. In the arterioles, endothelial cells are densely arranged and are separated from the muscular layer by the internal elastic membrane.

In the middle membrane of the arterioles, smooth myocytes are arranged in a single layer. The outer membrane is formed by fibrous connective tissue. The internal diameter of the arterioles ranges from 12.6 to 21.0 μm, averaging 19.1 ± 0.42 μm, while their wall thickness varies from 4.2 to 8.4 μm, averaging 5.8 ± 0.21 μm.

Morphometric analysis of the parenchyma-stromal ratio showed that the relative area of parenchyma varies between 50 and 65%, averaging 58.0 ± 0.8%, and the proportion of stromal tissue fluctuates between 35 and 50%, averaging 42.0 ± 0.8%.

In the experiment, thickened collagen fibers occupy all interepithelial and periductal areas of the stroma. In some regions, a coarse network of collagen fibers is formed in the interacinar stroma (Fig. 4.2.14). The thickness of the collagen fiber bundles ranges from 8.4 to 12.6 μm, averaging 9.24 ± 0.21 μm.

The study showed that in 18-month-old rats of the experimental group, 80% of the acini exhibited a folded appearance with epithelial-stromal outgrowths. The epithelium was predominantly cuboidal, with flat epithelium observed in some areas (Fig. 4.2.15). The thickness of the epithelial lining ranged from 4.2 to 8.4 μm, averaging 5.8 ± 0.21 μm.

In certain areas of the epithelium, foci of epithelial stratification were observed, with disruption of the normal layering, cell polymorphism, and the

presence of large, multiple nucleoli in the nuclei. Mitotic cells were visualized in some regions (Fig. 4.2.16).

The terminal sections of the glands were predominantly irregular and oval in shape, and the lumens of the acini were convoluted (Fig. 4.2.15). The diameter of the gland lumen varied from 210.0 to 420.0 μm, with an average of 288.5 ± 8.8 μm. The number of acini in the field of view ranged from 25 to 40, averaging 32.5 ± 0.8. All acini lumens (100%) were devoid of secretion (see Appendix 6), and no desquamated epithelial cells were detected.

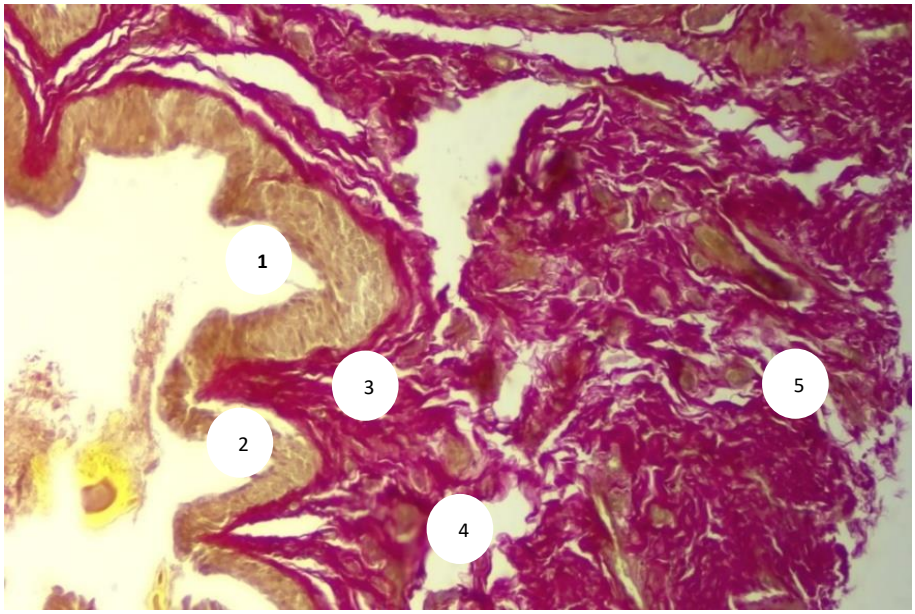

Fig.4.2.14. Prostate of a 12-month-old rat from the experimental group. Van Gieson staining. 1-acinus lumen, 2-desquamated epithelial cells, 3-folded epithelium of the acinus, 4-coarse network of collagen bundles in the subepithelial layer, 5-pathological proliferation of collagen fibers in the stroma. Approx. 10 x vol. 20.

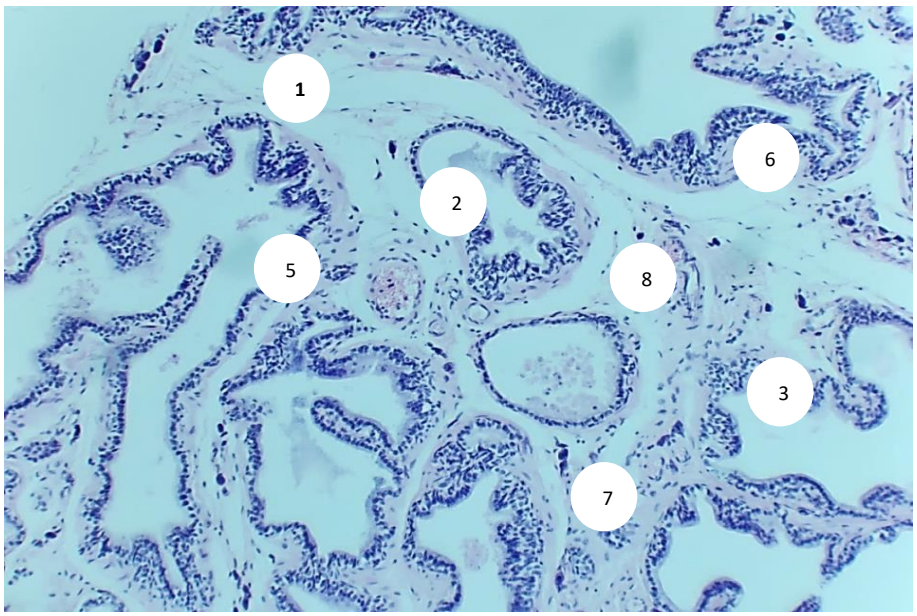

Fig.4.2.15. Prostate of 18-month-old rat of the experimental group. Hematoxylin and eosin staining. 1-gland capsule, 2-irregular acinus, 3-oval acinus with flat epithelium, 4-dilated stromal septa with exposed zones and tissue destruction, 5-intraluminal diffuse lymphocyte clusters, 6-diffuse lymphocyte clusters in the subcapsular zone, 7-diffuse lymphocyte clusters in the subepithelial layer, 8-full-blooded stromal vessels, lymphocyte infiltration of the perivascular zone. Approx. 10 x vol. 20.

In 18-month-old rats of the experimental group, a pronounced degree of lymphocytic infiltration with tissue destruction and nodular formation is noted. A large number of diffusely scattered lymphocytes are visualized in the interacinar stroma. Most preparations show intraluminal diffuse clusters of lymphocytes, diffuse clusters of lymphocytes in the subcapsular zone, in the subepithelial layer and epithelial-stromal outgrowths. In places around the full-blooded vessels of the intralobular stroma, diffuse clusters of lymphocytes infiltrating the vessel walls are detected. In some preparations, lymphoid nodules of irregular and rounded shapes are determined (Fig. 4.2.15, 4.2.17). It was not possible to count the number of lymphocytes in the stroma (in the field of view) due to their large quantity. In experiments

on one-and-a-half-year-old rats, a pronounced proliferation of connective tissue was observed in the subcapsular zones and central regions of the gland, with the septa enlarged in 7–10 fields of view out of 10. In some areas of the subcapsular zone, regions were exposed where the tissue structure of the organ was no longer visible.

The thickness of the stromal septa between the acini in the subcapsular zone ranged from 96.6 to 231.0 μm, averaging 162.1 ± 7.1 μm. In the central regions of the prostate, the thickness of the stromal layers varied from 40 to 80 μm.

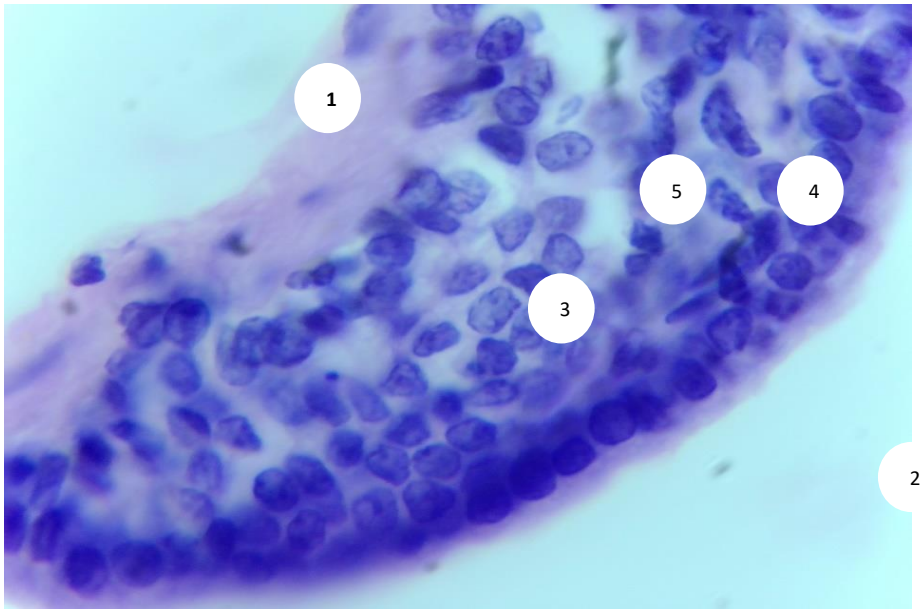

Fig.4.2.16. Prostate of an 18-month-old rat from the experimental group. Hematoxylin and eosin staining. 1-interglandular stroma, 2-acinus lumen, 3-epithelial stratification focus (multi-row and polymorphic cells are noted), 4-cells with large and multiple nucleoli, 5-mitotic cells. Approx. 10 x vol. 40.

A large number of venules, capillaries, and arterioles were observed in the interglandular stroma. Stasis of formed blood elements was detected in the vessels, accompanied by areas of stromal hemorrhage (Fig. 4.2.18). The number of stromal vessels in the field of view ranged from 14 to 25, with an average of 18.8 ± 0.6. The

walls of the venules are constructed from a single layer of endothelial cells located at a distance of 5-7 μm from each other. A great many veins are found in the subcapsular zones of the gland. The internal diameter of venules ranges from 29.4 to 46.2 μm, with an average of 42.0 ± 0.9 μm. The thickness of their walls varies from 4.2 to 8.4 μm, averaging 5.4 ± 0.21 μm. The endothelial cells of capillary walls are oriented perpendicular to the lumen. Capillary diameters range from 16.8 to 25.2 μm, with an average of 20.1 ± 0.42 μm, and their wall thickness ranges from 4.2 to 8.4 μm, averaging 4.5 ± 0.21 μm.

Arterioles have a three-layered wall, consisting of an internal endothelial membrane, a middle muscular layer, and an adventitia composed of connective tissue bundles. In many preparations, the arteriole membranes are not clearly distinguishable. The internal diameter of arterioles varies from 16.8 to 21.0 μm, averaging 19.5 ± 0.21 μm, and their wall thickness ranges from 4.2 to 8.4 μm, with an average of 5.4 ± 0.21 μm (see Appendix 7).

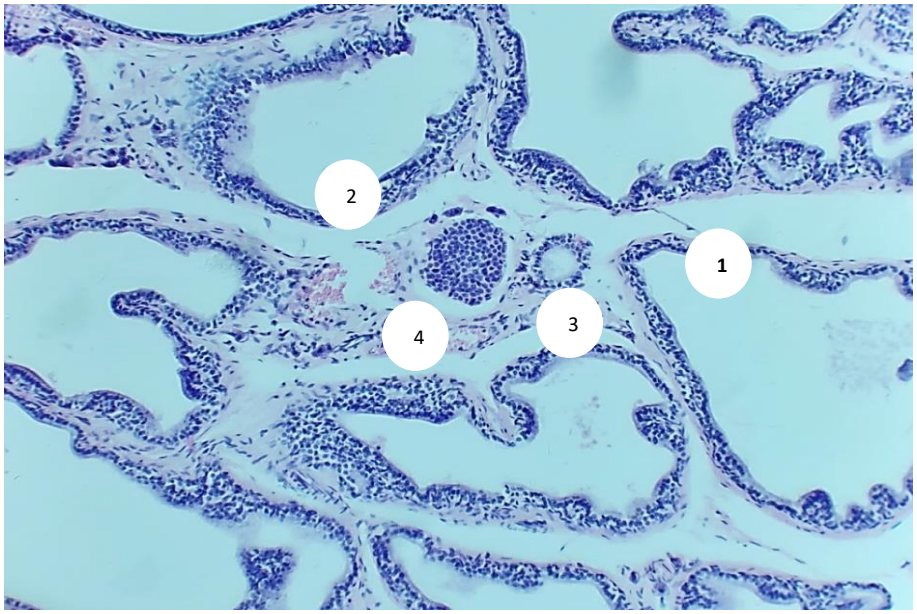

2

Fig.4.2.17. Prostate of an 18-month-old rat from the experimental group. Hematoxylin and eosin staining. 1-a round lymphoid nodule in the stroma, 2-bare areas of the stroma, no tissue structure, 3-damaged vessel wall with areas

of stromal hemorrhages, 4-diffuse lymphocyte clusters in the subepithelial layer and epithelial-stromal outgrowths. Approx. 10 x vol. 20.

Morphometric analysis of the parenchyma-stromal ratio revealed that the relative area of parenchyma varies from 20% to 46%, with an average of 34.1 ± 1.4%. The proportion of stromal tissue fluctuates between 54% and 80%, averaging 65.9 ± 1.4%(see Appendix 8).

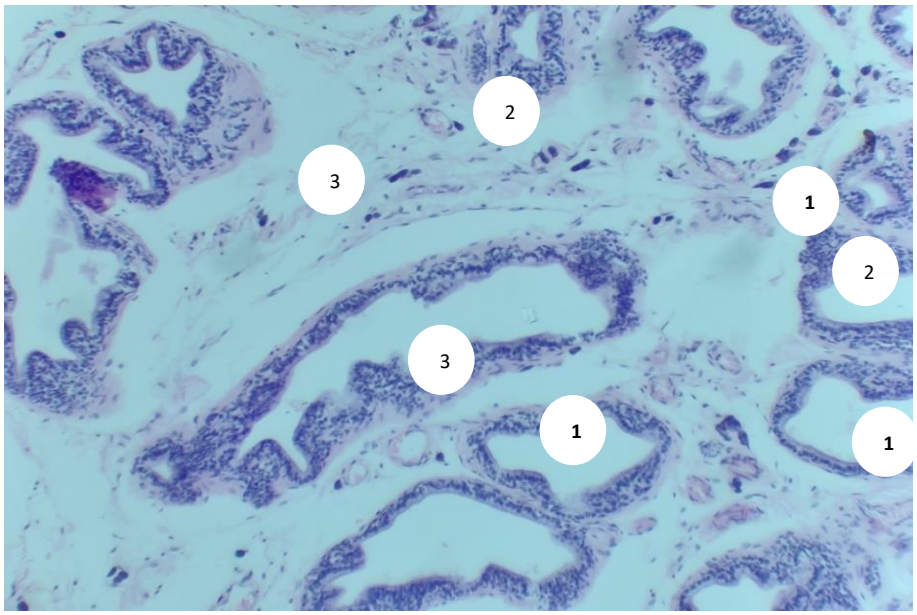

Fig. 4.2.18. Prostate of an 18-month-old rat from the experimental group. Hematoxylin and eosin staining. 1-a large number of intraorgan vessels in the interglandular stroma with stasis and areas of stromal hemorrhages, 2-expanded stromal septa with exposed areas, 3-diffuse lymphocyte clusters in the subepithelial layer. Approx. 10 x vol. 20.

In the experiment, pathological proliferation of collagen fibers was observed throughout almost the entire fibromuscular stroma. Numerous, massive bundles of collagen fibers were formed, occupying all areas around the acini and ducts of the gland. In some regions, a coarse network of collagen fibers was detected in the interacinar stroma (Fig. 4.2.19). The thickness of the collagen fiber bundles ranged from 4.2 to 8.4 μm, averaging 7.69 ± 0.21 μm.

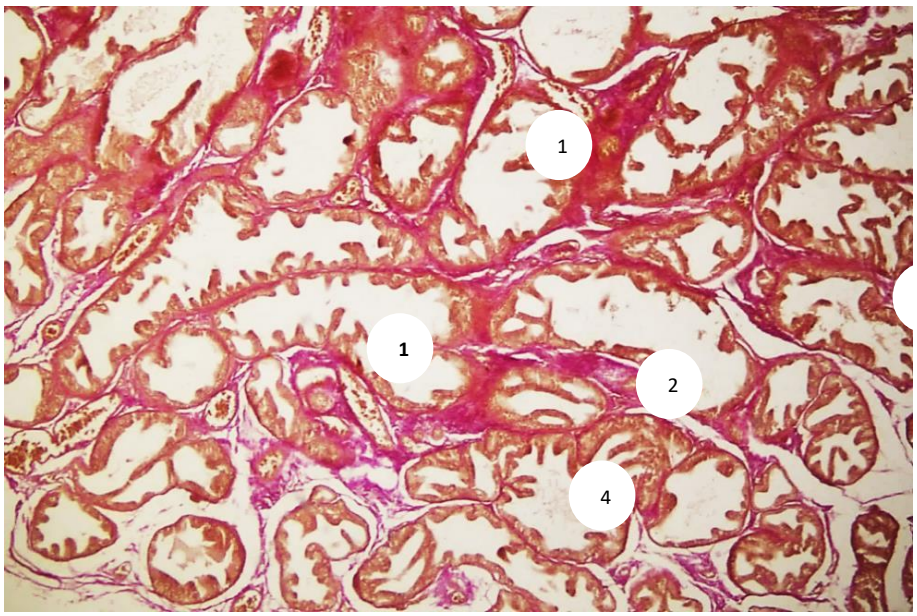

Fig. 4.2.19. Prostate of 18-month-old rat of the experimental group. Van Gieson staining. 1-acini with a large number of epithelial-stromal outgrowths, 2-pathological proliferation of collagen fibers in the stroma, 3-bundles of collagen fibers around the acini, 4-coarse network of collagen fibers in the subepithelial layer. Approx. 10 x vol. 20.

4.3-§. Immunohistochemical characteristics of the prostate gland of rats of the experimental group

Immunohistochemical study showed that 3-month-old rats of the experimental group exhibited pronounced proliferative activity in the structures of the stromal layer and parenchyma (Fig. 4.3.1).

In 6-month-old rats of the experimental group, immunohistochemical staining with antibodies to Ki-67 revealed moderate expression of the marker in the stroma and singly in the glandular epithelium (Fig. 4.3.2).

In 9-month-old animals of the experimental group, moderate reaction activity was determined. Reaction products in the form of brown precipitates were present in the stroma and vessels (Fig. 4.3.3).

In 12-month-old rats of the experimental group, immunohistochemical staining

with antibodies to Ki-67 revealed moderate proliferative activity in the stroma and vessels (Fig. 4.3.4).

In 18-month-old animals of the experimental group, a high level of expression was determined in the structures of the stromal layer and vessels (Fig. 4.3.5).

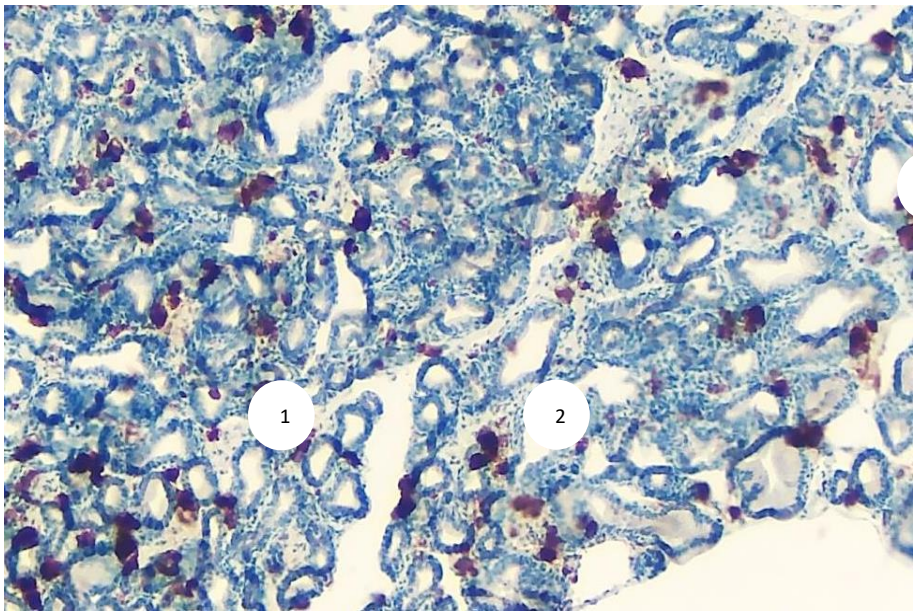

Fig.4.3.1. Prostate of a 3-month-old rat from the experimental group. Immunohistochemical staining with antibodies to Ki-67, chromogen diaminobenzidine, counterstaining with Mayer's hematoxylin. High expression of the marker in tissue stromal structures and in the epithelium of the terminal sections. 1-terminal secretory sections, 2-interlobar stroma.
Approx. 10 x vol. 20.

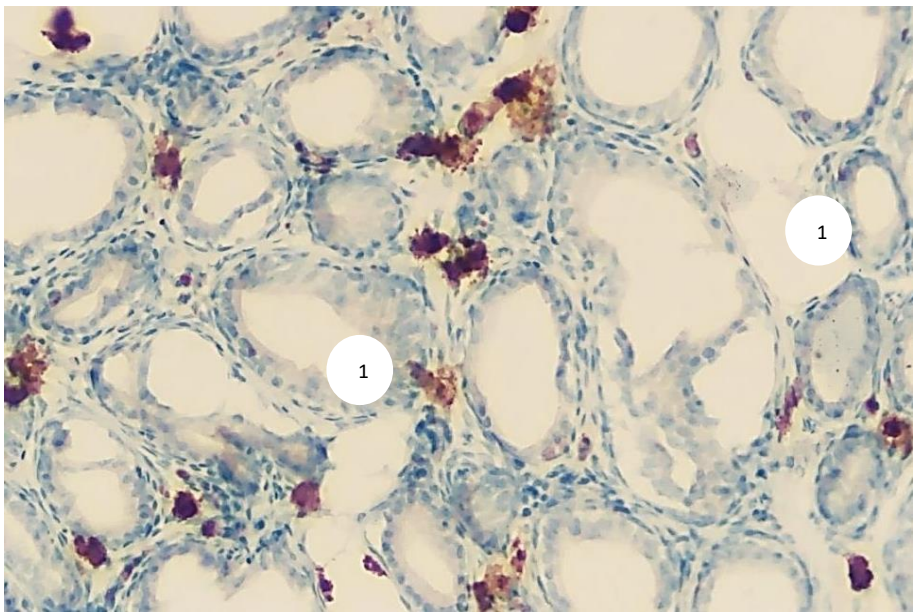

2

Fig.4.3.2. Prostate of a 6-month-old rat from the experimental group. Immunohistochemical staining with antibodies to Ki-67, chromogen diaminobenzidine, counterstaining with Maye 1 hematoxylin. Moderate proliferative activity. In the stroma and singly in the epithelium there are reaction products in the form 1 f violet-brownish precipitates. 1-acini, 2-interglandular stroma. Approx. 10 x vol. 20.

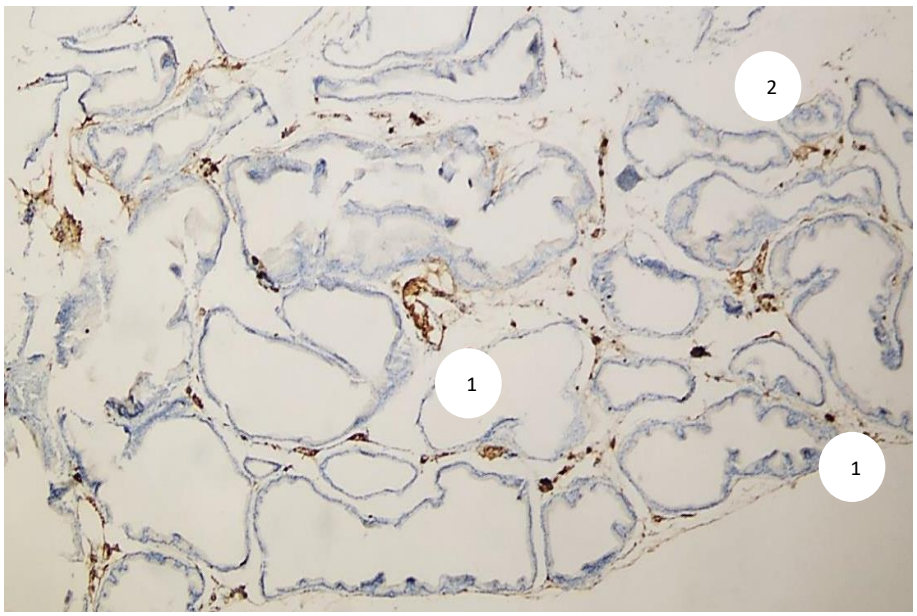

2

Fig.4.3.3. Prostate of a 9-month-old rat from the experimental group. Immunohistochemical staining with antibodies to Ki-67, chromogen

diaminobenzidine, counterstaining with Mayer's hematoxylin. Moderate expression. Reaction products in the form of brown precipitates are present in the stroma and vessels. 1-terminal glandular sections, 2-interlobular stroma.

Approx. 10 x vol. 20.

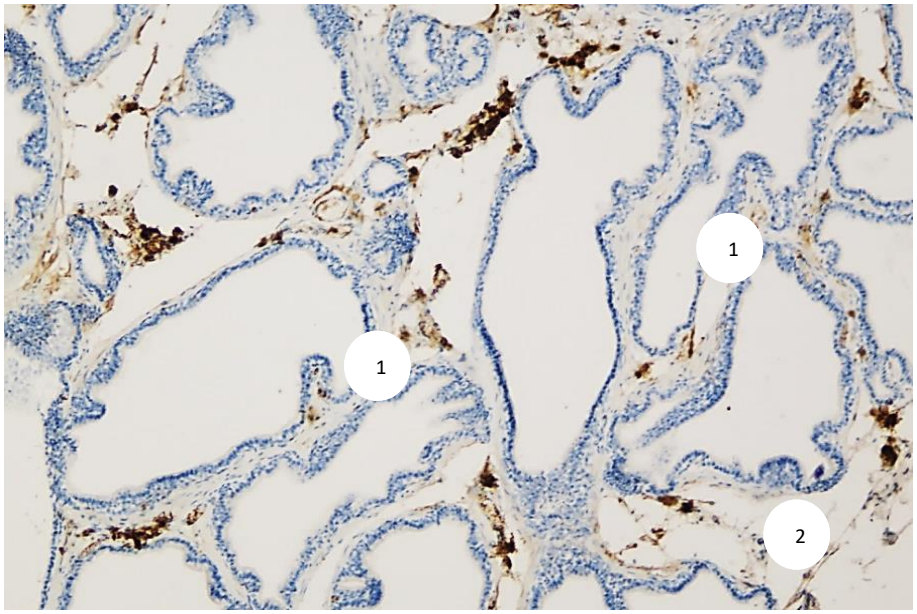

Fig.4.3.4. Prostate of a one-year-old rat of the experimental group. Immunohistochemical staining with antibodies to Ki-67, chromogen diaminobenzidine, counterstaining with Mayer's hematoxylin. Moderate proliferative activity. Reaction products in the form of brown precipitates are present in the stroma and vessels. 1-acini,
2-interglandular stroma. Approx. 10 x vol. 20.

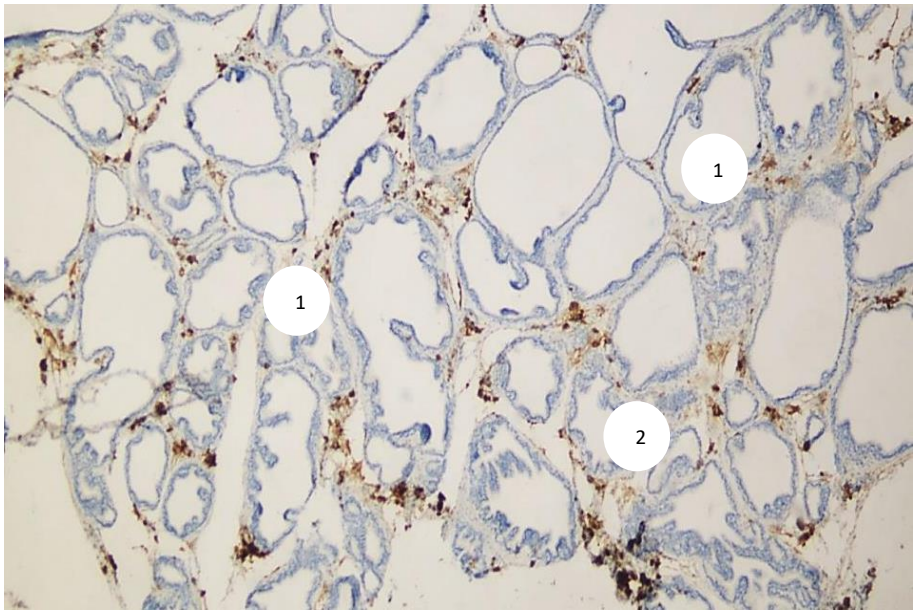

Fig. 4.3.5. Prostate of a one-and-a-half-year-old rat from the experimental group. Immunohistochemical staining with antibodies to Ki-67, chromogen diaminobenzidine, counterstaining with Mayer's hematoxylin. High level of expression in the structures of the stromal layer and vessels. 1-terminal secretory sections, 2-intralobular stroma. Approx. 10 x vol. 20.

Immunohistochemical study established that in 3-month-old rats of the experimental group, moderate expression of T-lymphocytes is determined in tissue stromal structures and in the epithelium of the terminal sections (Fig. 4.3.6). In 6-month-old animals of the experimental group, moderate activity of the T-lymphocyte reaction is observed in the stroma and epithelium of the terminal secretory sections, while the reaction products in the form of blue-violet precipitates are present in the epithelium and stroma (Fig. 4.3.7).

In the experiment, moderate expression of T-lymphocytes in tissue stromal structures and in the epithelium of the terminal sections is noted in 9-month-old rats (Fig. 4.3.8).

In 12-month-old rats of the experimental group, immunohistochemical study revealed moderate activity of the T-lymphocyte reaction in the stroma and epithelium of the secretory sections (Fig. 4.3.9).

In the experiment, pronounced expression of T-lymphocytes in tissue stromal structures and in the epithelium of the terminal sections is determined in 18-month-old rats of the experimental group (Fig. 4.3.10).

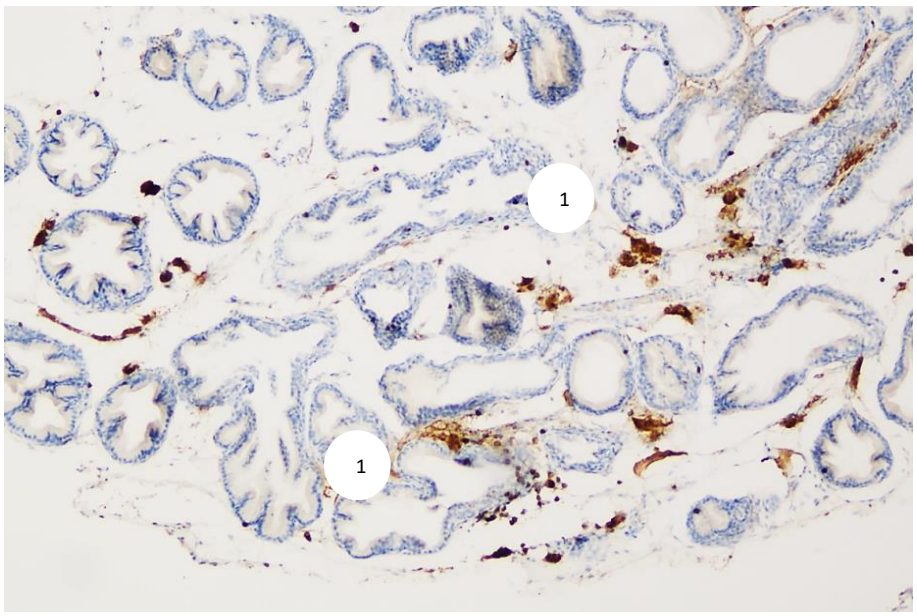

Fig.4.3.6. Prostate of a 3-month-old rat from the experimental group. Immunohistochemical staining with the CD3 marker, chromogen diaminobenzidine. Moderate expression of T-lymphocytes in tissue stromal structures and in the epithelium of the terminal sections. 1-glandular sections, 2-intralobular stroma. Approx. 10 x vol. 20.

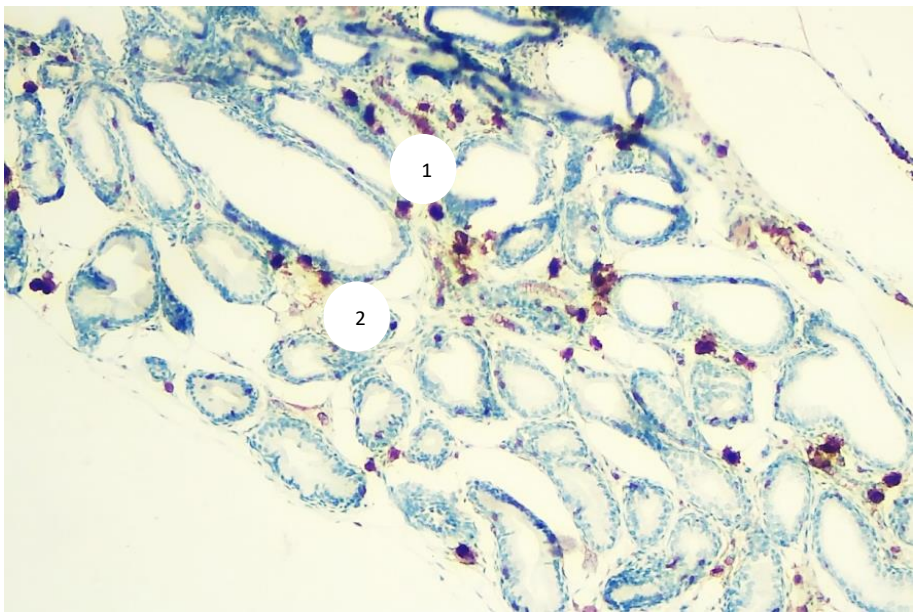

Fig.4.3.7. Prostate of a 6-month-old rat from the experimental group. Immunohistochemical staining with the CD3 marker, chromogen diaminobenzidine. Moderate activity of the T-lymphocyte reaction in the stroma and epithelium of the

terminal sections. Reaction products in the form of blue-violet precipitates are present in the epithelium and stroma. 1-secretory sections, 2-intralobular stroma. Approx. 10 x vol. 20.

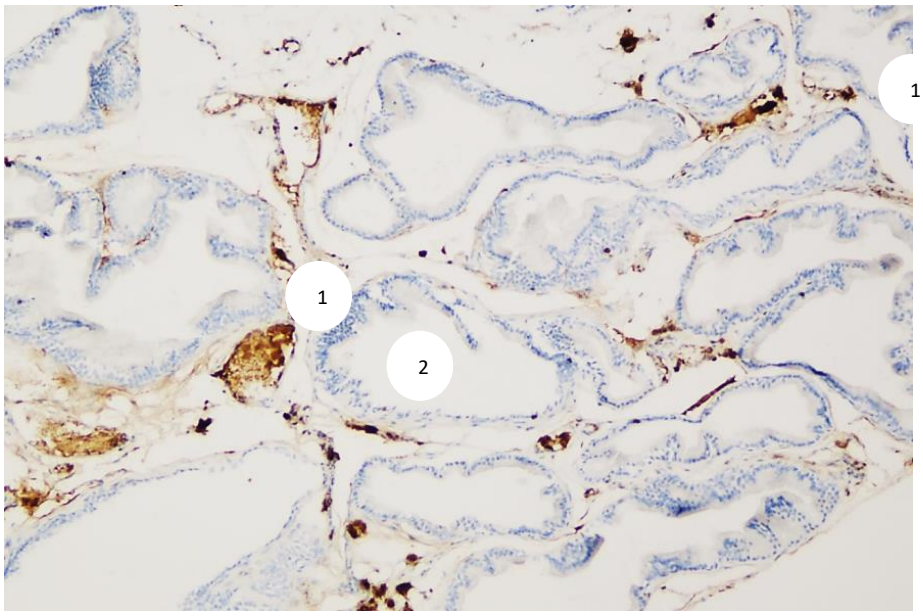

Fig.4.3.8. Prostate of a 9-month-old rat from the experimental group. Immunohistochemical staining with the CD3 marker, chromogen diaminobenzidine. Moderate expression of T-lymphocytes in tissue stromal structures and in the epithelium of the terminal sections. 1-acini, 2-interglandular stroma. Approx. 10 x vol. 20.

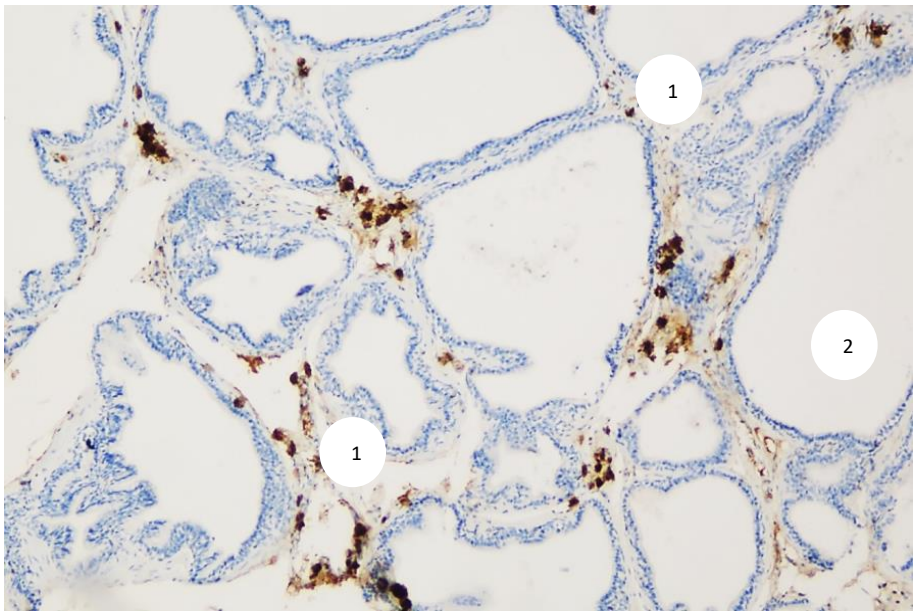

Fig.4.3.9. Prostate of a 12-month-old rat from the experimental group. Immunohistochemical staining with the CD3 marker, chromogen diaminobenzidine. Moderate activity of T-lymphocyte reaction in the stroma and epithelium of the terminal sections. 1-secretory sections, 2-intralobular stroma. Approx. 10 x vol. 20.

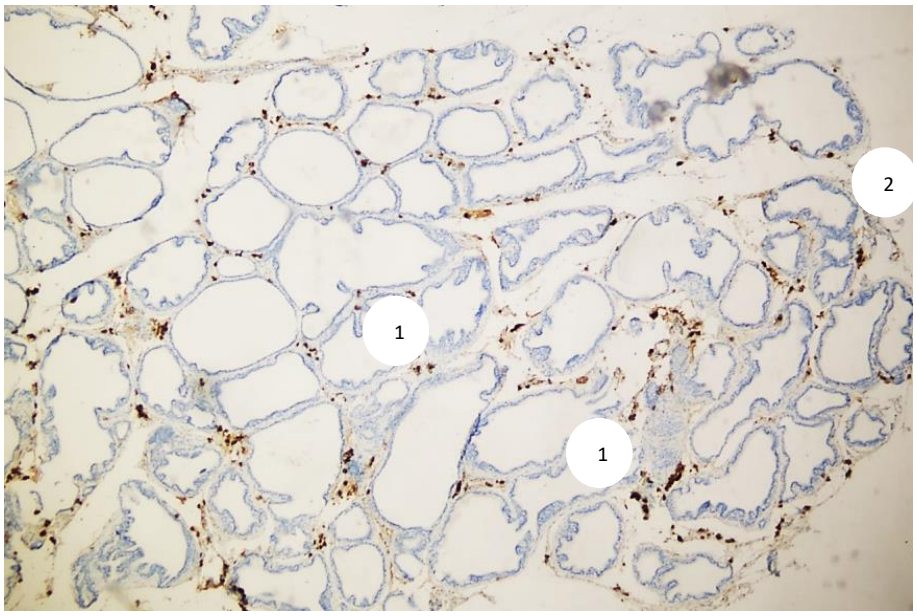

Fig.4.3.10. Prostate of an 18-month-old rat from the experimental group. Immunohistochemical staining with the CD3 marker, chromogen diaminobenzidine. Pronounced expression of T-lymphocytes in tissue stromal structures and in the epithelium of the terminal sections. 1-terminal secretory sections, 2-periglandular stroma. Approx. 10 x vol. 20.

DISCUSSION OF THE OBTAINED DATA AND CONCLUSION

The think about has set up that in infant rats, in a few cases, overview microscopy uncovers shaped secretory terminal segments of the organs, whereas in others, epithelial strings are show, which speak to the starting organize of postnatal morphogenesis of the prostate organ. Within the to begin with case, the secretory areas are spoken to by alveolar-tubular organs with as of now shaped lobules, their epithelium is lined with a single-layer low kaleidoscopic epithelium. Within the second case, epithelial (compact) strings are decided within the organ, which are circular or oval arrangements constrained by the basal layer, filled with epithelial cells. In this case, the epithelial cells have huge cores that are not polarized with regard to the basal film. In a few acini, the epithelium is freely found, the cell

boundaries are hazy, multi-row and polymorphism of the cells are famous. Cells with huge and different nucleoli and mitotic cells are uncovered.Until the end of the lactation period, that is, up to 21 days, differentiation of the glandular-stromal elements of the gland occurs due to the proliferation and branching of epithelial strands. Subsequently, the epithelium progressively differentiates, the cell rows acquire an ordered character, and from the age of one month it acquires a phenotype closer to the structure of the organ of an adult animal.

Our data are consistent with studies of prostate development in newborn boys and in rats at birth (Petko I. A., Usovich A., 2019; Bruni-Cardoso A., 2007), which found that at birth, the prostate epithelium consists of compact strands. Bruni-Cardoso A. (2007), Petko I. A. (2019) believe that by the time of birth, the prostate is morphologically formed and its transformations are aimed at further morphofunctional development. The formation of prostatic ducts from epithelial strands and their subsequent transformation into secretory terminal sections of the glands continues after birth.

Corbier P. et al. (1995) and Hayward S.W., Cunha G.R. (2002) share a similar opinion that the prostate gland of rodents is characterized by a postnatal stage of development, which occurs during the first 3 weeks after birth in response to a surge in testosterone that occurs on the day of birth.

We cannot but agree with the statement of Vilamaior P.S. et al. (2006) that the formation of the lumen in the prostate of rats occurs during the first 3 postnatal weeks.

During postnatal ontogenesis, typical alveolar-tubular glands covered with high and low cylindrical epithelial cells surrounded by stromal layer structures were found in the prostate gland, which correlates with the descriptions of a number of authors (Hayashi N., 1991; Banerjee P.P., 1994; Nemeth J.A., 1996, 1997; Bossland M.C., 1998; Suwa T., 2001; Odum J., 2009). It is possible that the differences in the morphological picture of the epithelium were associated with the wave-like course of secretory processes. The greatest increase in the thickness of the epithelial lining

of the acini is observed on days 6-11 of development. This coincides with the literature data (Zondek L. H., 1980; Bruni-Cardoso A., 2007) that progressive growth of the prostate gland is observed immediately after birth, and then until puberty it remains relatively passive. At the age of 12 months, the height of the epithelial layer decreases by 52.3%, at the age of 18 months - by 10.6%, which may be associated with age-related involutional changes in the organ. In animals aged 18 months, areas of cellular proliferation are detected in the epithelium of the secretory sections, where the epithelium becomes multi-row, a similar picture is observed in the epithelium of the prostatic urethra and excretory ducts. A number of authors (Tam N.C. et al., 2003; Gomes N.N. et al., 2004; Homma Y. et al., 2004; Pechenino A.S., 2006; Bethel C.R., 2009) obtained similar results in the prostate gland of rats during aging and oxidative stress. They are of the opinion that the basis for the development of cell proliferation is an increase in the activity of 5α-reductase, which transforms testosterone into dihydrotestosterone. Due to the dual activity of dihydrotestosterone, it promotes protein synthesis in the epithelial cells of the gland. Androgens stimulate epithelial proliferation indirectly, through growth factors formed by epithelial-stromal cells.

In the experiment, at all ages, a significant flattening of the epithelial cells was observed, which allowed us to speak of focal atrophy of the epithelial layer. The greatest flattening of the epithelial lining was observed in the 9th month of the experiment (61.6%). This is consistent with the data of Cagnon V. H. A. et al. (2001), who observed a sharp atrophy in the secretory epithelium of cuboidal cells in adult mice after chronic alcohol consumption. Martinez F. E. et al. (1993) observed a similar result in the seminal vesicles and ventral lobe of the prostate gland of rats. Cagnon V.H.A et al. (1998), Garcia P.J. et al., (1999) conducting an ultrastructural analysis of the prostate gland of rats subjected to chronic consumption of sugar cane brandy, revealed progressive atrophy of the glandular epithelium, which coincides with the results of our studies.

In the rats we studied, foci of epithelial stratification (prostatic intraepithelial neoplasia) were detected at all age periods of the experiment, which is also confirmed by the data of studies by E.M. Candido et al. (2013), who observed similar changes in 3-month-old rats exposed to alcohol. According to some authors (Xie W. et al., 2000; Alberts S.R., Blute M.L., 2001), intraepithelial neoplasia of the prostate gland is classified as a precancerous condition that can cause malignant neoplasm as a result of focal epithelial stratification, decreased secretory activity, or nuclear deformation. Cornell R.J. et al. (2003) believe that stromal cells associated with tumor cells, under the influence of androgens and growth factors, affect stromal-epithelial interaction. This can lead to apoptosis and metastasis processes (Wong Y.C. et al., 2000; Cunha G.R. et al., 2002; Cornell R.J. et al., 2003).

In an experiment in rats aged 6-12 months, areas of cellular proliferation were detected in the epithelium of the secretory sections.

A number of authors (Aboyan I.A. et al., 2020; Gandaglia G. et al., 2017; Magri V. et al., 2019) believe that the inflammatory process is of no small importance in triggering proliferative processes in prostate tissue and their progression. The presence of inflammation in the prostate tissue leads to a progressive deterioration of metabolic processes in the gland and increases the proliferation processes in the gland tissue, which leads to its growth (Spivak L.G., Platonova D.V., 2017; Aboyan I.A. et al., 2020; Gandaglia G. et al., 2013; Xu D., 2019). Some lymphocytes, due to the secretion of anti-inflammatory cytokines and growth factors, have the ability to activate cell proliferation. And in the case of an inflammatory process in the prostate tissue, the production of these factors increases, which can significantly accelerate proliferative processes in the gland (Ren X. et al., 2016; Xu D. et al., 2019).

Another distinctive feature that we discovered in the secretory sections of the rat prostate, which is mentioned in the works (Banerjee P.P., 1994; Suwa T., 2001; Odum J., 2009) is the folds of the epithelium penetrating the lumens of the terminal sections. In the control, folds or epithelial-stromal outgrowths appear at the

beginning of late postnatal ontogenesis, that is, by the 1st month of life of animals, reaching 100% at 1.5 years.

In the experiment, compared with the control, a decrease in stromal outgrowths in the secretory sections of the gland is noted in all age groups. The results of our studies coincide with the data of E. M. Candido et al. (2013), who observed similar changes in rats exposed to alcohol. A. F. Budnik et al. (2016) share a similar opinion, that in the prostate of mature men with chronic alcohol intoxication, the number of folds decreases. From birth to one year of age, the secretory sections have an oval and round shape; in animals aged one and a half years, acini of irregular shapes predominate.

At all ages of the experiment, polygonality of the glands in shape and size is noted, and at the same time, acini of irregular shape predominate.

In early postnatal ontogenesis, the largest diameter of acini was found in newborn rats, which is possibly due to the significant influence of the mother's sex hormones on the morphology of the prostate at this age. Then this indicator gradually decreases. In the late postnatal period, the greatest increase in the diameter of the secretory sections is observed in rats in the period of 1-3 months (95.7% and 83.3%) and at 18 months of age (98.6%), which may be associated with age-related congestion in the gland.

Accordingly, in the lactation period, the smallest number of acini in the field of vision is noted in newborns, the largest - in 21 day old animals. In late ontogenesis, the smallest number is observed at the 9th month of life, the largest - at the age of 1 month. In the experiment, the diameter of the secretory sections decreases at all ages, especially at 3 months of age (62.2%). Sayapina I.Yu. et al. (2018) believe that the decrease in the lumen of the secretory sections may be associated with a spasm of the smooth muscles of the stroma in response to alcohol.

Our data are consistent with the results of studies by E. M. Candido et al. (2013), who observed similar changes in 3-month-old rats with chronic exposure to

alcohol. Similar changes are described in the work of Sattolo S. et al. (2004) on the histological material of the ventral prostate in rats of the alcoholic group. Yurov M.A. (2012) is of the opposite opinion, that chronic alcohol intoxication in rats leads to an expansion of the lumens of the terminal sections of the prostatic glands. At the 12th month of the experiment, under conditions of a hypersecretory state at this age (100%), such congestive anomalies as a sharp expansion of the secretory sections by 2.3 times and overflow of the acini with secretion are observed.

In the experiment, an increase in the number of acini in the field of view is observed due to a decrease in their diameter, only at the age of 12 months is a decrease in the number of acini due to an increase in their diameter noted.

In the lactation period, the highest secretory activity of acini is observed in newborns - 82.7%, which is possibly due to the organ's response to a surge in testosterone that occurs on the day of birth. Further, up to and including the 21st day of development, the secretory activity of the terminal sections is zero. In late ontogenesis, the highest growth rate of acini with secretion is noted at the age of 3 months, when it increases by 3.8 times compared to the previous age, which is possibly due to the onset of sexual maturity in animals. At 12-18 months of development, the secretory activity of the terminal sections increases to 100%, which indicates congestion in the prostate gland. In the experiment, the percentage of acini with secretion (secretory activity) decreases compared to the control, especially at 3 and 18 months of development. At one year of age, secretory activity is 100%, which is associated with cognitive phenomena in the organ.

In the control, the largest number of desquamative epithelial cells in the acini were found in newborns (7.5±0.4), then this indicator gradually decreases, starting from the age of 6 months, desquamated epithelial cells in the acini are not detected. These cells and formations in the secretory sections of the gland can be regarded as a structural basis for the formation of prostatic stones. In 18-month-old animals, concretions and single concretions were found in 50.0% of the acini, which in places destroyed the epithelial lining of the acini.

Alterative changes within the prostate organ beneath persistent liquor introduction were showed basically by desquamation of the epithelium, which showed an increment within the secretory movement of the acinar epithelium and the passing of epithelial cells in them. Articulated desquamation of epithelial cells into the lumen of the acini in creatures of the test group is watched in all age bunches, particularly within the 6th month of the test, when the number of desquamated epithelial cells within the lumen of the acini increments by 9.1 times.

At the age of one year, total desquamation of the epithelium with closure of the lumens of the acini is observed. This may be due to a drop in the level of testosterone in the blood of animals, and as a consequence, it is combined with the total death of epithelial cells in the secretory sections by apoptosis, as indicated by a number of authors (Banerjee S. et al., 2000; Omezzine A. et al., 2003).

It should be noted that no concretions or stones were found in the micropreparations of animals of the experimental group throughout the entire development process. The study found that in the control, the greatest increase in the number of lymphocytes in the field of vision during the suckling period is observed in 6-day-old animals (26.7%), in late ontogenesis - in 6-month-old (75.4%) and 18-month-old (58.4%) rats. In 18-month-old individuals, merging fields of lymphocytes without tissue destruction and lymphoid nodular formation were detected. Evaluation of the degree of lymphocytic infiltration in the gland tissues of animals of the experimental group showed that in the 3rd month of the experiment, a moderate degree of lymphocytic infiltration is observed without tissue destruction and lymphoid nodular formation. Up to one and a half years of age inclusive, a pronounced degree with tissue destruction, nodular formation, accumulation of lymphocytes in the lumens of the secretory sections and a violation of the integrity of the epithelium is noted. In the experiment, a relationship was observed between the level of lymphocytic infiltration and the presence of lymphocytes in the lumens of the secretory sections. The greatest reactive inflammatory changes with a noticeable increase in the number of lymphocytes were detected at the 9th and 18th

months of the experiment, when, due to their very large number, it was practically impossible to count them. The inflammation process, according to Billis A. (2000), is the result of excess prostate gland secretion and extravasation of secretion into the stroma after duct obstruction.

In animals of the control group, the greatest thickness of stromal septa during the lactation period was observed in newborn rats (28.6 ± 1.7 μm). In late postnatal ontogenesis, particularly in 12–18-month-old rats, areas of connective tissue proliferation were detected, mainly in the subcapsular zones.

In the experiment, throughout postnatal ontogenesis, an expansion of connective tissue layers was observed, indicating interstitial edema. At 3–6 months, a moderate form of connective tissue proliferation was noted, whereas at 9–18 months, a pronounced form was observed, with thickening of stromal layers occurring mainly in the subcapsular zones. In the central areas, the thickness of the layers remained largely unchanged.

By the 18th month of the experiment, an increase in the thickness of stromal septa predominated in the central zones, where it increased up to eight times compared to the control. In the subcapsular zones, the thickness increased by 49.0%. Compared to the control, the greatest expansion of stromal layers in the experiment was observed at 6–9 months, increasing by 4.6 and 6.1 times, respectively.

In the control, collagen fibers in the form of rims surround the secretory sections, forming a fine-mesh network in the stroma. The greatest increase in the thickness of collagen fiber bundles is noted on the 6th day and on the 3rd month, at 18 months of age, the thickness of the bundles decreases by 21.1%, which is possibly due to the compaction of collagen fiber bundles.

In animals of the experimental group, the number of thickened collagen fibers is increased, they occupy all interepithelial areas of the stroma. In parallel, they are determined around the secretory sections and excretory ducts, where they tightly

envelop the smooth myocytes of the stroma. In places, a coarse network of collagen fibers is formed in the interacinar stroma. The greatest compaction of collagen fiber bundles is observed at 6-9 months of the experiment.

During postnatal development, the highest rate of increase in the number of vessels in the visual field is observed in 6-month-old animals, and the growth rate in late postnatal ontogenesis is much higher than in the lactation period.

In the experiment, an increase in the number of vessels in the visual field is observed. The greatest increase in the number of vessels is noted at 3 months (82.0%) and 9 months (71.1%) ages, especially in the subcapsular zones.

During postnatal ontogenesis, the greatest increase in the diameter and wall thickness of venules, capillaries, arterioles is observed on the 6-11th day and 6-9 months of life, and the increase in these indicators drops sharply in 12-18-month-old animals. In 18-month-old animals, blood filling of the lumens of almost all vessels, especially venules, is noted. Around the vessels, clusters of lymphocytes are determined, which infiltrate the vessel walls.

In the experiment, the greatest expansion of the diameter of stromal vessels was detected in animals at 3, 12, 18 months of the experiment, a decrease in wall thickness at 12, 18 months. At the 3rd month, vascular changes are observed in the form of lymphocytic infiltration of the perivascular zone, from the 6th month, stasis of formed elements in the vessels and ruptures with massive hemorrhages in the stroma are added. Damage is most pronounced on the periphery of the organ, while in the central areas, compensatory and restorative processes dominate. These processes are aimed at restoring circulatory disorders, which is expressed in an increase in the number of vessels in the field of vision and an expansion of their diameter.

Budnik A.F. et al. (2016) in the prostate of mature men with chronic alcohol intoxication noted a similar expansion of the average diameter of blood vessels and an increase in their number in the field of vision.

Sherstyuk O.A. (2013), Emberton M. (2010), Abdelwahab O. et al. (2012) believe that microcirculatory changes (plethora and stasis) and, as a result, disorganization of the prostate structure underlie various diseases of the male reproductive system. In animals of the control group, secretory elements prevail over stromal ones. The highest percentage of glandular tissue in the prostate is detected at 9 months of age (the period of greatest functional activity), the lowest - at 18 months. The highest rate of stromal growth is noted in the 3rd month of life, when it increases by 2.1 times. At the same age, the highest secretory activity of acini is observed, when it increases by 3.8 times. Our data coincide with the results of the studies by Trotsenko B.V. (2006) that as secretory processes develop, the number of muscular-stromal elements increases, providing secretion drainage due to their powerful contractile effect. In the experiment, the proportion of glandular tissue decreases in all age periods, this is most pronounced in 9-month-old animals (65.0%). At the same time, the proportion of stromal tissue during this period increases by 5.9 times compared to the control, which is also confirmed by the data of the studies by Favaro W.J., Cagnon V.H.A. (2006) in rats of the same age with experimental alcoholism. Yurov M.A. (2012) when modeling alcohol intoxication in male Wistar rats with an initial body weight of 220-260 g, observed a decrease in the parenchyma area in the prostate by 10.0% and an increase in the stroma by 32.4%.

Thus, the development of the structural components of the prostate is carried out alternately and interrelated at all stages of postnatal life, while having individual characteristics. The data obtained can be used for the basic assessment of the morphology of the organ in pathological conditions. The growth process of epithelial-stromal elements of the gland with chronic exposure to alcohol is characterized by unevenness and depends on the anatomical and physiological, age-related characteristics of the body and the time when the body was exposed to chronic alcohol.

Immunohistochemical study using the Ki67 proliferative activity marker revealed a wide range of proliferative activity in animals of the control group and in the experiment.

The immunohistochemical reaction to the proliferation marker was presented in the form of nuclei clearly stained brown with more intense staining of the nucleoli; the staining of the nuclei was granular.

In animals of the control group, from the neonatal period to the 21st day of development inclusive, a high level of expression of the Ki67 marker is observed in the structures of the stromal layer and epithelial cords, which is consistent with the results of our histological studies, according to which the differentiation of epithelial-stromal elements in the rat prostate occurs during the first three postnatal weeks.

Starting from the age of one month and up to one and a half years, low proliferative activity is noted in the stroma and epithelium of the secretory sections, which is possibly associated with the completed differentiation of the organ.

The animals of the experimental group showed a moderately expressed immunopositive reaction with antibodies to Ki67, which indicates an increase in proliferative activity. At 6, 9, 12 months, moderate expression of the marker was noted, at 3, 18 months, a high rate of positively stained nuclei for the Ki67 protein was detected. It should be noted that from the 9th month of the experiment, the marker was determined in the structures of the stromal layer and in the vessels.

The assessment of the state of T-cell immunity showed that in animals of the control group, weak expression of the CD3 marker in the structures of the stromal layer and glandular epithelium is determined throughout the entire postnatal ontogenesis.

In the experiment, this marker is moderately expressed in rats up to 12 months of age, at 18 months, pronounced expression of the marker is observed, which indicates an increase in reactive processes in the organ in response to alcohol.

Thus, based on the results of the study, the following conclusions can be made:

1. Until the conclusion of the lactation period, due to the multiplication and branching of epithelial strands, separation of glandular-stromal components of the organ happens, which is affirmed by the multi-row epithelium, adjusted, huge cores and an wealth of mitotic figures. In this way, the epithelium dynamically separates, involving one layer of cells, and from the age of one month it secures a phenotype closer to the structure of an grown-up creature. At the 12th month of improvement, involutional changes win within the organ tissues within the shape of a sharp diminish within the tallness of the epithelial layer by 52.3%, a diminish within the breadth of the terminal segments by 63.9% and a diminish in secretory action.

2. In animals with chronic alcoholism, polygonality of the glands in shape and size, a decrease in the size, folding, secretory activity of the acini and the volume fraction of the glandular parenchyma in the organ structure, alternative changes in the form of focal desquamation of varying severity are observed, indicating accelerated elimination of glandular epithelial cells. In some places, acini with foci of epithelial stratification are detected, which can subsequently cause a malignant neoplasm.

3. Alcohol exposure leads to vascular changes manifested by an increase in the number and diameter of all vessels, a decrease in their wall thickness mainly in the subcapsular parts of the organ and lymphoid infiltration of the perivascular zones; there are phenomena of stasis of blood cells in the vessels, especially in venules with extensive areas of stromal hemorrhages.

4. Until the end of the lactation period, the epithelium of the acini and stromal structures demonstrate pronounced expression of the Ki67 proliferation marker, which correlates with the results of our histological study on the ongoing

differentiation of the gland up to the 21st day of development. At later stages, the organ structures exhibit weak immunopositive properties. With chronic exposure to alcohol, moderately high proliferative activity is observed, and from the 9th month the marker is determined both in the structures of the stromal layer and in the vessels. 5. In animals of the control group, weak activity of the CD3 marker reaction in the structures of the stromal layer and glandular epithelium is noted throughout postnatal ontogenesis. In the experiment, this marker is moderately expressed, crowding of lymphocytes is noted, which indicates an increase in the reactivity of cellular immunity in order to maintain antigen homeostasis in the body.

LIST OF REFERENCES

1. Aboyan I.A., Tolmachev A.N., Lemeshko S.I. Morphological characteristics of prostate hyperplasia tissue in chronic prostatitis // Experimental and Clinical Urology. - 2020. - No. 4. - P. 38-46.

2. Avtandilov, G.G. Medical morphometry / G.G. Avtandilov. - M: Medicine, 1990. - 384 p.

3. Badluev E.B. Structure and some histochemical indices of the rabbit prostate gland / E.B. Badluev. - Text: direct // Morphology. - 2000. - V.117.- №3.- P. 17.

4. Batueva A. B. Histological structure of the prostate gland of silver-black foxes and the content of carbohydrate components in it / A. B. Batueva. - Text: direct // Morphology. - 2000. - V.117. - №3. - P. 19-28.

5. Borovskaya T. G. The state of spermatogenesis in rats after administration of the antitumor drug paclitaxel / T. G. Borovskaya, V. Ye. Goldberg, O. A. Rumpel et al. // Bulletin of Experimental Biology and Medicine. - 2009. - Vol. 147. - № 6. - P. 655-658.

6. Budnik A.F., Bogatyreva O.E., Musukaeva A.B. Morphological characteristics of the human prostate in chronic alcohol intoxication // International Research Journal. - 2016. - No. 3 (45). - P. 50-52.

7. Gorbunova E.N., Davydova D.A. Krupin V.N. Chronic inflammation and fibrosis as risk factors for prostatic intraepithelial neoplasia and prostate cancer // Clinical Medicine. - 2011. - No. 1. - P. 79-83.

8. Evtushenko V.M., Sirtsov V.K. Immunohistochemical features of the endocrine function of the human prostate gland in adulthood // “World of Medicine and Biology”, issue 2, 2013, pp. 29-31.

9. Evtushenko V. M. Analysis of morphofunctional and immunomorphological characteristics of the prostate gland in adolescence // Biomedical and biosocial anthropologi. - 2015. - No. 24. - P. 53-57.

10. Zadonskaya V. Yu. Histological features of the prostate gland of male American mink / V. Yu. Zadonskaya. - Text: electronic // Materials of the scientific and practical conference of young scientists "Innovative ideas of young researchers

for the agro-industrial complex of Russia" (March 29-30, 2018) / Ministry of Agriculture [and others]. - Penza: Penza State Agrarian University, 2018. - P. 45-48.

11. Zapadnyuk V. I. On the issue of age periodization of laboratory animals // Cell aging. - Kyiv, 1971. - P. 433-438.

12. Zapadnyuk I.P., Zapadnyuk V.I., Zakharia E.A. Laboratory animals. Breeding, maintenance, use in the experiment. - Kyiv: Vyshcha shkola. - 1983. - 383 p.

13. Zakharov A.A. Features of morphometric parameters of the prostate gland of immature rats after the use of an immunosuppressant // Bulletin of the Smolensk State Medical Academy. - 2017. - Vol. 16. - No. 4. - P. 12-18.

14. WHO Information Bulletin. Alcohol [Electronic resource] // World Health Organization. - September, 2018. URL: https://www.who.int/ru/news-room/fact-sheets/detail/alcohol.

15. Kashchenko S.A., Zakharov A.A. Features of the morphostructure of the prostate gland and seminal vesicles of animals in the period of pronounced senile changes during cyclophosphamide-induced immunosuppression // Crimean Journal of Experimental and Clinical Medicine. Vol. 8, No. 3, 2018, pp. 35-42. UDC: 611.659.084:615.37.

16. Knysheva L.P. et al. Criteria for the reliability of reproducing an experimental model of chronic alcohol intoxication // Volgograd Scientific Medical Journal. - 2016. - No. 4. - P. 48-51.

17. Koptyaeva K.E., Muzhikyan A.A., Gushchin Ya.A., Belyaeva E.V., Makarova M.N., Makarov V.G. Methodology for dissection and extraction of organs of laboratory animals // Communication 1: rat. Laboratory animals for scientific research. - 2018. - No. 2. - P. 71-92. DOI: 10.29296/ 10.29296/2618723X-2018-02-08.

18. Lugin I. A., Trotsenko B. V. Development of prostatitis under hypokinetic stress // Modern medicine: Current issues. - 2014. - No. 37. - P. 47-80. ISSN: 2309-3552.

19. Makarov V. G., Makarova M. N., Abrashova T. V., Gushchin Ya. A., Kovaleva M. A., Rybakova A. V., Selezneva A. I., Sokolova A. P., Khodko S. V. Handbook. Physiological, biochemical and biometric parameters of the norm of experimental animals. SPb.: Publishing house "LEMA", 2013.- 116 p.

20. Nefedchenko A. V., I. V. Naumkin. Splanchnology of domestic animals: the reproductive system: a textbook and method manual / Novosibirsk State Agrarian University, State Scientific Institution IEVSiDV of the Russian Agricultural Academy; - Novosibirsk: NGAU Publishing House, 2012. - 101 p.

21. Neimark A.I. et al. Pathomorphological changes in the prostate gland in vibration disease // BULLETIN OF THE SB RAMS - 2008. - No. 6 (134). - P. 145-150.

22. Nikitin, A.I. Harmful environmental factors and the human reproductive system (responsibility to future generations) / A.I. Nikitin. - St. Petersburg: El-bi-SPb, 2005. - 216 p.

23. Petko I. A., Usovich A. K. Formation and transformation of the human prostate glands in the prenatal and neonatal periods // Ontogenesis. - 2019, Vol. 50. - No. 2. - P. 141-146.

24. Petko I. A., Usovich A. K. Morphometric indices of the epithelium in the prostate of boys. Modern morphology: problems and development prospects // Collection of papers of the scientific and practical conference with international participation dedicated to the 90th anniversary of the birth of the Honored Scientist of the Republic of Belarus, laureate of the State Prize of the Republic of Belarus, professor Pyotr Iosifovich Lobko, October 3-4, 2019. Minsk, Republic of Belarus. - Pp.43-45.

25. Rybakova A.V. Methods of euthanasia of laboratory animals in accordance with the European Directive 2010/63 / A.V. Rybakova, M.N. Makarova // International Bulletin of Veterinary Medicine. - 2015. - No. 2. - P. 96-107.

26. Sayapina I.Yu., Tseluiko S.S., Lashin S.A., Ostronkov V.S. Functional morphology of the organs of the male reproductive system during adaptation to low temperatures against the background of correction with dihydroquercetin. Monograph. Blagoveshchensk: OOO "Tipografiya". - 2018. - 179 p.

27. Sidorov P.I. Use of laboratory animals in toxicological experiments: guidelines. Ed. Sidorov P.I. Arkhangelsk. - 2002. - 15 p.

28. Skorodok P. M., Savchenko O. N. Disorders of sexual development in boys. Publishing house Medicine, Moscow. - 1984. - 240 p.

29. Spivak L. G., Platonova D. V. Efficacy and safety of the drug Vitaprost Plus in patients with chronic bacterial prostatitis, as well as in patients with benign prostatic hyperplasia before and after transurethral resection for the prevention of complications. Effective pharmacotherapy // Urology and nephrology. - 2017. - No. 24. - P. 10-14.

30. Stepanova E. F., Evseeva M. M., Karagulov H. G. Use of Tambuil suppositories in rats with interstitial prostatitis (experimental study) // Scientific News Series Medicine. Pharmacy. - 2011.- No. 22 (117). Issue 16/2. - P. 35-38.

31. Telenkov V. N. Comparative morphology of the prostate gland in caged fur animals: diss. Cand. of Veterinary Sciences: 16.00.02 / Telenkov V. N. - Omsk, 2001.- 193 p.

32. Telenkov V. N. Morphofunctional features of the genitourinary organs of males in representatives of the orders of carnivores and lagomorphs: diss. ... Doctor of Veterinary Sciences: 16.00.02 / Telenkov V. N. - Omsk, 2022, - 325 p.

33. Trotsenko, B.V. Comparative analysis of the morphogenesis of the prostate gland in human and rat fetuses / B.V. Trotsenko, I.A. Lugin // In the collection "Karpov readings". - Dnepropetrovsk: Porogi, 2006. - 86 p.

34. Khibkhenov L.V., Zamyanov I.D. The prostate gland of the yak in the prenatal and postnatal period of ontogenesis // Almanac of modern science and education. - Tambov, 2011. - No. 11 (54). - P. 83-87

35. Khorosh V.Ya., Mysak A.I. Experimental cytotoxic lesion of the prostate gland in the modeling of chronic prostatitis // Experimental and clinical urology. - 2013. - No. 2. - P. 35-37. 36. Tsvetkov I. S. Structural and functional changes in the prostate gland and immune system organs of Wistar rats with chronic autoimmune inflammation under normo- and hyperandrogenemia: author's abstract. diss. ... candidate of biological sciences / Tsvetkov I. S. - Moscow, 2012. - 26 p.

37. Tsydypov R. Ts. Morphology and histochemistry of the prostate gland of farm animals in comparison // Mongolian Journal of Agricultural Sciences. - 2014. - No. 13 (02). - P. 29-32.

38. Sharypova N. V. Concentration of hormones regulating sexual function under prolonged exposure to stress factors of extreme intensity / N. V. Sharypova, A. A. Sveshnikova // Fundamental research. – 2013. – № 3. – P. 404-410.

39.Sherstyuk O.A. et al. The role of anatomical knowledge in diagnostics and treatment of prostate diseases // Bulletin of problems of biology and medicine. – 2013. – Vol. 2, № 3. – P. 56-61. [Sherstjuk O.A. and dr. Visnyk problem biologii i medycyny. Bulletin of Biology and Medicine. – 2013. – Vol. 2, N3. – P. 56-61. (in Russian).

40.Yurov M.A. Structural changes in the prostate and lymph nodes in modeling alcohol intoxication in combination with venous congestion and phytocorrection: author's abstract. diss. … candidate of medicine. Sciences / Yurov M. A. - Novosibirsk, 2012. 28 pp.

41. Abdelwahab O., El-Barky E., Khalil M.M., Kamar A. Evaluation of the resistive index of prostatic blood flow in benign prostatic hyperplasia / O. Abdelwahab, E. El-Barky, M.M. Khalil, A..Kamar // Int. Braz. J. Urol. – 2012. – Mar-Apr; 38(2) – R. 250-255; discussion 255-257.

42.Adebayo A., Akinloye A., Olukole S., Ihunwo A., Oke B. Anatomical and immunohistochemical characteristics of the prostate gland in the greater cane Rat (Thryonomys swinderianus). Anatomia, Histologia, Embryologia. 2014. 1-8 doi: 10.1111/ahe.12122.

43.Akmal Yusrizal, Chairun Nisa, Savitri Novelina. "Morfologi Kelenjar Aksesori Kelamin Jantan pada Trenggiling (Manis javanica) (Morphology of the male sex accessory glands of the pangolin (manis javanica)) // Jurnal Veteriner 20, no. 1 (May 2019): 38.

44.Akbari G., Kianifard D. (2017). Anatomy, Histology and Histochemistry of Accessory sex glands in male Persian squirrel (Sciurusaomalus) // Italian Journal of Anatomy and Embryology, 122: 17-26.

45.Alsafy M.M.A., Abumandour A.A.K., El-Bakary R., Seif M.A., Roshdy K. Morphological examination of the accessory sex glands of the Barki bucks (Capra hircus) // Folia Morphol. (Warsz). – 2021. - Jun 1. P. 28-39.

46.Alberts S.R., Blute M.L. Chemoprevention for prostatic carcinoma: The role of flutamide in patients with prostatic intraepithelial neoplasia // Urology. -2001; 57 (4A): 188-190.

47.Amin Ali, Alexander Du Feu, Pedro Oliveira, Ananya Choudhury, Robert G. Bristow, Esther Baena. Prostate zones and cancer: lost in transition // Nature Reviews Urology, 10.1038/s41585-021-00524-7, 19, 2, (101-115), (2021).

48.Banerjee P.P. Age - and lobe-specific responses of the brown Norway rat prostate to androgen / B.B. Banerjee, S. Banerjee, R. Dorsey et al. // Biology of Reproduction. – 1994. – Vol. 51, № 4. – P. 675-684.

49.Banerjee. S. Castration-induced apoptotic cell death in the Brown Norway rat prostate decreases as a function of age / S. Banerjee, P.P. Banerjee, T.R. Brown // Endocrinology. – 2000. – Vol. 141, № 2. – P. 821-832.

50.Bethel C.R. Gene expression changes are age-dependent and lobe specific in the Brown Norway rat model of prostatic hyperplasia / C.R. Bethel, J. Chaudhary, M.D. Anway et al. // The Prostate. – 2009. – Vol. 69, № 8. – P. 838-850.

51.Billis A. Sistema Genital Masculino. In: Bogliolo L, editor. Patologia. 6th ed. Rio de Janeiro: Guanabara Koogan; - 2000. - p. 514.

52.Bosland M.C. Proliferative lesions of the prostate and other accessory sex glands in male rats / M.C. Bossland, D.L. Tuomari , M.R. Elwell et al. // In Guides for Toxicologic Pathology. – Washington: DC, 1998. – P. 1-20.

53.Bruni-Cardoso A. Dynamics of the epithelium during canalization of the rat ventral prostate / A. Bruni-Cardoso, H. F. Carvalho // Anat Rec. - 2007. - Vol. 290. - P. 1223–1232.

54.Cagnon V.H.A., Garcia P.J Martinez F.E. Martinez M. and Padovani C.R. 1996. Ultrastructural study of the coagulating gland of wistar rats submitted to experimental chronic alcohol ingestion // The Prostate., 28, 341-346.

55.Cagnon, V.H.A., Garcia, P.J., Guazzelli Filho, J., Martinez, F.E., Mello, Jr. W. and Martinez M. 1998. Ultrastructural study of the lateral lobe of the prostate of Wistar rats submitted to experimental chronic alcohol ingestion // J. Submicrosc. Cytol. Pathol., 30(1), 77-84.

56.Cagnon V. H. A., Tomazini F. M., Garcia P. J., Martinez F. E., Martinez M., Padovani C. R. Structure and ultrastructure of the ventral prostate of isogenic mice (C57B1/6J) submitted to chronic alcohol ingestion Tissue & Cell, 2001, 33 (4) 354-360.

57.Campos S.G.P., Zanetoni C., Scarano W. R., Vilamaior P.S.L., Taboga S. R. Age-related histopathological lesions in the Mongolian gerbil ventral prostate as

a good model for studies of spontaneous hormone-related disorders // Int. J. Exp. Path. (2008), 89, 13–24.

58.Candido E.M. Experimental alcoholism and pathogenesis of prostatic diseases in UChB rats / Candido E.M., Carvalho C.A., Martinez F.E. et al. // Cell Biology International. – 2013. – Vol. 31, № 5. – P. 459-472.

59.Carolyn King, David Forsyth. The Handbook of New Zealand Mammals. Csiro Publishing, 2021, 576 p. ISBN 14863062929781486306299.

60.Cordeiro R.S., Scarano W.R., Goes R.M., Taboga R.B. (2004) Tissue alterations in the guinea pig lateral prostate following antiandrogen flutamide therapy // Biocell. 28: 21-30.

61.Cornell R.J., Rowley D., Wheller T., Ali N., Ayala G., 2003. Neuroepithelial interactions in prostate cancer are enhanced in the presence of prostatic stroma // Urology 61, 870–875.

62.Corbier P., Martikainen P., Pestis J., Harkonen P. 1995. Experimental research on the morphofunctional differentiation of the rat ventral prostate: roles of the gonads at birth // Arch Physiol Biochem 103: 699–714.

63.Creasy D., Bube A., de Rijk E., Kandori H., Kuwahara M., Masson R., Nolte T., Reams R., Regan K., Rehm S. et al. Proliferative and Nonproliferative Lesions of the Rat and Mouse Male Reproductive System // Toxicol. Pathol. 2012, 40, 40–121.

64.Cunha G.R., Donjacour A.A., Cooke P.S., Mee S., Bigsby R.M., Higgins S.J., Sugimura Y. (1987) The endocrinology and developmental biology of the prostate // Endocrine Rev. 8: 338–362.

65.Cunha G.R., Hayward S.W., Wang Y.Z., 2002. Role of stroma in carcinogenesis of the prostate // Differentiation 70, 473–485.

66.Cunha G.R., Sinclair A., Ricke W. A., Robboy S. J., Cao M., Baskin L. S., Reproductive tract biology: Of mice and men // Differentiation, 10.1016/j.diff.2019.07.004, 110, (49-63), (2019).

67.Dalga S., Aslan K. (2020) Anatomi of urogenital system in rabbits. Van international applied sciences congress, 24-25 Julya Van, TURKEY, P. 190-203

68.El-Shahat A.E. Altered testicular morphology and oxidative stress induced by cadmium in experimental rats and protective effect of simultaneous green tea extract / A.E. El-Shahat, A. Gabr, A.R. Meki et al. // International Journal of Morphology. – 2009. – Vol. 27, № 3. – P. 757-764.

69.El-Alfy M., Pelletier G., Hermo L.S., Labrie F. Unique features of the basal cells of human prostate epithelium // Microsc. Res. Tech. 2000; 51:436–446. doi: 10.1002/1097-0029(20001201)51:5<436::AID-JEMT6>3.0.CO;2-T.

70.Emberton M. Progression of benign prostatic hyperplasia: a systematic review of patients treated with placebo in clinical trials / J.M. Fitzpatrick, M. Garcia-Losa, N. Qizilbash, B. Djavan // International abstract journal Urology. – 2010. – No. 1. – P. 46-54

71.Evans H. E., de Lahunta A. Mıller's Anatomy of the Dog. 4nd edition. WB Saunders Company. Philadelphia, London, Sydney, Tokyo. 2013: 1062–1067. ISBN: 978-143770812-7.

72.Fabiane F. Martins, Mateus R. Beguelini, Cintia C.I. Puga, Eliana Morielle-Versute, Patricia S.L. Vilamaior, Sebastiao R. Taboga, Morphophysiology and ultrastructure of the male reproductive accessory glands of the bats Carollia perspicillata , Glossophaga soricina and Phyllostomus discolor (Chiroptera: Phyllostomidae), Acta Histochemica, 10.1016/j.acthis.2016.07.005, 118, 6, (640-651), (2016).

73.Fardous S. K., Zahran N.M. Histological study of the effect of pumpkin seed oil on experimentally induced benign prostatic hyperplasia of the ventral prostate in

adult male albino rats // The Egyptian Journal of Histology 2015, 38: 286-294 25 (1522-2015) DOI: 10.1097/01.EHX.0000464781.75492.17.

74.Favaro W.J., Cagnon V.H.A., Morphometric and morphological features of the ventral prostate in rats submitted to chronic nicotine and alcohol treatment // Tissue and Cell 38 (2006) 311–323.

75.Fernandez D.S., Ferraz R.H.S., Melo A.P.F., Rodrigues R.F., Souza W.M. (2010). Análise histológica das glandulas uretrais da capivara (Hydrochoerus hydrochaeris) // Pesq. Vet. Bras. 30(4): 373–378.

76.Fernando Leis-Filho A.; Fonseca-Alves C.E. Anatomy, Histology, and Physiology of the Canine Prostate Gland. Vet. Anat. Physiol. 2018. In book: Veterinary Anatomy and Physiology (pp.1-14).

77.Fonseca-Alves C.E., Kobayashi P.E., Rivera Calderon L.G., Felisbino S.L., Rinaldi Jd.C., Drigo S.A., et al. (2018) Immunohistochemical panel to characterize canine prostate carcinomas according to aberrant p63 expression. PLoS ONE 13(6): 39-49 e0199173. https://doi.org/10.1371/journal. pone.0199173.

78.Gandaglia G., Briganti A., Gontero P., Mondaini N., Novara G., Salonia A., et al. The role of chronic prostatic inflammation in the pathogenesis and progression of benign prostatic hyperplasia (BPH) // BJU Int. 2013; 112 (4): 432-441.

79.Gandaglia G, Zaffuto E, Fossati N, Cucchiara V, Mirone V, Montorsi F, et al. The role of prostatic inflammation in the development and progression of benign and malignant diseases // Curr. Opin. Urol. 2017; 27 (2): 99-106. https://doi.org/: 10.1097/MOU.0000000000000369.

80.Garcia P.J., Cagnon V.H.A., Mello W.Jr., Martinez M. and Martinez F.E. 1999. Ultrastructural observations of the dorsal lobe of the prostate of rats (Rattus norvegicus) submitted to experimental chronic alcohol ingestion // Rev. Chil. Anat., 17 153-159.

81.Gervaise H. Henry, Alicia Malewska, Diya B. Joseph, Venkat S. Malladi, Jeon Lee, Jose Torrealba, Ryan J. Mauck, Jeffrey C. Gahan, Ganesh V.

Raj, Claus G. Roehrborn, Gary C. Hon, Malcolm P. MacConmara, Jeffrey C. Reese, Ryan C. Hutchinson, Chad M. Vezina, Douglas W. Strand, A Cellular Anatomy of the Normal Adult Human Prostate and Prostatic Urethra, Cell Reports, 10.1016/j.celrep. 2018.11.086, 25, 12, (3530-3542), (2018).

82.Ginja M., Maria J. P., Gonzalo-Orden J.M., Seixas F., Correia-Cardoso M., Ferreira R., Fardilha M., Oliveira P. A. , Faustino-Rocha A. I. Anatomy and Imaging of Rat Prostate: Practical Monitoring in Experimental Cancer-Induced Protocols // Diagnostics (Basel). - 2019. - Jun 30; 9(3): 68. 2-16 doi: 10.3390/diagnostics9030068.

83.Gomes I.C., Cagnon V.H., Carvalho C.A., De Luca I.M. 2002. Stereology and ultrastructure of the seminal vesicle of C57/BL/6J mice following chronic alcohol ingestion // Tissue Cell, 34, 177–186.

84.Gofur M. Anatomy and histomorphometry of accessory reproductive glands of the Black Bengal buck // Eur. J. Anat. 2015; 19 (2): 171-178.

85.Hayward S.W., Cunha G.R. 2000. The prostate: development and physiology // Radiol. Clin. North Am. 381:1–14.

86.Hayashi N. Morphological and functional heterogeneity in the rat prostate gland / N. Hayashi, Y. Sugimura, J. Kawamura et al. // Biology of Reproduction. – 1991. – Vol. 45, № 2. – P. 308-321.

87.Homma Y. Promotion of carcinogenesis and oxidative stress by dietary cholesterol in rat prostate / Y. Homma, Y. Kondo, M. Kaneko et al. // Carcinogenesis. – 2004. – Vol. 25, № 6. – P. 1011-1014.

88.Ismail A. H. R., Landry F., Aprikian A. G., Chevalier S. (2002). Androgen ablation promotes neuroendocrine cell differentiation in dog and human prostate // Prostate, 51(2), 117– 125.

89. Ittmann M. Anatomy and Histology of the Human and Murine Prostate // Journal List Cold Spring Harb Perspect Med. - 2018 - v.8 (5). - P.38-49.

90.Joon Hyuk Sohn, Dai Fukui, Taro Nojiri, Kazuhiro Minowa, Junpei Kimura, Daisuke Koyabu, Three-Dimensional and Histological Observations on Male Genital Organs of Greater Horseshoe Bat, Rhinolophus ferrumequinum //

Journal of Mammalian Evolution, 10.1007/s10914-020-09525-6, 28, 2, (559-571), (2020).

91.Kheddache A., Moudilou E. N., Zatra Y., Aknoun-Sail N., Amirat Z., Exbrayat J., Khammar F. Seasonal morphophysiological variations in the prostatic complex of the Tarabul's gerbil (Gerbillus tarabuli) // Tissue and Cell, 10.1016 /j.tice.2017.01.004, 49, 2, (345-357), (2017).

92.Knoblaugh S., Tretiakova M., Hukkanen R. Male reproductive system. In Comparative Anatomy and Histology: A Mouse, Rat and Human Atlas; Treuting, P., Dintzis, S., Montine, K., Eds.; Academic Press: Cambridge, MA, USA, 2017; pp. 335–338.

93. Lai C.L. van den Ham R., van Leenders G., van der Lugt J., Teske E. Comparative characterization of the canine normal prostate in intact and castrated animals // The Prostate. 2008; 68: 498-507. DOI: 10.1002/pros.20721.

94. Leav I., Schelling K. H., Adams J. Y., Merk F. B., Alroy J. (2001). Role of canine basal cells in postnatal prostatic development, induction of hyperplasia, and sex hormone-stimulated growth; and the ductal origin of carcinoma // Prostate, 48(3), 210– 224.

95.Leroy B. E., Northrup N. (2009). Prostate cancer in dogs: Comparative and clinical aspects // Veterinary Journal, 180(2), 149– 162.

96.Mahmud Muhammad Abdullahi, Josephat Edoga Onu, Sani Abdullahi Shehu, Abubakar Abubakar Umar, Abubakar Danmaigoro. Histomorphology of accessory sex glands in one-humped camel bull (Camelus dromedarius), Uda Rams and Red Sokoto Buck // World Journal of Biology and Biotechnology 5, no. 3, 28 - 37 (August 2020): 23. http://dx.doi.org/ 10. 33865/ wjb. 005. 03.0308.

97. Mangera A., Osman N. I., Chapple C. R. (2013). Anatomy of the lower urinary tract (pp. 319– 325). Elsevier Ltd.

98. Magri V., Boltri M., Cai T., Colombo R., Cuzzocrea S., De Visschere P.et al. Multidisciplinary approach to prostatitis // Arch. Ital. Urol. Androl. 2019; 90 (4): 227-248.

99. Martinez F.E., Garcia P.J., Padovani C.R., Cagnon V.H.A. and Martinez, M. 1993. Ultrastructural study of the ventral lobe of the prostate of rats submitted to experimental chronic alcoholism. Prostate, 22, 317-324.

100. McVary K.T., McKenna K.E., Lee C. Prostate innervation // Prostate Supl. 1998, 8, 2–13.

101. McNeal J.E., 1983. Relationship of the origin of benign prostatic hypertrophy to prostatic structure of man and other mammals. In: F. Hinman, editor. Benign prostatic hypertrophy. New York: Springer-Verlag. p. 152– 166.

102. Mendes L.O. Mast cells and ethanol consumption: interactions in the prostate, epididymis and testis of UChB rats // L.O. Mendes, J.P. Amorim, G.R. Teixeira et al. // American Journal of Reproduction Immunology. – 2011. – Vol. 66, № 3. – P. 170-178.

103.Miniati D.N., Chang Y., Shu W.P., Peehl D.M., Liu B.C. (1996) Role of prostatic basal cells in the regulation and suppression of human prostate cancer cells // Cancer Lett 104: 137–144.

104.Miotti M.D., Mollerach M.I., Barquez R.M. (2018) Anatomy and histology of the prostate and glands of Cowper in three species of Neotropical bats // J. Morphol. 279: 294–301.

105.Mollineau W.M., Adogwa A.O., Garcia G.W. (2009) The gross and micro anatomy of the accessory sex glands of the male agouti (Dasyprocta leporina) // Anat. Histol. Embryol. 38: 204-207.

106.Moura F., Sampaio L., Kobayashi P., Laufer-Amorim R., Ferreira J.C., Watanabe T.T.N., Fonseca-Alves C.E. Structural and Ultrastructural Morphological Evaluation of Giant Anteater (Myrmecophaga tridactyla) Prostate Gland // Biology 2021, 10, 231-242.

107. Nemeth J.A. Prostate ductal system in rats: regional variation in stromal organization / J.A. Nemeth, C. Lee // The Prostate. – 1996. – Vol. 28, № 2. – P. 124-128.

108.Odum J. Guidance document for histologic evaluation of endocrine and reproductive tests in rodents / J. Odum, D. Creasy, J. Cartwright et al. // ENV/JM/MONO. – 2009. – Vol. 11, № 106.

109.Oliveira D.S., Dzinic S., Bonfil A.I., Saliganan A.D., Sheng S., Bonfil R.D. Bosn. The mouse prostate: a basic anatomical and histological guideline // J. Basic Med. Sci. 2016 Feb 10; 16 (1): 8-13. doi: 10. 17305 /bjbms. 2016. 917. PMID: 26773172.

110.Oliveira C., Ferreira A.L. 1987. Effect of alcohol on the rat justa prostatic pelvic ganglia and gonads // Gegenbaurus Morphol. Jahrb., 133, 771-780.

111.Omezzine A. Caspase-3 and -6 expression and activation are targeted by hormone action in the rat ventral prostate during the apoptotic cell death process / A. Omezzine, C. Mauduit, E. Tabone et al. // Biology of Reproduction. – 2003. – Vol. 65, № 3. – P. 752-760.

112.Paner G. 2010. Prostate gland and seminal vesicle. In Diagnostic pathology: Genitourinary (ed. Amin M, et al.), Section 3, pp. 4–156. Amirysis, Salt Lake City, UT.

113.Pathak A., Katiyar R., Sharma D., Farooqui M., Prakash A. Gross anatomical, histological and histochemical studies on the postnatal development of the prostate gland of Gaddi goat // Int. j. morphol. 2012; 30 (2): 731-739.

114.Pechenino A.S. Superoxide dismutase in the prostate lobes of aging Brown Norway rats / A.S. Pechenino, T.R. Brown // The Prostate. – 2006. – Vol. 66, № 5. – P. 522-535.

115.Picut C.; Remick A. Male reproductive system. In Atlas of Histology of the Juvenile Rat; Parker, G., Picut, C., Eds.; Academic Press - Elsevier: Cambridge, MA, USA, 2016.rita T, Medina RT, Mills AA and Cunha GR: Role of P63 and basal cells in the prostate. Development 131: 4955-4964, 2001.

116.Randazzo M. Grobholz R. (2020) Prostata: Anatomie und Physiologie // J. Urol. 14: 48-61.

117.Renata T. S. Santos, Laís R. M. Pires, Edna S. S. Albernaz, Cleber S. Andrade, Cornelio S. Santiago, Eliana Morielle Versute, Sebastiao R.

Taboga, Mateus R. Beguelini. Morphological analysis of the male reproductive accessory glands of the bat Artibeus lituratus (Phyllostomidae: Chiroptera) // Journal of Morphology, 10.1002/jmor.20767, 279, 2, (228-241), (2017).

118.Ren X., Wu C., Yu Q., Zhu F., Liu P., Zhang H. Correlation of IL-8 and IL-6 in prostatic fluid with serum prostate-specific antigen level in patients with benign prostatic hyperplasia complicated by prostatitis. Nan Fang Yi Ke Da Xue Xue Bao 2016; 36(1): 135-139.

119.Riede U.N., Werner M. Allgemeine und Spezielle Pathologie, DOI 10.1007/978-3-662-48725-9_52, © Springer-Verlag GmbH Deutschland, 2017: 58.

120.Rochel S.S., Bruni-Cardoso A., Taboga S.R., Vilamaior P.S.L., Goes R.M. (2007) Lobe identity in the Mongolian gerbil prostatic complex: a new rodent model for prostate study // Anat Rec 290:1233–1247.

121.Roy-Burman Wu H., Powell W.C., Hagencord J., Cohen M.B. Genetically defined mouse models that mimic natural aspects of human prostate cancer development // Endocr Relat Cancer. 2004 Jun; 11(2): 225-254. doi: 10. 1677/ erc. 0.01 10225.

122.Ruetten H., Cole C., Wehber M., Wegner K.A., Girardi N.M. (2020) An immunehisto chemical prostate cell identification key indicates that aging shifts procollagen 1A1 production from myofibroblasts to fibroblasts in dogs prone to prostate-related urinary dysfunction. PLOS ONE 15(7): 232-264.

123.Santamaría L., Ingelmo I., Alonso L., Pozuelo J., Rodriguez R. The prostate of the rat. In Neuroendocrine Cells and Peptidergic Innervation in Human and Rat Prostate; Springer: Berlin/Heidelberg, Germany, 2007; pp. 39–42.

124.Sattolo S., Carvalho C.A.F., Cagnon V.H.A., 2004. Influence of hormonal replacement on the ventral lobe of the prostate of rats (Rattus norvegicus albinus) submitted to chronic ethanol treatment // Tissue Cell. 36, 417–430.

125.Smith J. Canine prostatic disease: A review of anatomy, pathology, diagnosis, and treatment. Theriogenology. 2008; 70: 375-383. DOI: 10. 1016 /j. therio geno logy. 2008.04.039.

126.Stefanov M., Martín-Alguacil N., Martín-Orti R. Distinct vascular zones in the canine prostate // Miicrosc. Res. Tech. 2000 Jul 15; 50 (2): 169-75. doi: 10.1002/1097-0029 (20000715) 50:2-169:AID-JEMT93.0.CO;2-P.

127.Sun F., Báez-Díaz C., Sánchez-Margallo F. M. (2017). Canine prostate models in preclinical studies of minimally invasive interventions: Part I, canine prostate anatomy and prostate cancer models. (pp. 538– 546). AME Publishing Company.

128.Suwa T. A Retrospective Analysis of Background Lesions and Tissue Accountability for Male Accessory Sex Organs in Fischer-344 Rats / T. Suwa, A. Nyska, J.C. Peckham et al. // Toxicologic Pathology. – 2001. – Vol. 29, № 4. – P. 467-468.

129.Shappell S.B., Thomas G.V., Roberts R.L., Herbert R., Ittmann M.M., Rubin M.A., Humphrey P.A., Sundberg J.P., Rozengurt N., Barrios R., Ward J.M., Cardiff R.D. 2004. Prostate pathology of genetically engineered mice: definitions and classification. The consensus report from the Bar Harbor meeting of the Mouse Models of Human Cancer Consortium Prostate Pathology Committee // Cancer Res. 64: 2270- 2305.

130.Ousset M., Van Keymeulen A., Bouvencourt G., Sharma N., Achouri Y., Simons B.D., Blanpain C. Multipotent and unipotent progenitors contribute to prostate postnatal development // Nat. Cell Biol. 2012; 14: 1131–1138.

131.Takis A. Impact of hypercholesterol diet (HD) on the antioxidant system of the rat ventral prostate / A. Takis, A. Kyroudi-Voulgari, K. Ploumidou et al. // European Urology. – 2009. – Vol. 8, № 4. – P. 208.

132.Tam N.C Androgenic Regulation of Oxidative Stress in the Rat Prostate: involvement of NAD (P) H oxidases and antioxidant defense machinery during prostatic involution and regrowth /N.C. Tam, Y. Gao, Y-K. Leung et al. // The American Journal of Pathology. – 2003. – Vol. 163, № 6. – P. 2513-2522.

133.Thomson A.A., Timms B.G., Barton L., Cunha G.R., Grace O.C. (2002) The role of smooth muscle in regulating prostatic induction // Development 129: 1905–1912.

134.Toby Ryman-Tubb, Jennifer H. Lothion-Roy, Veronika M. Metzler, Anna E. Harris, Brian D. Robinson, Albert A. Rizvanov, Jennie N. Jeyapalan, Victoria H. James, Gary England, Catrin S. Rutland, Jenny L. Persson, Lukas Kenner, Mark A. Rubin, Nigel P. Mongan, Simone Brot, Comparative pathology of dog and human prostate cancer // Veterinary Medicine and Science, 10.1002/vms3.642, 8, 1, (110-120), (2021).

135.Toivanen R., Shen M.M. Prostate organogenesis: Tissue induction, hormonal regulation and cell type specification // Development. 2017; 144: 1382–1398. doi: 10.1242/dev.148270.

136.Vilamaior P.S., Taboga S.R., Carvalho H.F. 2006. Altenating proliferative and secretory activities contribute to the postnatal growth of rat ventral prostate // Anat. Rec. A Discov Mol. Cell. Evol. Biol. 288: 885–892.

137.Wendell Smith C., 2000: Terminology of prostate and related structures // Clin. Anat. 13, 207–213.

138.Whitney K. Male accessory sex glands. In Boorman´s Pathology of the Rat: Reference and Atlas; Suttie A., Leininger J., Bradley A., Eds.; Academic Press – Elsevier: Cambridge, MA, USA, 2018; pp. 579–586.

139.Wong Y.C., Xie W., Tsao S.W. Structural changes and alteration in expression of TGF-bI and its receptors in Prostatic Intraepithelial Neoplasia (PIN) in the ventral prostate of Noble rats // Prostate 2000; 45: 289- 298.

140.Wong Y.C., Tam N.N. (2002) Dedifferentiation of stromal smooth muscle as a factor in prostate carcinogenesis // Differentiation 70: 633–645.

141.Xie W., Wong I.C., Tsao S.W. Correlation of increased apoptosis and proliferation with development of prostatic intraepithelial neoplasia (PIN) in ventral prostate of the Noble rat // Prostate June 15, 2000; 44(1): 31-39.

142.Xu D., Chen P., Xiao H., Wang X., Di Santo M.E., Zhang X. Upregulated Interleukin 21 receptor enhances proliferation and epithelial-mesenchymal transition process in benign prostatic hyperplasia // Front. Endocrinol. 2019; 10 : 4.

143.Yassa H.A. Subchronic toxity of cannabis leaves on male albino rats /H.A. Yassa, W. Dawood Ael, M.M. Shehata et al. // Human & Experimental Toxicology. – 2010. – Vol. 29, № 1. – P. 37-47.

144.Zondek L. H. Observations on the prostatic utricle in the fetus and infant / L. H. Zondek, T. Zondek // Acta Paediatr. Scand. 1980. Vol. 69. P. 257–258.

145.Zordo T.D., Aigner F., Frauscher F. (2021): Prostata und Samenblasen. In: Hofmann R., Hegele A., Honacker A. (Hrsg.), Ultraschall in der Urologie. Springer, Berlin, 226.

APPLICATIONS

Appendix 1.

Morphological parameters of the prostate of control group rats in early postnatal ontogenesis

age / features	newborns	6 - day	11 -day	16 -day	21 -day
number of acini in the visual field	23-37 29,7±0,8	40-55 47,5±0,8*	65-85 77,0±1,1*	60-80 73,2±1,1	75-110 92,5±1,9*
acinus diameter (μm)	50,4-197,4 116,8±5,9	29,4-54,6 37,8±1,1*	16,8-29,4 23,1±0,5*	21,0-63,0 37,0±1,7*	25,2-105,0 55,4±3,4*
height of acinar epithelium (μm)	4,2-8,4 6,3±0,21	4,2-12,6 8,4±0,42*	8,4-12,6 11,3±0,21*	8,4-16,8 12,6±0,4	8,4-16,8 14,0±0,4
proportion of acini with secretion (%)	70-94 82,7±1,3	0	0	0	0
proportion of acini without secretion (%)	6-30 17,3±1,3	100	100	100	100

Note: * - significance of differences in relation to the previous age ($P \leq 0.05$).

Appendix 2.

Intraorgan vessels of the prostate gland of control group rats in postnatal ontogenesis

vessels / age	number of vessels in the field of view	venule (μm)		capillary (μm)		arteriole (μm)	
		inner diameter	wall thickness	inner diameter	wall thickness	inner diameter	wall thickness
Newborns	3-5 3,6±0,1	8,4-12,3 10,5±0,21	2,1-4,2 3,0±0,13	4,2-8,4 4,8±0,21	2,1-4,2 2,4±0,13	4,2-8,4 5,6±0,21	4,2-8,4 4,5±0,21
6-day	3-6 3,9±0,2	12,6-16,8 12,9±0,21*	2,1-4,2 3,2±0,13	4,2-8,4 5,4±0,21	2,1-4,2 2,7±0,13	4,2-8,4 6,3±0,21	4,2-8,4 4,8±0,21
11-day	3-6 4,4±0,2	12,6-16,8 14,5±0,21*	2,1-6,3 3,7±0,21	4,2-8,4 6,3±0,21	2,1-4,2 3,0±0,13	4,2-12,6 8,4±0,42*	4,2-8,4 5,4±0,21
16- day	3-6 4,5±0,2	12,6-21,0 16,8±0,42*	2,1-6,3 4,2±0,21	4,2-8,4 6,3±0,21	2,1-4,2 2,9±0,13	8,4-12,6 9,2±0,21	4,2-8,4 5,8±0,21
21- day	4-7 4,6±0,2	12,6-25,2 18,0±0,67	4,2-8,4 4,8±0,21	4,2-12,6 7,4±0,42	2,1-4,2 3,1±0,13	8,4-12,6 10,5±0,21*	4,2-8,4 6,3±0,21
1-month	3-7 4,7±0,2	12,6-25,2 18,9±0,67	4,2-8,4 5,0±0,21	4,2-12,6 8,4±0,42	2,1-4,2 4,0±0,13*	8,4-16,8 12,6±0,42*	4,2-8,4 7,0±0,21
3- month	3-8 5,0±0,3	16,8-29,4 20,6±0,67	4,2-8,4 4,7±0,21	8,4-12,6 9,6±0,21	2,1-4,2 4,1±0,13	8,2-16,4 13,8±0,46	4,2-8,4 7,5±021
6- month	4-9 7,0±0,3*	21,0-29,4 24,8±0,42*	4,2-8,4 5,8±0,21	8,4-16,8 13,1±0,42*	2,1-4,2 4,2±0,13	12,6-16,8 14,7±0,21	4,2-8,4 7,7±0,21

9- month	7-10 9,0±0,2*	21,0-33,6 29,8±0,67*	4,2-8,4 7,5±0,21	12,6-16,8 15,2±0,21*	4,2-8,4 5,0±0,21	12,6-16,8 15,1±0,21	4,2-8,4 8,0±0,21
12- month	8-12 10,2±0,2	21,0-33,6 29,9±0,67	4,2-8,4 7,7±0,21	12,6-16,8 15,9±0,21	4,2-8,4 6,1±0,21	12,6-16,8 15,5±0,21	4,2-8,4 8,2±0,21
18- month	11-15 13,0±0,2*	25,2-33,6 30,7±0,42	4,2-8,4 7,9±0,21	12,3-16,8 16,3±0,21	4,2-8,4 6,5±0,21	12,3-16,8 15,8±0,21	4,2-12,3 8,4±0,42

Note: * - significance of differences in relation to the previous age ($P \leq 0.05$).

Appendix 3.

Morphometric indices of the prostate of control group rats in early postnatal ontogenesis

age / features	newborns	6 - day	11 -day	16 -day	21 -day
number of acini with epithelial desquamation	4-12 7,5±0,4	4-8 6,5±0,2	5-8 7,0±0,2	5-8 6,7±0,2	2-5 3,6±0,2*
number of lymphocytes in the stroma	2-4 3,0±0,1	3-5 3,8±0,1*	3-5 4,0±0,1	4-6 4,7±0,1*	4-6 5,0±0,1
thickness of stromal septa	16,8-50,4 28,6±1,7	12,6-33,6 24,8±1,3	8,4-16,8 13,9±0,4*	8,4-21,0 14,7±0,7	4,2-16,8 9,5±0,7*
volume fraction of glandular tissue (%)	60-89 72,2±1,6	68-80 73,1±0,6	54-75 64,7±1,1*	64-84 73,1±1,1*	59-85 70,6±1,4
volume fraction of stromal tissue (%)	11-40 27,8±1,6	20-32 26,9±0,6	25-46 35,3±1,1*	16-36 26,9±1,1*	15-41 29,4±1,4

Note: * - significance of differences in relation to the previous age ($P \leq 0.05$).

Appendix 4.

Morphological parameters of the prostate of rats in the control group in late postnatal ontogenesis

age / features	1 – month	3 – month	6 - month	9 – month	12 - month	18 - month
number of acini in the visual field	60-90 78,1±1,6	38-66 51,8±1,5*	18-28 22,0±0,5*	10-21 14,9±0,6*	16-26 20,1±0,5*	18-34 25,9±0,9*
acinus diameter (μm)	63,0-168,0 108,4±4,2	105,0-298,2 198,7±8,0*	210,0-441,0 330,5±9,7*	336,0-840,0 531,7±20,6*	147,0-252,0 191,9±4,2*	252,0-504,0 381,8±10,5*
height of acinar epithelium (μm)	8,4-16,8 14,9±0,4	8,4-21,0 16,5±0,6*	12,6-21,0 17,8±0,4	16,8-21,0 19,7±0,2*	4,2-12,6 9,4±0,4*	4,2-12,6 8,4±0,4
proportion of acini with secretion (%)	15-30 22,1±0,8	70-93 83,5±1,3*	90-100 93,3±0,5*	85-100 92,0±0,8	 100	90-100 95,0±0,5

proportion of acini without secretion (%)	70-85 77,9±0,8	7-30 16,5±1,3*	0-10 6,7±0,5*	0-15 8,0±0,8	 0	0-10 5,0±0,5

Note: * - significance of differences in relation to the previous age ($P \leq 0.05$).

Appendix 5.

Morphometric indices of the prostate of rats of the control group in late postnatal ontogenesis

age / features	1 – month	3 – month	6 - month	9 – month	12 - month	18 - month
number of acini with epithelial desquamation	3-6 4,6±0,2	0-4 1,7±0,2*	 -	 -	3-6 4,4±0,2	 -

number of lymphocytes in the stroma	4-6 5,2±0,1	4-9 5,7±0,3	8-12 10,0±0,2*	9-14 12,5±0,3*	16-25 18,5±0,5*	20-35 29,3±0,8*
thickness of stromal septa	4,2-16,8 12,6±0,7	8,4-25,2 15,5±0,9	12,6-33,6 23,1±1,1*	42,0-71,4 53,3±1,7*	37,8-84,0 64,7±2,5	50,4-168,0 108,8±6,3*
объёмная доля железистой ткани (%)	82-90 86,5±1,0	62-80 71,0±1,0*	77-90 82,5±0,7*	85-91 88,2±0,3*	60-85 70,3±1,4*	45-75 61,3±1,6
volume fraction of stromal tissue (%)	10-18 13,5±1,0	20-38 29,0±1,0*	10-23 17,5±0,7*	9-15 11,8±0,3*	15-40 29,7±1,4*	25-55 38,7±1,6

Note: * - significance of differences in relation to the previous age ($P \leq 0.05$).

Appendix 6.

Morphological parameters of the prostate of rats of the experimental group

age / features	1 – month	3 – month	6 - month	9 – month	12 - month
number of acini in the visual field	54-96 74,2±2,3*	20-52 35,9±1,7*	12-34 23,5±1,2*	10-22 15,7±0,6*	25-40 32,5±0,8*
acinus diameter (μm)	25,2-126,0 75,2±0,4*	105,0-327,6 204,1±9,2*	231,0-483,0 354,9±10,5*	336,0-672,0 448,1±13,9*	210,0-420,0 288,5±8,8*
height of acinar epithelium (μm)	4,2-16,8 9,1±0,6*	4,2-12,6 9,8±0,4*	4,2-12,6 7,6±0,4*	4,2-8,4 7,7±0,2	4,2-8,4 5,8±0,2*
proportion of acini with secretion (%)	15-46 29,2±1,7*	85-95 87,8±0,5*	50-70 58,8±1,1*	100	0
proportion of acini without secretion (%)	54-85 70,8±1,7*	5-15 12,2±0,5*	30-50 41,2±1,1*	0	100

Note: * - significance of differences in relation to control (P≤ 0.05).

Appendix 7.

Intraorgan vessels of the prostate gland of rats of the experimental group

vessels / age	number of vessels in the field of view	venule (μm)		capillary (μm)		arteriole (μm)	
		inner diameter	wall thickness	inner diameter	wall thickness	wall thickness	inner diameter
3-month	6-12 9,1±0,3*	16,8-37,8 25,2±1,13	2,1-4,2 3,6±0,13	8,4-16,8 12,6±0,46*	2,1-4,2 3,5±0,13	12,6-21,0 17,5±0,46*	4,2-8,4 5,6±0,21*
6- month	7-12 9,9±0,3*	25,2-33,6 29,8±0,42*	4,2-8,4 4,5±0,21*	12,6-16,8 15,8±0,21*	2,1-4,2 3,7±0,13	12,6-21,0 17,9±0,42*	4,2-8,4 6,1±0,21*
9- month	12-18 15,4±0,3*	25,2-37,8 34,4±0,67*	4,2-8,4 6,3±0,21	12,6-21,0 17,6±0,42*	2,1-4,2 3,7±0,13*	12,6-21,0 17,7±0,42*	4,2-8,4 5,6±0,21*
12- month	13-19 16,0-0,3*	29,4-42,0 38,1±0,67*	4,2-8,4 6,0±0,21*	12,6-21,0 18,7±0,42*	2,1-4,2 3,8±0,13*	12,6-21,0 19,1±0,42*	4,2-8,4 5,8±0,21*
18- month	14-25 18,8±0,6*	29,4-46,2 42,0±0,9*	4.2-8,4 5,4±0,21*	16,8-25,2 20,1±0,42*	4,2-8,4 4,5±0,21*	16,8-21,0 19,5±0,21*	4,2-8,4 5,4±0,21*

Note: * - significance of differences in relation to control ($P \leq 0.05$).

Appendix 8.

Morphometric indices of the prostate of rats of the experimental group

age / features	1 – month	3 – month	6 - month	9 – month	12 - month
number of acini with epithelial desquamation	4-10 7,5±0,3*	5-11 9,1±0,3	3-6 5,1±0,2	8-20 13,7±0,6*	-
number of lymphocytes in the stroma	15-40 26,0±1,4*	30-70 46,0±2,2*	∞	17-26 20,0±0,5	∞
thickness of stromal septa	21,0-75,6 40,7±2,9*	75,6-201,6 122,6±6,7*	252,0-462,0 326,3±11,3*	151,2-252,0 189,4±5,5*	96,6-231,0 162,1±7,1*
volume fraction of glandular tissue (%)	32-55 40,6±1,2*	37-55 43,6±0,1*	17-52 30,9±1,9*	50-65 58,0±0,8*	20-46 34,1±1,4*
volume fraction of stromal tissue (%)	45-68 59,4±1,2*	45-63 56,4±0,1*	60-83 69,1±1,2*	35-50 42,0±0,8*	54-80 65,9±1,4*

Note: * - significance of differences in relation to control (P≤ 0.05).